IDENTIFICATION OF *IKBKB* AS A NOVEL REGULATOR OF MACROPHAGE PHAGOCYTOSIS THAT SUPPRESSES ANTITUMOR IMMUNITY IN HEPATOCELLULAR CARCINOMA

CHAN SZE MAN

PhD

The Hong Kong Polytechnic University

2026

The Hong Kong Polytechnic University

Department of Applied Biology and Chemical Technology

Identification of *IKBKB* as a Novel Regulator of Macrophage Phagocytosis That Suppresses Antitumor Immunity in Hepatocellular Carcinoma

CHAN Sze Man

A thesis submitted in partial fulfilment of the requirements for the degree of Doctor of Philosophy

December 2025

CERTIFICATE OF ORIGINALITY

I hereby declare that this thesis is my own work and that, to the best of my knowledge and belief, it reproduces no material previously published or written, nor material that has been accepted for the award of any other degree or diploma, except where due acknowledgement has been made in the text.

_____(Signed)
CHAN Sze Man (Name of Student)

Abstract

Hepatocellular carcinoma (HCC) presents a significant clinical challenge owing to the high prevalence of primary and acquired resistance to current standard-of-care treatments, a problem often linked to an immunosuppressive TME. Cancer cells evolved to evade from clearance of macrophages by overexpressing the "don't eat me" signal or antiphagocytic protein on the cell surface. Therapeutic strategies antagonizing the interaction of "don't eat me" signals with macrophage-expressed receptors have been investigated in multiple cancer types, yet remain underexplored in HCC. Here, we aim to identify protein kinases governing resistance to phagocytosis in HCC. To this end, we employed an *in vitro* CRISPR-based kinome screen targeting 713 mouse kinase genes in a co-culture system in which mouse HCC cells (RIL-175) interacted with RAW 264.7 macrophages.

Our analysis revealed that inhibitor of kappaB kinase beta (IKKβ), encoded by the *IKBKB* gene, emerged as a top sensitizer for macrophage-mediated phagocytosis, serving as a novel master regulator of anti-phagocytosis that facilitates immune evasion in HCC. Perturbation of *Ikbkb* significantly enhanced HCC cell phagocytosis and promoted macrophage activation under co-culture conditions. Depletion of *Ikbkb* suppressed HCC tumor growth, accompanied by increased *in vivo* macrophage phagocytosis and infiltration. The tumor-promoting role of *Ikbkb* through its anti-phagocytic function was further demonstrated by the observation that the growth-suppressive effect in *Ikbkb* knockout cells was offset by *in vivo* depletion of macrophages using clodronate liposomes. Mechanistically, *Ikbkb* facilitates evasion from macrophage-mediated phagocytosis by driving transcriptional activation of the anti-phagocytic checkpoints CD47 and PD-L1 via canonical NF-kB signaling.

The immunomodulatory role of HCC cell-specific *Ikbkb* targeting was next assessed in immunocompetent murine models. Overexpression of *Ikbkb* in hepatocytes fosters tumor progression with a signature of compromised innate and adaptive immunities characterized by reduced infiltration and activation of innate immune cells, such as macrophages and dendritic cells, as well as dampened cytotoxic T cell activation and help T cells infiltration. Concordantly, cancer cell-specific *Ikbkb* depletion results in enhanced antitumor activities of both innate and adaptive arms, and remarkable tumor clearance. Interestingly, antigen cross-presentation was enhanced in splenic macrophages, suggesting systemic antigen spread and potentially accounting for the active immune surveillance of the adaptive arm and tumor clearance observed.

Plausible therapeutic targeting was investigated using an IKKβ-targeting peptide, TAT-NEMO^{Actpep}. In cell models, treatment with TAT-NEMO^{Actpep} showed pro-phagocytic effects, resembling the results of gene depletion assays. Most critically, using the hydrodynamic tail vein injection (HTVI) model for hepatocarcinogenesis, which is known to generate HCC resistant to anti-PD-1 monotherapy, combining TAT-NEMO^{Actpep} with PD-1 blockade yielded effective tumor control without overt toxicity. Taken together, these findings establish IKKβ inhibition as an efficacious and bifunctional strategy to disrupt cancer cell defences and reprogram the immunosuppressive niche, providing a compelling rationale for co-targeting with immunotherapy to overcome treatment resistance in HCC.

(453 words)

Publications

Chan MS, Lee TK^. Unveiling TRIB3: A New Mediator in MET-Driven Hepatocellular Carcinoma Progression. Clin Mol Hepatol 2025, doi: 10.3350/cmh.2025.0452.

Ying F[#], **Chan MS**[#], Lee TK^. Cancer-associated fibroblasts in hepatocellular carcinoma and cholangiocarcinoma. Cell Mol Gastroenterol Hepatol 2023;15(4):985-999.

Lee, C., Mu, W., Chen, X. J., **Chan, M. S**., Chen, Z., Yeung, S. F., Chan, H. H., Chow, S. T., Ko, B. C., Chan, D. W., Cho, W. C., Lui, V. W., & Tsui, S. K. (2025a). Oncogenic activity and sorafenib sensitivity of Araf P.S214C mutation in Lung Cancer. Cancers, *17*(13), 2246. doi: 10.3390/cancers17132246

Leung CON#^, Gurung S#, Chung KPS#, Leung RWH, Lei MM, **Chan MSM**, Muliawan GK, Khan SA, Wu XQ, Yu J, Zhu HL, Lu YY, Ma S, Wu XP, Hoo RL, Lee TK^. Adipocyte-derived FABP4 promotes metabolism-associated steatotic liver-induced hepatocellular carcinoma by driving ITGB1-mediated β-catenin activation. J Clin Invest 2025; 135(24):e182322.

Lei MML, Leung CON, Leung RWH, Wu XQ, Chung KPS, Gu CY, **Chan MSM**, Chau WK, Mu QH, Ng JK, Tong M, Yun JP, Teo JM, Ling CS, Wong PP, Chan SL, Xiong ZW, Cheng AS, Ding J, Ma S, Lee TK^. Wild-type KRAS activation drives evasion of interferon-mediated immunity and resistance to immunotherapy in hepatocellular carcinoma. Nat Commun 2025, 16:9913.

Conference Presentations and Awards

Chan MS, Lee TK. 'Identification of IKBKB as a Novel Regulator of Macrophage Phagocytosis That Enhances Antitumor Immunity in Hepatocellular Carcinoma' The Liver Week 2025, Gyeongju, Korea. 2025.

This presentation was awarded the Travel Award and Best Presentation Award.

Chan MS, Lee TK. 'Identification of IKBKB as a Novel Regulator of Macrophage Phagocytosis That Enhances Antitumor Immunity in Hepatocellular Carcinoma' FASEB Science Research Conferences, HKU. 2025.

Chan MS, Lee TK. 'CRISPR-based Kinome Screen Identifies *Ikbkb* as a Regulator of Cancer Cell Phagocytosis in Hepatocellular Carcinoma' American Association for Cancer Research (AACR 2024), San Diego. 2024.

Chan MS, Lee TK. 'CRISPR-based Kinome Screen Identifies Ikbkb as a Master Regulator of Phagocytic Checkpoints in Hepatocellular Carcinoma' 5th ABCT Research Postgraduate Symposium in the Biology Discipline, 2024.

This presentation was awarded the Best Poster Presentation Award and People's Choice Award.

Chan MS, Lee TK. 'CRISPR-based Kinome Screen Identifies Regulators of Phagocytic Evasion in Hepatocellular Carcinoma' 4th ABCT Research Postgraduate Symposium in the Biology Discipline, 2023.

This presentation was awarded the Best Poster Presentation Award.

Acknowledgements

I want to express my sincere appreciation to my supervisor, Professor Terence Lee Kin Wah, for his invaluable mentorship and support throughout my doctoral journey. His expertise, guidance, and encouragement have been the foundation of this endeavour. He generously shared his time and wisdom, offering insightful advice that shaped the direction of my research. I am thankful for his prompt and thoughtful responses to my questions and for his guidance during challenging moments. His mentorship has been essential in the completion of this thesis as well as in my development as an independent researcher, for which I will remain ever grateful.

My heartfelt thanks also go to my colleagues and lab mates, Dr. Carmen Oi Ning LEUNG, Dr. Sherry Xue Qian WU, Dr. Sara Ying, Dr. Shakeel KHAN, Dr. Martina Mang Leng LEI, Dr. Catherine Yu Jia GU, Dr. Yitain CHEN, Dr. Huihai Yang, Ms. Rainbow Wing Hei LEUNG, Miss Candy Chin Ngok CHU, Mr. Gregory Kenneth MULIAWAN, and Ms. Wing Ki CHAU for their scholarly discussions, shared expertise, technical support, and other forms of practical assistance. My doctoral journey would have been more challenging without their collective support.

Finally, I would like to acknowledge the unwavering love and patience of my family and friends, whose constant belief in me, even during the most challenging times of this journey, granted me the emotional basis and strength necessary to persevere. To them, I owe my deepest personal gratitude.

Table of Contents

List of Figures & Tables

List of Abbreviations

APCs	Antigen-presenting cells
CRISPR	Clustered Regularly Interspaced Short Palindromic Repeats
CD	Cluster of Differentiation (e.g., CD47, CD80, CD86)
cDC	Conventional Dendritic Cell
DAPI	4',6-diamidino-2-phenylindole
DC	Dendritic Cell
DEGs	Differentially Expressed Genes
EGFR	Epidermal Growth Factor Receptor
FACS	Fluorescence-Activated Cell Sorting
gDNA	Genomic DNA
GFP	Green Fluorescent Protein
HCC	Hepatocellular Carcinoma
HTVI	Hydrodynamic Tail Vein Injection
ICI	Immune Checkpoint Inhibitor
IHC	Immunohistochemistry
IKKβ / IKBKB	Inhibitor of nuclear factor kappa B kinase subunit beta (gene/protein)
IL	Interleukin (e.g., IL-12)
IP	Intraperitoneal (injection)

LIHC	Liver Hepatocellular Carcinoma
mAb	Monoclonal Antibody
MHC	Major Histocompatibility Complex
MMP	Matrix Metalloproteinase
MOI	Multiplicity of Infection
mRNA	Messenger RNA
NF-κB	Nuclear factor kappa-light-chain-enhancer of activated B cells
NGS	Next-Generation Sequencing
OVA	Ovalbumin
PFS	Progression-free survival
PD-1	Programmed Cell Death Protein 1
PD-L1	Programmed Death-Ligand 1
sgRNA	Single-Guide RNA
SIRPα	Signal Regulatory Protein Alpha
TAM	Tumor-Associated Macrophage
TAT-NEMOActpep	Trans-Activator of Transcription-NF-kappa-B Essential Modulator activation peptide
TCGA	The Cancer Genome Atlas
Tc	Cytotoxic T cell

TCR	T-Cell Receptor
Th	T helper cell (e.g., Th1, Th17)
TKI	Tyrosine Kinase Inhibitor
TLR	Toll-Like Receptor
TME	Tumor Microenvironment
TNF-α	Tumor Necrosis Factor-alpha
TPM	Transcripts Per Million
Treg	Regulatory T cell
UMAP	Uniform Manifold Approximation and Projection

CHAPTER 1 Introduction

1.1 Introduction to Hepatocellular Carcinoma (HCC)

Liver cancer represents a major clinical challenge, it is the sixth most prevalent cancer and fourth leading cause of cancer mortality around the globe, accounting for more than 800,000 deaths in 2020, with its annual incidence projected to surpass one million cases by 2025 (Yang et al., 2023; Llovet et al., 2021; Sung et al., 2021). Projections from the World Health Organization indicate the annual mortality from this disease is expected to rise to over one million by the year 2030 (Villanueva, 2019). As the dominant histological subtype, hepatocellular carcinoma (HCC) is responsible for an estimated 90% of all liver cancer diagnoses (Yang et al., 2023). Major etiological factors include chronic infection with hepatitis B virus (HBV) or hepatitis C virus (HCV), contributing to the most incidence cases worldwide (Llovet et al., 2008). Additional important risk factors include cirrhosis, chronic alcohol abuse, and metabolic conditions such as diabetes and obesity, the latter often correlated with non-alcoholic fatty liver disease (NAFLD) (Wei et al.,2019). While surgical resection is considered the foremost curative option for HCC, the combination of delayed symptom emergence, a lack of sensitive diagnostic biomarkers, and the cancer's aggressive nature means the majority of patients present with late-stage, non-resectable disease. Consequently, the outcome for advanced HCC remains severe, characterized by a short median survival (~8 months) and a five-year survival rate of only 10%, which often confines the range of viable treatments (Cabibbo et al., 2010). For advanced HCC, standard treatment involves systemic therapies including monoclonal antibodies, tyrosine kinase inhibitors (TKIs) and immune checkpoint blockers (Llovet et al., 2018). It is estimated that these systemic therapies are applicable to roughly 50–60% of patients, and over the past decade, they have proven effective in improving the clinical prognosis and life quality for those diagnosed with HCC (Llovet et al., 2018).

1.2 Treatment landscape for advanced HCC

1.2.1 Current systemic therapies

1.2.1.1 First-line therapies

Currently, two multi-kinase inhibitors, sorafenib and lenvatinib, are approved by FDA for initial systemic treatment of advanced HCC (Cheng et al., 2018; Llovet et al., 2021). Sorafenib, which inhibits Raf, VEGF, and PDGF receptor tyrosine kinases, was the first such agent to show clinical benefit and has been a mainstay therapy for over a decade (Wilhelm et al., 2008;

Cheng et al., 2009). A pivotal trial (SHARP) established that it extends overall survival by roughly three months (Llovet et al., 2008). Subsequent analysis indicated its efficacy is greater in patients with HCV-related, non-metastatic disease (Bruix et al., 2017). However, treatment response is limited to about 30% of patients, and resistance typically develops within six months, leading to failure (Llovet et al., 2008).

Lenvatinib, another first-line monotherapy, targets VEGFR 1-3, FGFR 1-4, and PDGF receptor (Okamoto et al., 2014). In the REFLECT trial, it demonstrated comparable overall survival compared to sorafenib (13.6 vs. 12.3 months) and significantly improved progression-free survival and objective response rate (Kudo et al., 2018; Llovet et al., 2021). Despite this, acquired resistance also curtails its long-term effectiveness. Notably, both sorafenib and lenvatinib are associated with severe adverse events in approximately half of patients, resulting in treatment discontinuation rates near 15% (Llovet et al., 2008; Kudo et al., 2018).

More recently, combination immunotherapies have emerged as superior first-line options. The atezolizumab (anti-PD-L1) plus bevacizumab (anti-VEGF) regimen, tested in the IMbrave150 trial, achieved a median survival of 19.2 months and improved both survival and tolerability over sorafenib (Finn et al., 2020; Richard et al., 2020), leading to FDA approval (Llovet et al., 2021). Similarly, the tremelimumab (anti-CTLA-4) and durvalumab (anti-PD-L1) combination (HIMALAYA trial) significantly extended overall survival and increased response rates compared to sorafenib, with severe adverse events occurring in about 25% of patients (Ghassan et al., 2022). This regimen has also received FDA approval for advanced HCC.

1.2.1.2 Second-line therapies

In the case of progression following single-agent treatments, three regimens (regorafenib, cabozantinib, and ramucirumab) have proven to improve patient clinical outcome in phase III clinical trials and have been approved as second-line approach for advanced HCC (Abou-Alfa et al.,2018; Zhu et al., 2019; Bruix et al., 2017). Regorafenib, a multi-kinase inhibitor blocking VEGFR 1–3 and other kinases, demonstrated in The RESORCE study that it improved patient survival over placebo (median OS of 10.6 months *vs.* 7.8 months, median PFS of 3.1 months *vs.* 1.5 months) in patients who progressed on prior sorafenib (Bruix et al., 2017). Cabozantinib is a multi-kinase inhibitor targeting VEGFR2, anexelekto (AXL), and Mesenchymal Epithelial Transition (MET). Cabozantinib treatment improved patients' overall and progression-free survival by 4.2 months and 3.3 months respectively, as compared to placebo in the

CELESTIAL trial (Abou-Alfa et al.,2018). Ramucirumab is a monoclonal antibody directed against VEGFR2. In the REACH-2 study, ramucirumab improved overall and progression-free survival by 1.2 months compared to placebo in patients with baseline α-fetoprotein levels of ≥400 ng/dl (Zhu et al., 2019). Grade 3 to 4 drug-associated adverse events were reported in the patients, resulting in a withdrawal rate of ~ 15% in these phase III trials.

Furthermore, three monoclonal antibody therapies (pembrolizumab, nivolumab, and nivolumab plus ipilimumab) were granted approval by the FDA as second-line treatments following sorafenib treatment owing to their marked clinical efficacies in phase Ib/II studies (El-Khoueiry et al., 2017; Yau et al., 2020; Zhu et al., 2018). Nivolumab and pembrolizumab are anti-PD1 inhibitors that were approved as single agents. In the CheckMate 040 trial, the median OS of patients receiving nivolumab was 15.6 months with a 14% objective response rate (ORR) (El-Khoueiry et al., 2017; Yau et al., 2020). The KEYNOTE-224 study showed an ORR of 17% and a median OS of 12.9 months with pembrolizumab (Zhu et al., 2018). Both agents showed durable responses and tolerable drug-related adverse effects. However, subsequent phase III studies of these agents did not show a significant improvement in patients' overall survival. CheckMate 459 reported that nivolumab only extended the median OS by 1.7 months relative to sorafenib, and KEYNOTE-240 showed that pembrolizumab extended the median overall survival by 3.3 months relative to placebo, but yet the results was not statistically significance (Yau et al., 2019; Finn et al., 2020). However, both agents remained approved because of durable responses in the patients. The combination of nivolumab plus ipilimumab (anti-CTLA-4 mAb) was assessed in patients who showed progression upon sorafenib treatment in the expansion arm of the CheckMate 040 trial (Thomas et al.,2020). The ORR was 31% with a median duration of response of 17 months and a median OS of 23 months (Thomas et al.,2020). Immune-related adverse effects were reported, and systemic corticoid was administered in half of the cases (Thomas et al.,2020). However, owing to its high treatment efficacy, the FDA approved this combination as a second-line treatment, and it is currently being assessed in a phase III trial (NCT04039607).

Agent	Target	Clinical stage	Study name (design)	Setting (number of patients)	Geographical area	Outcome	Safety profile
Sorafenib	VEGFR1–3, PDGFR, RAF, KIT	FDA-approved (2007)	SHARP (sorafenib vs placebo)	1L (602)	Global (121 centres in 21 countries)	OS: 10.7 vs 7.9 months (HR 0.69, *P*<0.001) TTP: 5.5 vs 2.8 months (HR 0.58, *P*<0.001) ORR: NA (PR 2 vs 1) Based on RECIST v1.0	Any grade TRAE: 80% vs 52% Grade 3 or 4 TRAE: NA
			Asia–Pacific Study (sorafenib vs placebo)	1L (271)	Asia (23 centres in the Asia–Pacific region)	OS: 6.5 vs 4.2 months (HR 0.68, *P*=0.014) TTP: 2.8 vs 1.4 months (HR 0.57, *P*=0.0005) ORR: 3.3% vs 1.3% Based on RECIST v1.0	Any grade HFSR: 45% vs 2.7% Grade 3 or 4 HFSR: 10.7% vs 0%
Regorafenib	VEGFR1–3, PDGFR, RAF, FGFR1–2	FDA-approved (2017)	RESORCE (regorafenib vs placebo)	2L (567)	Global (152 centres in 21 countries)	OS: 10.6 vs 7.8 months (HR 0.63, *P*<0.0001) PFS: 3.4 vs 1.5 months (HR 0.43, *P*<0.0001) ORR: 6.6% vs 2.6%	Any grade TRAE: 92.5% vs 51.8% Grade 3 or 4 TRAE: 50.0% vs 16.6%
Lenvatinib	VEGFR1–3, PDGFR, FGFR1–4, RET	FDA-approved (2018)	REFLECT (lenvatinib vs sorafenib)	1L (954)	Global (154 centres in 20 countries)	OS: 13.6 vs 12.3 months (HR 0.92, non-inferiority) PFS: 7.3 vs 3.6 months (HR 0.65, *P*<0.0001) ORR: 18.8% vs 6.5%	Any grade TRAE: 94% vs 95% Grade ≥3 TRAE: 57% vs 49%
Pembrolizumab	PD1	FDA-approved (2018)	KEYNOTE-394 (pembrolizumab vs placebo)	2L (453)	Asia	OS: 14.6 vs 13.0 months (HR 0.79, *P*=0.0180) PFS: 2.6 vs 2.3 months (HR 0.74, *P*=0.0032) ORR: 13.7% vs 1.3%	Any grade TRAE: 66.9% vs 49.7% Grade ≥3 TRAE: 14.4% vs 5.9%
Cabozantinib	VEGFR1–3, MET, RET	FDA-approved (2019)	CELESTIAL (cabozantinib vs placebo)	2L (707)	Global (95 centres in 19 countries)	OS: 10.2 vs 8.0 months (HR 0.76, *P*=0.005) PFS: 5.2 vs 1.9 months (HR 0.44, *P*<0.001) ORR: 3.8% vs 0.4%	Any grade all-cause AEs: 98.5% vs 92.4% Grade 3 or 4 all-cause AEs: 67.7% vs 36.3%
Ramucirumab	VEGFR2	FDA-approved (2019)	REACH-2 (ramucirumab vs placebo)	2L (292)	Global (92 centres in 20 countries)	OS: 8.5 vs 7.3 months (HR 0.71, *P*=0.0199) PFS: 2.8 vs 1.6 months (HR: 0.45, *P*<0.0001) ORR: 4.6% vs 1.1%	Any grade TRAE: 10.7% vs 5.3% Discontinuation: 19.8% vs 16.8%
Atezolizumab + bevacizumab	PDL1 + VEGFA	FDA-approved (2020)	IMbrave150 (combination vs sorafenib)	1L (501)	Global (111 centres in 17 countries and regions)	OS: 19.2 vs 13.4 months (HR 0.66, *P*<0.001) PFS: 6.9 vs 4.3 months (HR 0.65, *P*<0.001) ORR: 29.8% vs 11.3%	Any grade TRAE: 86.3% vs 94.9% Grade 3 or 4 TRAE: 43.5% vs 46.2%
Durvalumab + tremelimumab	PDL1 + CTLA4	FDA-approved (2022)	HIMALAYA (combination vs sorafenib)	1L (782)	Global (181 centres in 16 countries)	OS: 16.4 vs 13.8 months (HR 0.78, *P*=0.0035) PFS: 3.8 vs 4.1 months ORR: 20.1% vs 5.1%	Grade 3 or 4 TRAE: 25.8% vs 36.9% Discontinuation: 8.2% vs 11.0%

Table 1 Approved therapies for advanced HCC (This table is adopted from Yang et al., 2023)

1.2.1.3 Limitations of current therapeutic strategies

Multi-kinase inhibitors have demonstrated efficacy in patients with advanced HCC and have been the standard of care in the last decade, yet their therapeutic effects are still far from satisfactory. Sorafenib can only extend patient survival for less than 3 months, and lenvatinib showed comparable overall survival benefits as sorafenib, and the treatment benefits and response rate of second-line multikinase inhibitors are also modest (Yang et al., 2023). On the other hand, although ICIs demonstrated remarkable survival benefits, high ORR, and durable

response for treating patients with advanced HCC, ICI treatments are not amenable for patients with certain complications, including patients with autoimmune disease and prior history of organ transplantation (Yang et al., 2023; Johnson et al., 2017). Thus, new therapeutic regimens are required to offer more therapeutic options for HCC patients and achieve better clinical responses.

1.2.2 Treatment approaches under clinical investigations

1.2.2.1 Molecular-targeted monotherapies

To date, molecular-targeted treatments are the mainstay of treatment for unresectable HCC. These treatments target tumor-promoting signaling pathways, and novel approaches can be broadly classified into new multi-kinase inhibitors sharing mechanisms similar to previous ones and small-molecule drugs that inhibit more specific targets. For instance, donafenib is a new multi-kinase inhibitor modified from sorafenib. It has been shown to have an improved pharmacokinetic profile and was found to improve patient overall survival relative to sorafenib in a phase III trial (HR 0.83, $P = 0.0245$) (Qin et al., 2021). Several small-molecule agents targeting MET and FGFR4 were found to be effective in phase I/II clinical trials. Tepotinib and capmatinib are two selective MET inhibitors with promising clinical efficacies and are well tolerated in patients with MET-high HCC in early phase clinical studies (Ryoo et al., 2021; Faivre et al., 2021; Qin et al., 2019). FGFR4 represents another target for HCC treatment, and its selective inhibitor fisogatinib was deemed effective in a phase I study, showing a 17% ORR in the FGF19+ group, indicating its therapeutic potential in biomarker-based therapy (Kim et al., 2019). However, the clinical utility of these agents has yet to be studied in late-stage clinical trials.

1.2.2.2 Combinational regimens with immune checkpoint inhibitors

In HCC, immune checkpoint inhibitors (ICIs) have demonstrated promising clinical efficacy when paired with complementary ICIs and anti-angiogenic agents (i.e., VEGF mAb). As aforementioned, several ICI-based combination regimens have recently been approved as first- or second-line therapies for advanced HCC. And their marked efficacies have promoted ongoing preclinical and clinical investigations of additional combinatorial approaches with ICIs. The combination of ICIs with multikinase inhibitors has been intensively investigated in

HCC to date, as several multikinase inhibitors have been approved for HCC treatment, and these inhibitors exert both anti-angiogenic effects by targeting VEGFR and additional immunomodulatory effects (Figure 1.1).

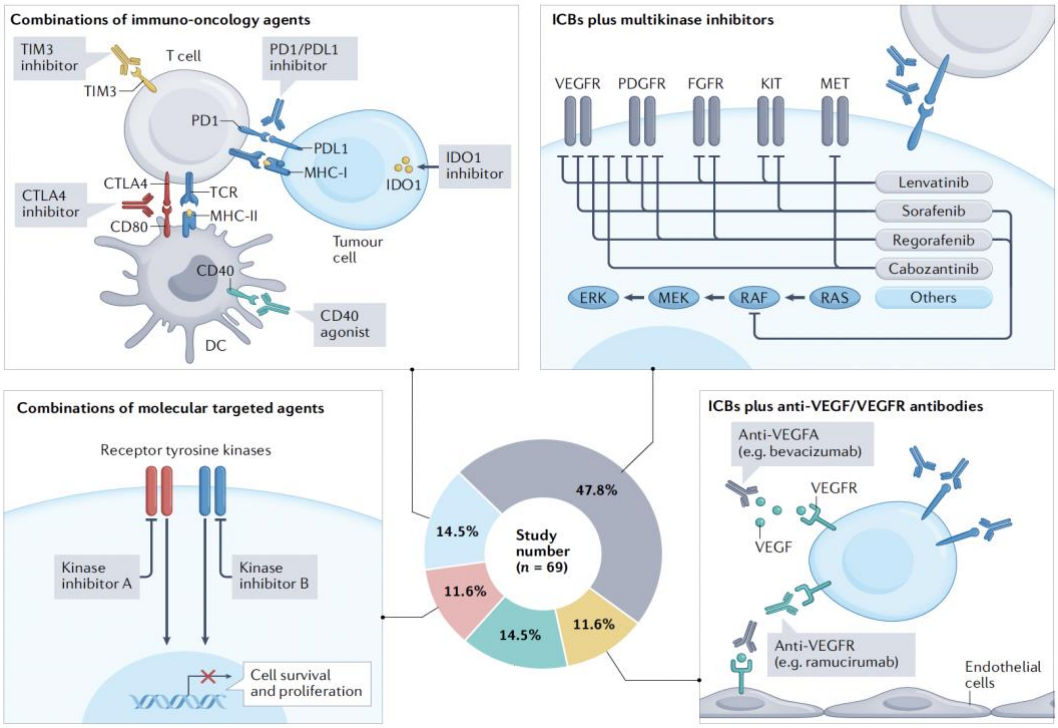

Figure 1.1 Combination approaches in HCC (This figure is adopted from Yang et al., 2023)

The VEGF pathway suppresses antitumor immunity by suppressing antigen-presenting cells (APCs) and effector cells, while stimulating immunosuppressive T regulatory (Treg) cells, myeloid-derived suppressor cells (MDSC), and tumor-associated macrophages (TAMs) (Rahma & Hodi, 2019). Thus, targeting the VEGF pathway could turn an immune cold tumor into a hot tumor, allowing additional effects of ICIs (Rahma & Hodi, 2019). Moreover, preclinical trials in cell and mouse models have reported immunostimulatory effects of multikinase inhibitors in HCC tumors. For example, sorafenib has been shown to promote M1 polarization through MAPK signaling; enhance CD8+ cell infiltration and activity through STAT3 suppression; and inhibit proliferation, activities, and migration of Tregs and MDSCs (Edwards et al., 2010; Chuang et al., 2014; Chen et al., 2014; Cao et al., 2019). Lenvatinib was found to promote cytotoxic (Tc) cell proliferation through the release of interferon-γ and granzyme B (Kato et al., 2019). The tumor-killing and tumor-necrosis activities of multikinase

inhibitors might induce tumor antigen release, thereby enhancing the immunogenicity of the tumor (Kudo 2021; Lin et al., 2018; Zhu et al., 2021).

Two phase III clinical trials, LEAP-002 and COSMIC-312, have evaluated the efficacy of combining multikinase inhibitors with ICIs as first-line modalities in treating advanced HCC (Llovet et al., 2023). In the LEAP-002 trial, lenvatinib plus pembrolizumab was compared to lenvatinib alone. Although the combination showed a higher objective response rate (26.1% vs. 17.5%) and a prolonged response (median duration of response 16.6 vs. 10.4 months), it did not achieve statistically significant improvements in the pre-specified endpoints of patient survival (OS 21.2 vs. 19.0 months; PFS 8.2 vs. 8.0 months) compared to the monotherapy (Llovet et al., 2023). In the COSMIC-312 trial, cabozantinib plus atezolizumab significantly improved progression-free survival over sorafenib (6.8 vs. 4.2 months) but failed to archive primary objective to improve patients' overall survival (15.4 vs. 15.5 months) (Llovet et al., 2023). Furthermore, the objective response rate for this combination was only 11%, which is lower than anticipated for such a regimen (Llovet et al., 2023).

Treatment toxicity is another major concern when combining ICIs with multikinase inhibitors. According to a large-scale meta-analysis on the safety profiles of combination therapies across cancer types, the combination of ICIs with multikinase inhibitors resulted in a high incidence (58.8%) of grade 3 or 4 treatment-related adverse effects (TRAEs), while the combination of ICIs only resulted in 35.9% of grade 3 or 4 TRAEs (Zhou et al., 2021). Consistently, in clinical trials of HCC, atezolizumab plus cabozantinib and pembrolizumab plus lenvatinib (combinations of ICIs with multikinase) resulted in 53.9% and 64.0%, respectively, of grade 3 or 4 TRAEs in HCC patients, in contrast to 25.8% of incidence in durvalumab–tremelimumab combination (combinations of ICIs) (Kelley et al., 2022; Abou-Alfa et al., 2022; Finn et al., 2020). Currently, there are many ongoing trials on dual ICIs inhibition, as well as combining ICIs with multikinase inhibitors, anti-VEGF/VEGFR antibodies, or targeted therapies for advanced HCC, and the follow-up of survival endpoint is still underway.

1.3 Macrophage-based cancer therapeutics

1.3.1 Pursuing alternative treatment modalities in HCC

Despite significant progress in cancer immunotherapy that adaptive ICIs have provided durable survival benefits for a subset of individuals with terminal cancers, including advanced

hepatocellular carcinoma, a substantial number of patients remain unresponsive to conventional adaptive ICIs. Another common clinical challenge is the development of treatment resistance, leading to disease progression upon follow-up (Feng et al., 2019). The efficacy of adaptive ICIs, such as PD-L1 and CTLA-4 inhibitors, is mechanistically dependent on the presentation of tumor neoantigens to activate specific T-cell clones. Consequently, tumors characterized by a low mutational burden, and thus limited neoantigen presentation, are often refractory to these therapies (Huntington, Cursons, and Rautela, 2020; Yarchoan, Hopkins, and Jaffee, 2017). In contrast, the innate immune system possesses the capacity for rapid tumor cell recognition via diverse surface molecules and the initiation of broad inflammatory responses, rendering it an alternative target for HCC treatment. Recent evidence has highlighted the critical role of innate immune checkpoints in facilitating tumor immune evasion by suppressing innate immune sensing and phagocytic functions, while targeting these checkpoints has emerged as a viable therapeutic strategy in oncology.

Macrophages, as key innate immune cells, infiltrate tumors and can destroy cancer through phagocytosis, sequential mechanism of identification, engulfment, and degradation (Anderson et al., 2020). However, tumors frequently escape this immune response by exploiting inhibitory signals, often by displaying high levels of checkpoint proteins on their cell surfaces (Barkal et al., 2019). Critical regulators of this evasion include phagocytosis checkpoints including cluster of differentiation 47 (CD47), major histocompatibility class I (MHC-I), cluster of differentiation 24 (CD24), PD-L1, disialoganglioside GD2, and Stanniocalcin-1 (STC-1), have emerged as critical checkpoints for cancer immunotherapy (Liu et al., 2023).

1.3.2 Role of macrophage within TME

1.3.2.1 Phenotypic heterogeneity of macrophages

Macrophages are highly plastic and possess different phenotypic states depending on environmental cues. Historically, macrophages have been classified into two functional states: M1 (or classic) macrophages exhibit pro-inflammatory function, while M2 (or alternative) macrophages poss anti-inflammatory abilities (Zheng et al., 2023). M1 polarization is induced by interferons released during type I immune responses mediated by Th1 cells and innate lymphoid cells and is implicated in initiating and sustaining inflammation. M2 polarization is driven by interferons released during type II immune responses and innate lymphoid cells and promotes tissue repair and remodelling. In the context of cancer, M1 is reported to generate

macrophage-dependent tissue damage and malignant cell killing. And M2 macrophages are shown to be pro-tumoral and suppresses effective adaptive immunity (Mantovani et al., 2022).

1.3.2.2 Immunosuppressive role of macrophages within TME

In general, mixed populations of tumor-associated macrophages (TAMs) with different functional states co-exist in the TME, as signals governing this plasticity vary drastically in different regions and stages of the same tumor. Tumor cell-released cytokines, including IL-10 and CSF-1, and chemokines, like CCL2, CCL18, CXCL4, and CCL17, induce M1 polarization of TAM; whereas cytokines such as IL-4 and IL-13, and neurotransmitter γ-aminobutyric acid (GABA) foster M2 transition (Mantovani et al., 2022). In most solid cancers, TAMs possess M2 phenotype, with elevated expression of arginase-1 and mannose receptor as well as low MHCII expression, and they contribute to cancer progression and metastasis (Duan & Luo, 2021). They extensively remodel the TME by secreting growth factors like EGF and VEGF, which directly stimulate malignant cell proliferation and drive angiogenesis which foster tumor progression and dissemination. Moreover, TAMs release various immunosuppressive molecules, such as IL-10, TGFβ, and PGE2, and elevate checkpoint ligands like PD-L1, which collectively suppress the induction and tumoricidal activity of T cells and NK cells, and establish an immune-permissive niche. By releasing matrix metalloproteinases (MMPs), such as MMP-2, MMP-9, and MMP-14, and other proteases like cathepsins, TAMs degrade the extracellular matrix (ECM) to foster local invasion and intravasation of cancer cells into circulation. TAMs also remodel the ECM structure by expressing the ECM proteins (fibronectin and collagens) as well as recruiting and activating cancer-associated fibroblasts that collectively contribute to fibrosis, and increased collagen deposition and cross-linking within the tumor, making the matrix stiffer, which favors cancer progression (Zheng et al., 2023).

In HCC, a highly immunosuppressive cancer, TAMs are the major immune cell population, representing 20-40% of the total infiltrating cells (Zheng et al., 2023). These TAMs are pivotal in promoting oncogenesis by facilitating processes like angiogenesis, metastasis, and the suppression of anti-tumor immunity (Zheng et al., 2023). The majority of TAMs in HCC display an M2-polarized state with a characteristic spindle-shaped appearance (Zheng et al., 2023). This phenotype contributes to tumor advancement and immune evasion through the

upregulation of factors such as MMP14, VEGFA, and the MRC1/CD206 receptor (Zheng et al., 2023).

1.3.3 Targeting macrophages in cancer treatments

1.3.3.1 Depletion of TAMs or preventing the recruitment of TAMs

Given that TAMs are generally regarded as pro-tumorigenic and immunosuppressive, studies have engrossed on eliminating TAMs from tumor or inhibiting their infiltration in the past decades. The dependency of macrophages on CSF1R signaling positions it as an attractive target for macrophage depletion. Various small molecules inhibitors and anti-CSF1R monoclonal antibodies have thus been generated and tested for the preclinical and clinical efficacies in treating solid tumors or haematological malignancies (Mantovani et al., 2022; Figure 1.2).

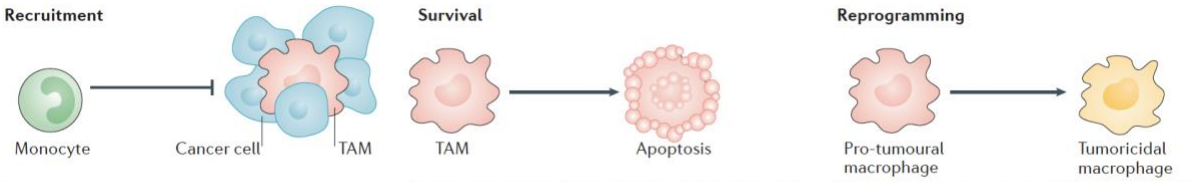

Drug name	Target	Inhibitor type
Carlumab	CCL2	mAb
PF04136309	CCR2	Small molecule
PLX3397	CSF1R	Small molecule
PLX7486	CSF1R	Small molecule
JNJ-40346527	CSF1R	Small molecule
ARRY-382	CSF1R	Small molecule
BLZ945	CSF1R	Small molecule
IMC-CS4	CSF1R	mAb
R05509554	CSF1R	mAb
RG7155	CSF1R	mAb
FPA008	CSF1R	mAb

Drug name	Target	Inhibitor type
Clodronate	NA	Small molecule
Zoledronic acid	NA	Small molecule
Trabectedin	Caspase 8	Small molecule
PLX7486	CSF1R	Small molecule
JNJ-40346527	CSF1R	Small molecule
ARRY-382	CSF1R	Small molecule
BLZ945	CSF1R	Small molecule
IMC-CS4	CSF1R	mAb
R05509554	CSF1R	mAb
RG7155	CSF1R	mAb
FPA008	CSF1R	mAb

Drug name	Target	Inhibitor type
Hu5F9-G4	CD47	mAb
CC-90002	CD47	mAb
TTI-621	SIRPα	Fusion protein
CP-870,893	CD40	Agonistic antibody
RO7009789	CD40	Agonistic antibody
Imiquimod	TLR7	Small molecule
852A	TLR7	Small molecule
IMO-2055	TLR9	Small molecule
BLZ945	CSF1R	Small molecule

Figure 1.2 Examples of anti-TAM therapies under clinical development (This figure is adopted from Cassetta & Pollard, 2018)

Small molecules targeting CSF1R under clinical development include PLX3397 (pexidartinib), PLX7486, BLZ945 and JNJ-40346527. PLX3397, either as a single agent or in combination with tyrosine kinase inhibitors dovitinib and vatalanib, was shown to be effective in controlling

tumor progression in preclinical models of glioma (Mantovani et al., 2022). In a phase II clinical trial, PLX3397 did not improve prognosis in patients with recurrent glioblastoma in which the progression-free survival of PLX3397 treatment group did not differ from the patients receiving radiotherapy and temozolomide (Mantovani et al., 2022). On the other hand, in late clinical studies of advanced tenosynovial giant cell tumors (TGCT), a cancer type with heightened expression of CSF1 and CSF1R, PLX3397 treatment was shown to have robust tumor response with sustained clinical benefits in phase III ENLIVEN study (NCT02371369), and was granted approval by the FDA in 2019 as the first systemic treatment for patients with TGCT (Tap et al., 2019). Despite the clinical success of PLX3397 in TGCT, its clinical utility in other solid tumors is limited, with no clinical benefits observed when used in combination with pembrolizumab in advanced melanoma and solid tumors (NCT02452424) or with radiotherapy and temozolomide in glioblastoma (NCT01790503). Other small-molecule CSF1R inhibitors (BLZ945 and JNJ-40346527), have progressed to Phase I/II evaluation for treating advanced-stage solid tumors either as single agents or combination treatments but further clinical development was halted owing to limited clinical benefits or safety concerns (NCT02829723) (Mantovani et al., 2022).

In addition, several mAbs targeting CSF1R (RG7155, IMC-CS4, FPA008, AMG 820, and ARRY-382) that have been evaluated clinically. RG7155 (emactuzumab), a humanized mAb that blocks CSF1R dimerization, was found to deplete CSF1R+CD163+ macrophages in preclinical models (Mantovani et al., 2022). For instance, RG7155 was shown to diminish TAMs infiltration while increasing the CD8+/CD4+ T cell ratio in colorectal cancer and fibrosarcoma (Mantovani et al., 2022). A Phase Ia/b study combining RG7155 (monotherapy or with paclitaxel) in patients with diffuse-type tenosynovial giant cell tumor (TGCT), RG7155 demonstrated promising results, with an ORR of 71%. Prompted by this promising clinical benefit, a late-stage clinical study (TANGENT) is currently being conducted for assessing the clinical utility of RG7155 in patients with TGCT who are not amenable to surgery (Gelderblom et al., 2025). In a phase 1b study of advanced solid cancers, RG7155 also showed signs of clinical activity, including partial metabolic responses and disease stabilization, when used in combination with atezolizumab (Gomez-Roca et al., 2022b). In other phase Ib/II trials, RG7155 did not show clinical response when used in combination with chemotherapy (paclitaxel) and anti-VEGF agent (Bevacizumab) in gynaecological neoplasms and ovarian cancer (NCT02923739) or in combination with anti-CD40 mAb (selicrelumab) in advanced solid tumors (NCT02760797). The other mAbs, IMC-CS4, FPA008, AMG 820, and ARRY-382,

did not progress beyond Phase I/II clinical development because of modest clinical responses in treating solid tumors (Wang-Gillam et al., 2019; Razak et al., 2020; Johnson et al., 2022).

Apart from the CSF1-CSF1R axis, CCL2-CCR2 signaling is another crucial pathway that induces monocytes recruitment and contributes to TAMs accumulation in the TME (Cassetta & Pollard, 2018). CCL2 released by tumor cells is a potent chemoattractant for monocytes that express CCR2 at the tumor site. The use of anti-CCL2 in cancer treatment is controversial. On one hand, some studies have reported that CCL2 targeting eased the tumor burden and metastatic progression in several malignancies including breast liver, lung and prostate cancers as well as melanoma (Cassetta & Pollard, 2018). Meanwhile, other groups have raised concerns regarding the long-term use of anti-CCL2 treatment. In breast cancer, treatment withdrawal resulted in a rebound of monocytes infiltration and lung metastasis, which led to death of the mice (Cassetta & Pollard, 2018). A similar observation was reported by another group that employed genetic depletion of CCR2 in the PyMT model, and they showed that the CCR2 loss in monocytes causes re-emergence of monocyte recruitment by an unknown redundancy mechanism (Cassetta & Pollard, 2018). Two plausible explanations are proposed for this observation. First, CCL2 depletion led to severe depletion of macrophages, and a compensatory mechanism was triggered to overcome the CCL2 deficiency, which drastically increased CCL2 levels and counteracted the therapeutic effect of the anti-CCL2 agent. Furthermore, there may be adaptive increase in the proliferation of tissue-resident macrophages when monocyte infiltration is inhibited (Cassetta & Pollard, 2018).

Nonetheless, owing to the elevated levels of CCL2 in patient serum and tumor and its association with poor survival, the use of anti-CCL2 mAb (Carlumab) or small inhibitor targeting CCR2 (PF-04136309) was evaluated clinically. Carlumab (CNTO888), a human immunoglobulin G1κ antibody that binds to CCL2, has been shown to reduce macrophage recruitment and vascular density, with diminished tumor burden in prostate cancer mouse models upon systemic administration (Cassetta & Pollard, 2018). In contrast to this preclinical finding, a phase II clinical trial showed that carlumab did not induce significant or long-term antitumor responses in patients with castration-resistant metastatic prostate cancer (Cassetta & Pollard, 2018). The therapeutic efficacy of PF-04136309 was assessed in pancreatic ductal adenocarcinoma (PDAC) in two clinical trials. A phase 1b clinical trial using the combination of PF-04136309 with FOLFIRINOX chemotherapy (oxaliplatin and irinotecan plus leucovorin and fluorouracil) demonstrated that the combination is safe, tolerable and effective for PDAC patients, with 32 of 33 patients showed local tumor control and 16 patients had objective tumor

response (Cassetta & Pollard, 2018). Despite this exciting finding, a recent Phase Ib study evaluating the combination of PF-04136309 and nab-paclitaxel/gemcitabine as first-line treatment for patients with metastatic PDAC reported significant safety concerns regarding synergistic pulmonary toxicity, with no efficacies observed in the combination group (Noel et al., 2019).

To date, a few clinical studies have tested the combination of anti-CSF1R antibodies, cabiralizumab and emactuzumab, with other agents in triple-negative breast cancer and PDAC (NCT04331067 and NCT03193190), as well as anti-CCR2/5 antagonist with nivolumab in HCC (NCT04123379) are still ongoing. Currently available phase II trials targeting TAM recruitment or accumulation have shown no durable clinical responses in most solid cancer types, except for TGCT and potentially in PDAC, and some treatment modalities were reported to have safety concerns. It is also noteworthy that CSF1R blockade, either with small inhibitors or mAbs, frequently causes periorbital oedema in patients. The mechanism involves dermal macrophage loss, which leads to pathological extracellular remodelling, matrix metalloproteinase activation and hyaluronan deposition, ultimately increasing fluid retention (Zheng et al., 2023). Beyond on-target toxicities, the effectiveness of TAM recruitment strategies is also impeded by the compensatory influx of immunosuppressive neutrophils, enhanced proliferation of tissue-resident macrophages, and inherit redundant chemokine system with multiple ligands and receptors acting on monocytes (Mantovani et al., 2022).

1.3.3.2 Functional reprogramming of TAMs – Macrophage activation

Despite being generally pro-tumoral, TAMs possess phenotypic plasticity that can, depending on the environmental cues, become tumoricidal and immunostimulatory, thus inhibiting tumor growth (Cassetta & Pollard, 2018). This macrophage plasticity property has been therapeutically exploited for cancer treatment (Cassetta & Pollard, 2018). This strategy involves in reprogramming of TAMs from pro-tumorigenic to tumoricidal state, that is switching them from their role in supporting angiogenesis, matrix remodelling, and immunosuppression to the one that promotes immune activation and direct tumor killing (Mantovani et al., 2022). The phenotypic conversion can be achieved by targeting key regulatory signals or receptors that govern the macrophage polarization. For instance, agonists of toll-like receptors (TLRs) or CD40 can skew TAMs towards the M1 subtype, which

possesses higher innate phagocytic, inflammatory and antigen presentation abilities for tumor killing, and can reverse the immunosuppressive TME (Figure 1.3; Mantovani et al., 2022).

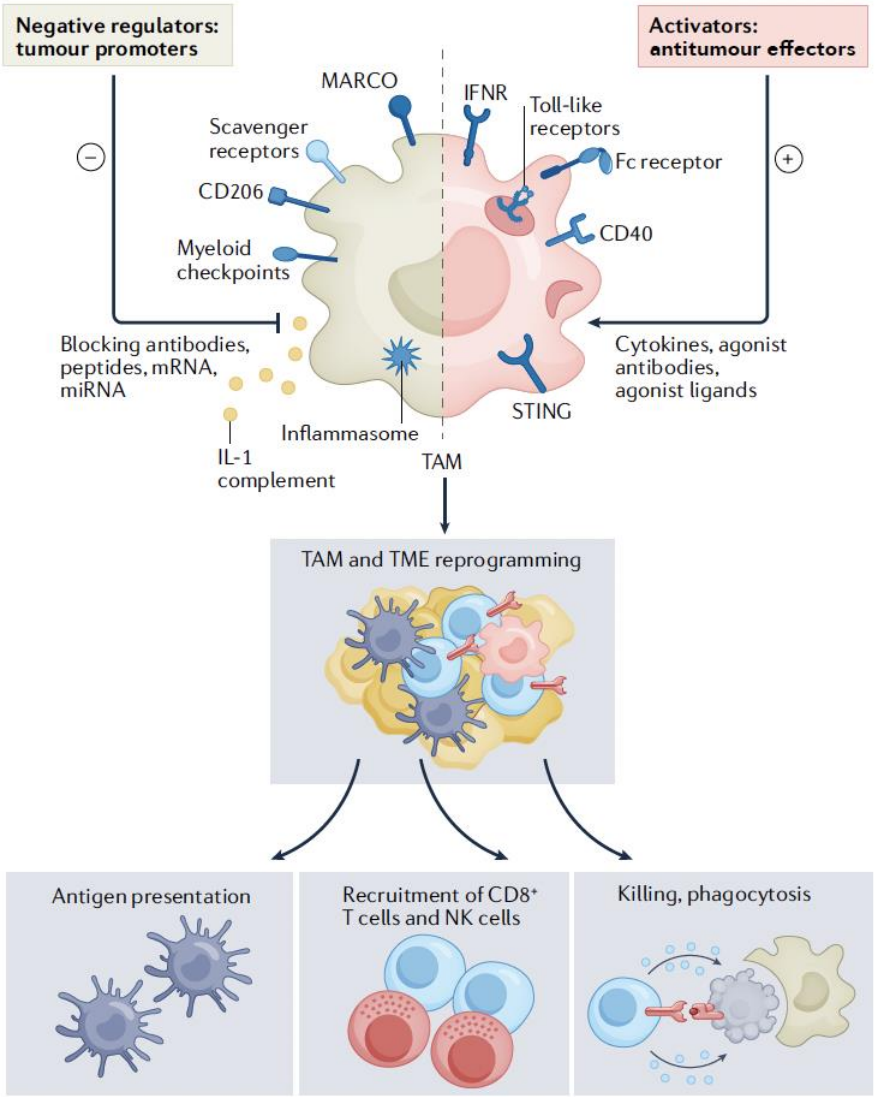

Figure 1.3 TAM reprogramming strategies. Cytokines (like interferons), TLRs, STING agonist and mAb that stimulate macrophage-mediated tumoricidal effect (red shading). Completement, inflammasomes activators, ligands for MARCO and CD206, as well as myeloid checkpoints shift macrophages to pro-tumorigenic phenotype (brown shading). IFNR, interferon receptor; NK, natural killer; TMAP, tumor-associated macrophages. (This figure is adopted from Mantovani et al., 2022)

The CD40 receptor belongs to the tumor necrosis factor (TNF) receptor family that expressed on antigen-presenting cells like macrophages and dendritic cells. It interacts with CD40 ligand (CD40L) on the activated Th cell surface and induces the generation of TNF and reactive oxygen and nitrogen species, which triggers the tumoricidal activity of macrophages. This

ligand-receptor interaction also activates T cell-mediated immune responses. Activating the CD40-CD40L axis with CD40 agonist mAbs repolarizes immunosuppressive TAMs to a tumoricidal state with heightened cytotoxic function, leading to immune surveillance and reduced tumor burden (Mantovani et al., 2022). The use of CD40 agonist mAbs has also been reported to cause TAMs to release CCL5, which triggers the recruitment of CD4+T cells to the tumor site (Mantovani et al., 2022). Recently, the safety profiles and clinical utilities of CD40 agonist mAbs (CP-870,893, SEA- CD40, APX005M, RO7009789, CDX-1140, and mitazalimab) in combination with other treatment regimens have been investigated intensively, and the currently available Phase I and II study results suggested that the combinations are safe and tolerable, and some studies reported encouraging antitumor activities and clinical responses to the treatments. Sotigalimab (APX005M) was assessed in phase I and II clinical trials for advanced melanoma patients as a single agent and in combination with nivolumab, respectively. Sotigalimab showed single-agent activity with a favorable safety profile in patients with advanced melanoma, and the subsequent phase II expansion study illustrated that a subset of patients harboring PD-1-resistant melanoma showed durable and prolonged responses to the sotigalimab plus nivolumab treatment regimen (Weiss et al., 2023). Another phase II study on upper gastroesophageal cancer also demonstrated that the use of sotigalimab with chemoradiotherapy as neoadjuvant treatment was effective and safe, with an improvement in the patient's complete response rate (Ko et al., 2025). The phase 1b/II PRINCE trial reported that sotigalimab administration with chemotherapy has immunostimulatory effects, inducing infiltration of CD4+ T cell and circulating differentiated CD4+ T cells and antigen-presenting cells (Padrón et al., 2022). Another CD40 agonistic mAb, mitazalimab, also showed a favorable clinical response when used in conjunction with chemotherapy. OPTIMIZE-1, a phase Ib/II clinical study completed in 2024, combined mitazalimab with modified FOLFIRINOX (mFOLFIRINOX; fluorouracil, leucovorin, oxaliplatin, and irinotecan) for treating patients with metastatic PDAC, and showed that the combination improves overall survival with an objective response rate of 42.1% and manageable treatment-related toxicities (Van Laethem et al., 2024). These encouraging results warrant further investigation in phase III clinical trials. Apart from sotigalimab and mitazalimab, several CD40 agonistic mAbs are currently being assessed for their clinical efficacy and safety in various types of malignancies (NCT05165433, NCT04616248, NCT04495257, NCT05029999, NCT03424005, NCT02588443).

Toll-like receptors (TLRs) are innate immunity pattern recognition receptors that trigger an innate immune response upon detecting pathogen-associated molecular patterns (PAMPs), such as bacterial lipopolysaccharides and lipoproteins, and viral nucleic acids. This activation polarizes macrophages towards a pro-inflammatory and antitumor phenotype (Cassetta & Pollard, 2018). Consequently, TLRs have been extensively investigated as immunomodulatory targets to re-educate TAMs within the TME. Multiple agonistic TLR molecules have been developed to achieve this, successfully reprogramming TAMs to become tumoricidal with increased release of immunostimulatory cytokines in various preclinical models (Mantovani et al., 2022). Early clinical successes of TLR agonists include the FDA-approved TLR2/4 agonist Bacillus Calmette-Guérin (BCG) for bladder cancer and the topical TLR7 agonist imiquimod for skin cancer. BCG, a live attenuated form of Mycobacterium bovis (i.e., tuberculosis bacteria) that activates TLR2 and TLR4, was approved by the FDA in 1990 for the treatment of early-stage bladder cancer and remains a standard treatment to date (Mantovani et al., 2022). Imiquimod was approved in 2004 for the topical treatment of superficial basal cell carcinoma. A derivative of imiquimod, motolimod (a TLR8 agonist), demonstrated potent immunostimulatory activity in preclinical models of multiple cancer types, and TAMs appear to be the major immune population that primes the antitumor immune response (Mantovani et al., 2022). The clinical efficacy of this drug was evaluated in a phase III Active8 study when combined with standard therapy (cetuximab and chemotherapy) for treating recurrent and/or metastatic head and neck cancer. The combination did not improve survival in the overall patient population but showed significant benefit in the HPV-positive subgroup, suggesting its plausible use in subset-selected patients (Ferris et al., 2018). The TLR3 agonist Poly(I:C) has shown significant antitumor activity in experimental settings (De Waele et al., 2021). To enhance its stability and delivery, a nanocomplex formulation with polyethyleneimine, known as BO-112, has been developed and evaluated in the phase II Clinical Trial SPOTLIGHT-203 for the use of intratumoral BO-112 plus intravenous pembrolizumab in patients with anti-PD1-resistant melanoma. The combination was shown to be well tolerated with promising improvement in patient survival and a 25% objective response rate, and the combination warrants future studies to validate the clinical benefits (Márquez-Rodas et al., 2025). It is noteworthy that early trials of TLR stimulation by systemic administration of TLR agonists often trigger severe inflammatory reactions, such as cytokine-related syndrome, high fever, chills, and hypotension. This toxicity profile likely accounts for the high rate of grade 3 or 4 adverse events observed in the combination arm (tilsotolimod, a TLR9 agonist, plus ipilimumab) of the ILLUMINATE-301

trial. Consequently, local or intratumoral administration is now considered the dominant strategy to maximize potent local immune activation within the tumor microenvironment while effectively minimizing systemic toxicity.

1.3.3.3 Functional reprogramming of TAMs – Targeting phagocytic checkpoints

Normal cells express ‘don’t eat me’ signals on their cell surface as a self-protective mechanism to prevent unwanted phagocytosis. Tumor cells hijack this mechanism by overexpressing these checkpoint molecules, effectively disguising themselves as 'self, and thus evading macrophage surveillance (Figure 1.4). Researchers have developed therapeutic agents that target these phagocytic checkpoints to reverse phagocytic inhibition. These strategies have been shown to enhance macrophage-mediated tumor control in several preclinical models. Over the past decade, the CD47/SIRPα, CD24/SIGLEC-10, and PD-L1/PD-1 signaling axes have emerged as the most extensively studied therapeutic targets. Their signaling mechanisms, key preclinical findings, and progress in clinical development are discussed in this section.

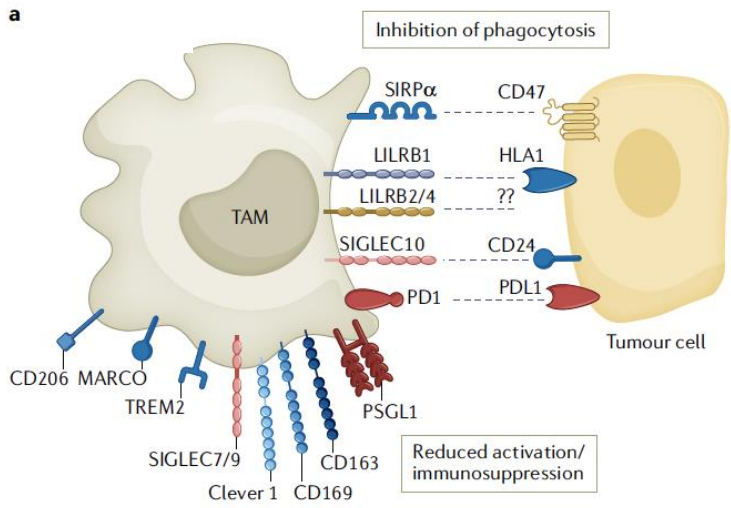

Figure 1.4 Myeloid checkpoints on macrophages and corresponding interacting partners on tumor cells (This figure is adopted from Mantovani et al., 2022)

CD47/SIRPα axis

CD47 is a ubiquitously expressed protein in normal cells that controls physiological processes such as cell migration, cytokine production, and T cell activation (Cassetta & Pollard, 2018).

CD47 interacts with signal regulatory protein-α (SIRPα), which is mainly expressed on macrophages, monocytes, and DCs (Cassetta & Pollard, 2018). This prevents myosin IIA accumulation at the phagocytic synapse, thereby inhibiting phagocytosis (Cassetta and Pollard, 2018). CD47 is overexpressed in various tumors, including ovarian cancer, HCC, cholangiocarcinoma (CCA), and haematological malignancies (Liu et al., 2023). This overexpression contributes to tumor invasion and metastasis and, more importantly, functions as a key antiphagocytic mechanism that enables tumors to resist innate immune surveillance (Cassetta & Pollard, 2018). Several preclinical studies have demonstrated that CD47/SIRPα inhibition with blocking antibodies enhances the phagocytosis of tumor cells by macrophages and reduces tumor burden in various tumor models, including lymphoma, melanoma, glioblastoma, breast and colorectal cancer, and liver cancers (Feng et al., 2019). In addition to its pro-phagocytic function, targeting this axis has been shown to activate macrophage cytokine release, which stimulates the immune system of patients (Liu et al., 2023). Prompted by these promising preclinical findings, therapies designed to disrupt CD47/SIRPα interactions have been investigated intensively in clinics for different malignancies in the past decade (Feng et al., 2019).

Magrolimab was the first CD47 targeting agent to enter clinical development and progressed to phase III ENHANCE-3 trial for treating acute myeloid leukemia (AML) in combination with venetoclax and azacitidine (Daver et al., 2025). Increased fatal adverse events and risk of death, primarily driven by grade 5 pneumonia and respiratory failure, were observed in the combination arm, and the clinical development of magrolimab was halted. This raises concerns regarding the overall toxicity profile of the drugs and the potential dysregulation or overactivation of the immune system upon administration of the combination regimen. Magrolimab's mechanism of action inherently leads to on-target toxicity against normal cells, given that CD47 is ubiquitously expressed in normal cells, particularly red blood cells (RBCs) and platelets. Systemic treatment with magrolimab results in unintended phagocytosis and clearance by macrophages, agglutination of RBCs, and cell lysis (Liu et al., 2023). This manifests clinically as anemia and thrombocytopenia, which are anticipated dose-limiting side effects observed in clinical trials (Mantovani et al., 2022). While this haematological toxicity was often manageable with a lower initial "priming" dose, it contributed to the drug's challenging safety profile, compounding the more severe immune-mediated toxicities that ultimately led to its clinical hold.

Considering this, novel strategies have been proposed to circumvent these on-target adverse effects. These approaches include engineered CD47 antibodies with minimal affinity to erythrocytes (e.g., ALX148, TJC4, TTI-622, and AO-176) and bispecific antibodies or fusion proteins that co-engage CD47 and a tumor-associated antigen to enhance tumor selectivity (for example TG-1801, IMM0306). ALX148, also known as evorpacept, is an engineered fusion protein with a high-affinity CD47-binding domain linked to an inactive human immunoglobulin Fc region. Its inactive Fc domain renders it incapable of triggering immune responses, such as ADCC and ADCP, thereby averting immune responses against normal CD47-expressing cells. Consequently, adverse effects on normal blood cells were not observed in preclinical models, highlighting an improved safety profile over earlier CD47-targeting agents. ALX148 has demonstrated antitumor activity in a phase I clinical trial of B-cell non-Hodgkin lymphoma in combination with lenalidomide and rituximab (Zhuang et al., 2025). Recently, the Phase II ASPEN-06 study demonstrated the promising activities of ALX148, including an increased objective response rate and longer duration of response when added to trastuzumab, ramucirumab, and paclitaxel for treating advanced HER2-positive gastric or gastroesophageal junction (GEJ) cancer (Shitara et al., 2025). In another phase Ib/II clinical trial for breast cancer, ALX148 also showed promising antitumor activity when used in combination with zanidatamab in HER2-positive patients, illustrating its effectiveness in HER-expressing tumors across different cancer types (Montero et al., 2025). Meanwhile, it is currently being investigated in combination with pembrolizumab in phase II trials for advanced solid tumors and lymphoma (NNCT04675294, NCT03013218). TJC4, or lemzoparlimab, is another modified CD47 mAb that is under early clinical development. Given that the molecular conformation of CD47 on tumor cells differs from that on blood cells, lemzoparlimab was designed to target a distinct and tumor-specific CD47 epitope, thereby sparing red blood cells and platelets (Liu et al., 2023). Lemzoparlimab has shown encouraging clinical activity as a single agent in AML and in combination with rituximab in lymphoma in two early clinical trials (Qi et al., 2020; Mehta et al., 2021). Nonetheless, its further clinical development has been halted owing to strategic focus and resource allocation.

IMM0306 is a novel tandem-targeting fusion protein that fuses the CD47 binding domain of SIRPα to the Fc region of a CD20-targeting antibody, rituximab, generating a bifunctional molecule that simultaneously blocks the “don't eat me” signal on tumor cells and directs this activity specifically to CD20-expressing cells (Yu et al., 2022). This reduces binding to red

blood cells and thus can avoid dose-limiting haematological toxicity, which is observed in first-generation CD47 inhibitors, indicating a potentially improved safety profile (Yu et al., 2022). IMM0306 is currently being evaluated in early clinical trials for patients with relapsed or refractory (R/R) CD20-positive B-cell lymphomas. It has been reported to have a favorable safety profile and preliminary efficacy in patients with B-cell lymphoma as a single agent or in combination with lenalidomide, and assessment is ongoing (Yang et al., 2024; Deng et al., 2024).

CD24/SIGLEC-10 axis

The CD24/Siglec10 axis is a physiological pathway that suppresses the inflammatory response and, thereby, pathological cell death (Liu et al., 2023). Mechanistically, this interaction reduces damage-associated molecular pattern (DAMP)- related inflammatory responses, such as sepsis and liver injury, as well as antigen sensing on the cell surface, thus dampening normal cell phagocytosis by macrophages (Liu et al., 2023). Malignant cells exploit this mechanism by overexpressing surface CD24, which engages Siglec10 on tumor-associated macrophages to transmit a potent 'don't eat me' signal via the phosphatases SHP-1 and SHP-2, thus inhibiting phagocytosis and evading macrophage surveillance (Liu et al., 2023). Meanwhile, this immunoinhibitory signaling cascade simultaneously weakens the killing activity of T and NK cells (Liu et al., 2023). CD24 overexpression has been reported in various cancers, including B cell lymphomas, breast cancer, gliomas, SCLC, and HCC, where it functions as a potent oncoprotein and a poor prognostic marker (Liu et al., 2023). Its high expression fosters immune evasion of tumors and directly fuels tumor progression by enhancing cell proliferation and metastasis. Preclinical studies have confirmed that disrupting this interaction by CD24 targeting increases macrophage-directed clearance of tumor cells and dramatically suppresses the growth of orthotopic tumors in mice, establishing CD24 as a viable new antitumor phagocytosis checkpoint (Liu et al., 2023). An alternative approach capitalizes on the sialic acid-dependent nature of these interactions. Studies have shown that antibody-sialidase conjugates can remove sialic acid from tumor cells, disrupting siglec acid engagement and enabling immune cell killing of desialylated cancer cells (Liu et al., 2023). Despite these encouraging preclinical findings, a significant challenge remains in the on-target, off-tumor expression of CD24 in immune cells, which poses a risk of adverse effects. Moreover, no CD24-targeting agents have entered clinical trials for cancer treatment.

PD-L1/PD-1 axis

The function of the PD-1/PD-L1 axis has been well-characterized in T cell immune checkpoints, and recent studies have reported that this axis is also crucial for regulating the phagocytic capacity of TAM (Feng et al., 2019). It is noteworthy that PD-1 expression is not restricted to T cells but also to other immune cells, such as DCs, B cells, and activated monocytes (Feng et al., 2019). Moreover, TAMs express high levels of PD-1, and its expression is elevated relative to that of circulating monocytes or splenic macrophages and is upregulated in a tumor growth-dependent manner (Feng et al., 2019). Most PD-1+TAMs are predominantly of the M2 phenotype, which is generally regarded as a pro-tumorigenic subtype (Feng et al., 2019). PD-1 knockout promotes M1 polarization through STAT1 signaling, suggesting that PD-1 may promote M2 polarization of TAMs, thereby reinforcing an immunosuppressive TME (Feng et al., 2019). Functionally, PD-1^+ TAMs exhibit markedly weaker phagocytic ability than their PD-1^- counterparts, suggesting that PD-1 on TAMs inhibits phagocytosis (Feng et al., 2019). This is further supported by the fact that PD-L1 blockade potentially increases phagocytosis by PD-1+ macrophages but has no effect on the PD-1 population (Feng et al., 2019). Crucially, PD-1/PD-L1 axis blockade induces phagocytosis and antitumor responses in NSG mice, which lack T cells but retain functional macrophages, confirming the functional role of this axis as a phagocytic checkpoint (Feng et al., 2019). The clinical relevance of this pathway is underscored by PD-L1 overexpression across various solid tumors, including HCC, its poor prognostic association, and the association between PD-1 + TAMs and patient survival (Feng et al., 2019). The dual role of the PD-1/PD-L1 axis rationalizes novel therapeutic strategies, such as combination with CD47/ SIRPα blockers and the development of bispecific agents targeting both pathways, to cooperatively unleash innate and adaptive immunity. (Feng et al., 2019; Mantovani et al., 2022)

1.3.3.4 Therapeutic potential of macrophage-based therapies in HCC

The therapeutic potential of macrophage-based treatments has been assessed primarily in hematologic cancers and other solid cancers, but rarely in liver cancer (Duan and Luo, 2021). In the HCC TME, liver-resident Kupffer cells (the main nonparenchymal cells, ~20%, in the liver) and liver-infiltrating macrophages constitute TAM. Although these phagocytes have been shown to play a pro-tumorigenic role and are functionally impaired with deprived phagocytic capability in the HCC TME, Willingham et al. demonstrated that the administration

of anti-CD47 mAb alone can induce TAM-mediated phagocytosis of liver cancer cells, highlighting the plasticity of macrophages whose phagocytic capacity can be readily re-elicited. Moreover, studies have shown that Kupffer cells exhibit high plasticity and are capable of eliciting potent phagocytic abilities (i.e., readily phagocytosing circulating B or T lymphoma cells) upon opsonization with tumor-targeting antibodies (Duan and Luo, 2021; Gül et al., 2014). The high abundance, intrinsic potency, and plasticity of macrophages in the HCC TME render them attractive targets for liver cancer treatment.

1.3.4 Macrophage bridges innate to adaptive immunity

1.3.4.1 Antigen presentation via MHCII for helper T cell activation

In addition to their direct tumoricidal role in engulfing tumor cells, macrophages serve as a pivotal bridge between innate and adaptive immunity by orchestrating T cell responses through antigen presentation and immunomodulatory signaling. This process begins with macrophages that engulf and proteolytically degrade tumor cells within the phagolysosome, generating peptide fragments that are then loaded onto Major Histocompatibility Complex class II (MHCII) molecules, forming a peptide-MHCII complex that is transported on the macrophage cell surface (Murray & Wynn, 2011). This peptide-MHCII complex interacts with the specific TCR of helper T (Th) cells and serves as signal 1 for their activation (Iborra & Sancho, 2015). Macrophages also provide signal 2 for the full activation of helper T cells (Iborra & Sancho, 2015). During phagocytosis, the engagement of innate activation signals, such as TLR, often triggers the upregulation of co-stimulatory molecules, such as CD80/86, on macrophages. These co-stimulatory molecules interact with the corresponding receptor, CD28, on CD4+ T cells (Chen and Flies, 2013). Upon receiving both signals, helper T cells become activated, proliferate, and differentiate into effector subsets (Th1, Th2, and Th17), predominantly into Th1 cells (Iborra & Sancho, 2015).

These Th1 cells then orchestrate an antitumor cytotoxic T cell response through multiple pathways: (1) they license APCs, including dendritic cells and macrophages, via CD40/CD40L interaction, potentiating their ability to prime and activate naïve T cells (Bennett et al., 1998; Schoenberger et al., 1998); (2) they secrete key cytokines, particularly IFNγ, which acts directly on CD8+ T cells to promote their clonal expansion, effector differentiation, and memory formation, and enhances MHCI expression on tumor cells, sensitizing them to Tc cell attack (Bevan, 2004); and (3) they provide critical signals to prevent T cell exhaustion

and sustain a functional Tc population within the TME by enabling CD8+T cells to differentiate into long-lived memory T cells (Borst et al., 2018). Moreover, this macrophage-T cell interaction is reciprocal, and CD40/CD40L engagement provides a potent feedback signal that further enhances macrophage antigen presentation and tumoricidal capacity, establishing a positive feedback loop crucial for effective cell-mediated immunity against cancer (Murray & Wynn, 2011).

In summary, macrophage phagocytosis drives CD4+ T cell activation by providing a constant source of antigens for the MHC II presentation pathway. This process indirectly but indispensably amplifies and polarizes the adaptive immune cascade within the peripheral tissue, effectively bridging the detection of tumor cells (innate immunity) with a targeted antigen-specific T cell response.

1.3.4.2 Antigen cross-presentation and cross-priming by macrophage

In addition to the indirect role in bridging the innate and adaptive immune responses through CD4+ T cell activation, macrophages have also been reported to directly activate adaptive immunity within the TME through antigen cross-presentation and cross-priming, a process involving APCs presenting the processed antigen of phagocytosed tumor cells on the MHCI molecule to naïve T cells to induce their activation (Feng et al., 2019). Cross-presentation is a critical adaptation of the classical MHC I pathway that enables APCs to present exogenous antigens to $CD8^+$ T cells. The cytosolic pathway is the major pathway for antigen cross-presentation. It involves the partial degradation of ingested tumor cells by acidic proteases in the phagolysosome and the regulated translocation of selected tumor antigens or fragments into the cytosol, which is facilitated by SEC61 translocon, recruited to the phagosomal membrane (Grotzke et al., 2017). Once in the cytosol, the antigens are cleaved into short peptides by proteasomes and transported to the ER lumen or back to the phagosome via retro-translocation by the Transporter Associated with Antigen Processing (TAP) (Lecoultre et al., 2020; Alloatti et al., 2015). Within the peptide-loading compartment, the peptide is further trimmed to an optimal length by aminopeptidase and loaded onto nascent MHCI molecules within the peptide-loading complex, which allows the selection of high-affinity peptides and stabilizes the complex. The stable MHCI-peptide complex is then released and transported to the plasma membrane to be surveyed by CD8+ T cells (Blum et al., 2013).

Following cancer cell phagocytosis, DNA from phagocytosed cells can escape into the cytosol, where it stimulates the cyclic GMP-AMP synthase stimulator of interferon genes (cGAS-STING) pathway (Lecoultre et al., 2020). In particular, the cytosolic DNA sensor cGAS binds to exposed tumoral DNA and becomes activated to catalyze the conversion of ATP and GTP to cyclic GMP-AMP (cGAMP), which functions to phosphorylate and activate STING, leading to transcription induction and release of interferons such as type I interferons (IFNs) and TNFα (Feng et al., 2019). Type I IFNs increase the pH of the phagolysosome of APCs, which can, in turn, extend the persistence of processed antigens, thereby increasing the cross-presentation ability of APCs (Lecoultre et al., 2020). Notably, macrophages express high levels of three-prime repair exonuclease 1 (TREX1), which degrades cytosolic DNA and thus dampens cGAS-STING pathway activation (Feng et al., 2019). This limits the ability of macrophages to cross-present antigens.

Furthermore, several other intrinsic properties of macrophages render them markedly less effective in cross-presentation than dendritic cells. First, macrophages possess higher proteolytic activity in the phagolysosome, leading to extensive degradation of internalized antigens and reducing the pool of intact peptides for cross-presentation (Lecoultre et al., 2020). Second, macrophages demonstrate limited translocation of antigens from phagosomes to the cytosol, which is a critical step in the cytosolic cross-presentation pathway (Lecoultre et al., 2020). Most importantly, cross-priming principally occurs in the draining lymph nodes. Unlike DCs, macrophages have poor migratory ability and are largely unable to be recruited to the draining lymph nodes to engage and prime naïve T cells (Lecoultre et al., 2020). Functionally, several studies have shown the importance of DCs in cross-presentation for T cell priming in *in vivo* models, while there was a limited contribution of macrophages to $CD8^+$ T cell activation (Lecoultre et al., 2020). Despite the known limitations of macrophages in cross-presentation, *in vitro* studies have suggested that enhancing macrophage phagocytosis can unlock their fundamental cross-presentation capacity, enabling them to cross-present tumor antigens to T cells (Lecoultre et al., 2020). Moreover, these functional limitations may be counterbalanced by their quantitative advantage within the TME: macrophages are typically more abundant and exhibit higher phagocytic activity than DCs (Lecoultre et al., 2020). This allows macrophages to facilitate comprehensive sampling of the entire tumor mass. In the context of tumor heterogeneity, where distinct antigenic subclones can limit T cell responses, this broad sampling by macrophages could present a wider repertoire of tumor antigens, thereby

broadening the resulting T cell response against tumor diversity (Lecoultre et al., 2020). Collectively, this rationale supports therapeutic strategies designed to boost macrophage phagocytosis to leverage their inherent cross-presentation machinery and potentiate a more comprehensive antitumor T-cell response.

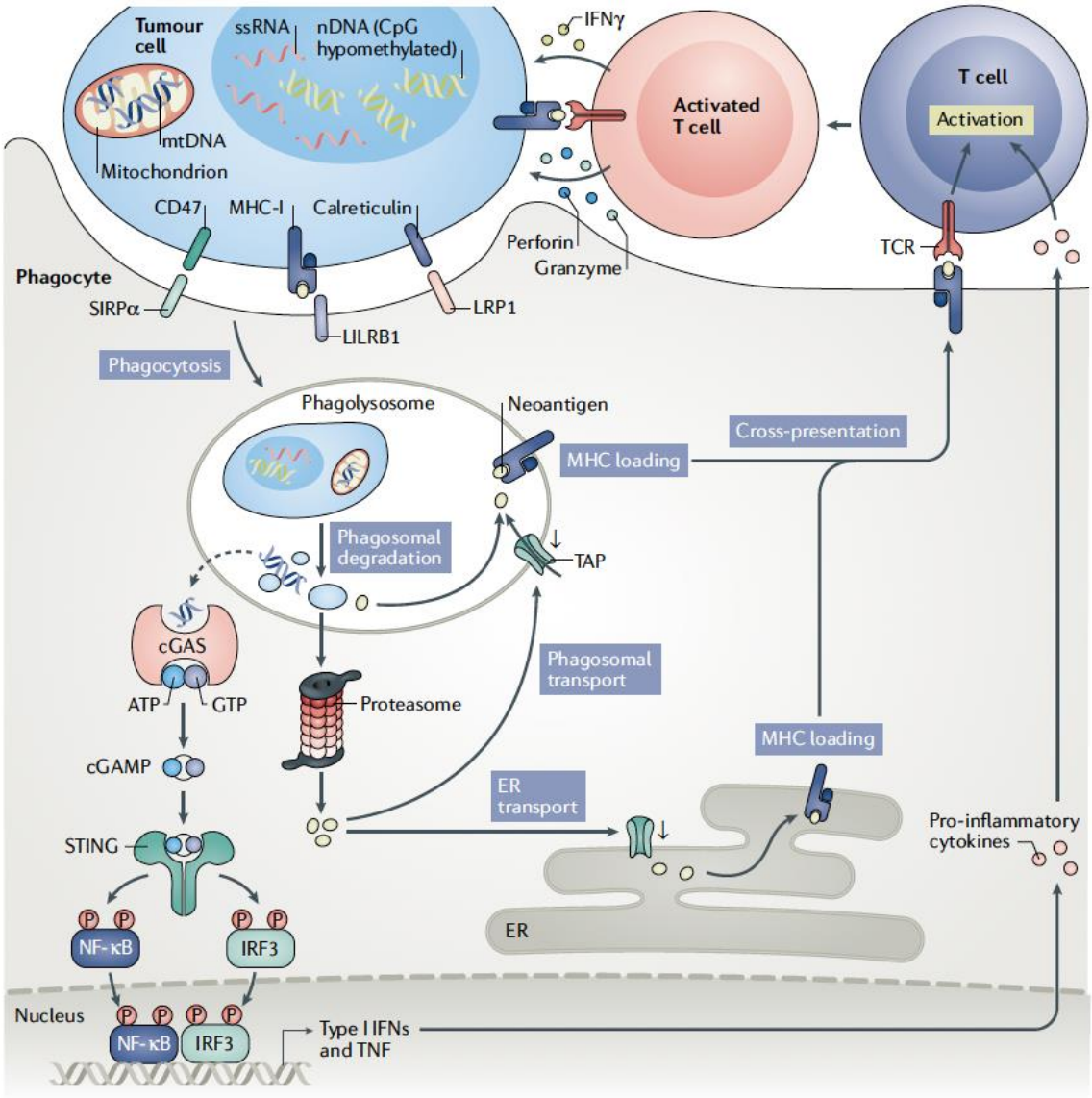

Figure 1.5 Cytosolic cross-presentation pathway (This figure is adopted from Zheng et al., 2023)

1.4 Aims of study

Based on the treatment efficacy of macrophage-based therapies in other solid malignancies, the unique advantages of targeting macrophages in liver cancer, and the plausible co-activation of innate and adaptive immunity by potentiating macrophage phagocytosis, we hypothesized that inducing macrophage phagocytosis may represent an efficacious therapeutic approach for HCC. Although a few anti-phagocytic axes have been identified and are under clinical investigation, redundant inhibitory signals are commonplace in immunoregulation. We aimed to identify additional inhibitory signals crucial for engaging macrophages in the elimination of cancer cells. Given the druggable properties of protein kinases and their regulatory effects on tumors, we focused on identifying specific protein kinases that play crucial roles in the regulation of HCC phagocytosis. To achieve this, we performed a kinome-wide CRISPR knockout screen in mouse HCC cells (RIL-175), followed by co-incubation with mouse macrophages (RAW264.7). Cells with depleted anti-phagocytic genes are phagocytosed and removed from the cell pool, and these anti-phagocytic genes can be identified using high-throughput sequencing. Next, we aimed to determine whether the candidate anti-phagocytic gene(s) are actionable target(s) in HCC. Specifically, we investigated whether knockout of candidate gene(s) by sgRNA would reinitiate the phagocytic clearance of HCC cells by macrophages and exhibit antitumor effects in a mouse model. We postulated that depleting cancer intrinsic antiphagocytic genes would invoke macrophage effector function(s) and augment tumor clearance. Finally, we aimed to elucidate the underlying mechanisms and develop novel therapeutic strategies for HCC treatment.

CHAPTER 2 Materials and Methods

2.1 Cell Cultures and animals

2.1.1 Cell Cultures

Cell culture media and conditions were as follows: PLC/PRF/5 and RAW264.7 cells were maintained in Dulbecco's Modified Eagle Medium (DMEM) supplemented with 10% fetal bovine serum (FBS) and 1% penicillin/streptomycin. RIL-175 cells were grown in complete RPMI-1640 medium containing HEPES buffer. THP-1 cells were cultured in suspension using complete RPMI-1640 medium, which was additionally supplemented with 5.5 μM 2-mercaptoethanol. THP-1 monocytes differentiation into M0 macrophages was done by plating cells at 1.5×10^6 cells per 60 mm dish and treating with 100 nM phorbol 12-myristate 13-acetate (PMA) for 24 hours. After PMA removal, cells were incubated in standard THP-1 medium for a further 48 hours. For polarization to the M1 phenotype, PMA-differentiated macrophages were stimulated for 72 hours with 20 ng/mL interferon-gamma (IFN-γ) and 100 ng/mL lipopolysaccharide (LPS) in complete RPMI-1640. All cells were incubated at 37°C in a humidified condition of 5% CO_2.

To generate a stable OVA-expressing murine cell line, RIL-175-NTC or RIL-175-sg*Ikbkb* cells were seeded in 6-well plates at a density of 1 x 10^5 cells per well 24 hours before the transduction. Then the cells were infected with pLVX-OVAL-IRES-Neo virus at an MOI of ~0.9 in the presence of 8μg/ml polybrene (MilliporeSigma). The viral medium was replaced by fresh medium 24 hours post-infection. Two days post-transduction, selection was initiated using 3mg/ml G418 (geneticin) sulfate (GoldBio) for 5 days, and the cells were maintained for selection at 1.5mg/ml G418. The expression of OVA was assessed by Western Blot analysis using rabbit anti-OVA antibody (Abcam, #ab17283; 1:250) followed by HRP-conjugated anti-mouse IgG (1:500), as well as by qPCR with using BrightGreen 2x qPCR Master Mix (Applied Biological Materials) and the following primers: primer 1- OVA forward: 5'-CTACTGCCCCATTGCCATCA-3'; OVA reverse: 5'-CTGTGTCCTGGTGCTGTCTT-3'; primer 2- OVA forward: 5'-TGCAGATCAAGCCAGAGAGC-3'; OVA reverse: 5'-TGAGAATCCACGGAGCTTGG-3'. GAPDH was used as an endogenous control.

To generate a stable GFP-expressing murine cell line, RIL-175-NTC or RIL-175-sg*Ikbkb* cells were seeded in 6-well plates at a density of 1 x 10^5 cells per well 24 hours prior to the transduction. Then the cells were infected with pLent-EF1a-FH-CMV-GFP-P2A-NEO virus (WZ Biosciences Inc.) at an MOI of ~0.9 in the presence of 8μg/ml polybrene. The viral medium was replaced by fresh medium 24hours post-infection. Two days post-transduction,

selection was initiated using 3mg/ml G418 for 5 days, and the cells were maintained for selection at 1.5mg/ml G418. The expression of GFP was assessed by flow cytometry analysis.

2.1.2 Mouse models

2.1.2.1 Subcutaneous and orthotopic tumor model

For the subcutaneous tumor model, BALB/c nude mice (aged 4–6 weeks, sourced from the Centralised Animal Facilities at The Hong Kong Polytechnic University) received injections of either 1×10^4 RIL-175-NTC or RIL-175-sgIkbkb cells, suspended in 100 µL of PBS, into their left and right flanks. In the xenograft model, 8×10^5 PLC/PRF/5-NTC or PLC/PRF/5-sgIkbkb cells, suspended in a 100 µL mixture of serum-free medium and Matrigel, were similarly injected into the bilateral flanks of the mice.

C57BL/6 male mice (8-10 weeks old) were purchased from the Centralised Animal Facilities in the Hong Kong Polytechnic University. For the orthotopic tumor model, 8 x 10^3 RIL-175, RIL-175-NTC-OVA, or RIL-175-sg*Ikbkb*-OVA cells were washed once in PBS, suspended in 15µl mixture of serum-free medium and Matrigel (Corning; 1:1 ratio). Mice were then anesthetized with a mixture of ketamine and xylazine. A small left lateral subcostal incision (~1 cm) was made to expose the left liver lobe, and it was slowly injected with 15 µL of the cell suspension. Flunixin meglumine (Banamine®; 0.006 mg/mL) was prepared in drinking water for postoperative analgesia for three days. Tumor growth was monitored weekly by in vivo bioluminescence imaging (IVIS Spectrum, PerkinElmer) after intraperitoneal injection of D-luciferin (100 mg/kg, GoldBio). Mice were euthanized when humane endpoints were reached (e.g., significant body weight loss >20%, ascites, or lethargy). Livers were harvested and weighed, and tumors were collected for immune profiling.

2.2.2.2 Hydrodynamic Tail Vein Injection (HTVI) for Liver Tumorigenesis

The Sleeping Beauty transposon system was used. The transposon plasmid pT3-EF1α-cmyc-IRES-luc (Addgene #129775), the transposase plasmid pCMV-SB13 (Addgene #34879), px330-sgTP53 (Addgene #59910), pT3-EF1α-EV, or pT3-EF1α-*IKBKB* (plasmid constructs were generated using the CloneEZ method provided by GenScript®) were used. For hydrodynamic injection, a sterile saline solution (0.9% NaCl) containing 15 µg of transposon plasmids and 2.5 µg of transposase plasmid in a total volume equivalent to 10% of the mouse

body weight (e.g., 2 mL for a 20g mouse) was prepared and filtered through a 0.22 μm filter. C57BL/6 male mice (8-10 weeks old) were placed in a restraining device, and the tail vein was dilated using a warm lamp. The plasmid solution was rapidly injected (<7 seconds) using a 27-gauge needle attached to a 3 mL syringe. Mice were recovered on a warm lamp.

For examining the effect of TAT-NEMO^{ActPep} and in combination with anti-PD-1 mAb (anti-mouse; BioXcell), we employed a 17-mer TAT-NEMO^{ActPep} oligopeptide with diglycine-linked N-terminal TAT peptides, which were synthesized by MOTIF BIOTECH. Peptides were dissolved in 1× PBS to stocks of 10 mM. IgG2A (rat isotype control; BioXcell) was used as a control for anti-PD-1 mAb. Treatment was initiated at day 10 post-HTVI following the bioluminescence signal randomization, TAT-NEMO^{ActPep} was administered via I.P. injection every two days at 20 μg/g for 2 weeks, and IgG2A or anti-PD-1 mAb was administered via I.P. injection at 4mg/kg twice a week for two weeks.

2.1.3 In vivo macrophage depletion

To deplete macrophages in vivo, mice were administered 200 μL of clodronate liposomes or a PBS liposome control via tail vein injection 24 hours prior to tumor inoculation. For the tumor model, 2 × 10^4 RIL-175-NTC or RIL-175-sgIkbkb cells in 100 μL PBS were injected subcutaneously into both flanks. Macrophage depletion was maintained by administering 100 μL of clodronate or control liposomes intraperitoneally twice weekly, beginning three days post-tumor injection. Tumor dimensions were measured using calipers to calculate volume, and animal body weight was monitored throughout the study. To confirm macrophage depletion, spleens were harvested, subjected to red blood cell lysis, and analyzed via surface marker staining, following the protocol outlined for the in vivo phagocytosis assay. Clodronate and control liposomes were commercially sourced.

2.2 CRISPR/Cas9 knockout library screen

The Mouse Kinome CRISPR Knockout Library (Brie), comprising 2,852 sgRNAs (4 per gene) targeting 713 kinase genes and 1,000 non-targeting controls, was introduced into RIL-175-Cas9 cells at a low multiplicity of infection (MOI 0.2-0.3) to achieve approximately 500-fold library coverage. Following 24-hour viral transduction, a mutant cell pool was established through puromycin selection (12μg/ml for 2 days) and a subsequent rest period. For the screen,

1×10^6 mutant cells were co-cultured with or without RAW264.7 mouse macrophages at a 1:1 ratio in serum-free medium for 16 hours. After co-culture, non-phagocytosed cells were recovered by isolating the top fraction, followed by a 2-day puromycin selection and a 2-day recovery period; this co-culture and selection cycle was then repeated.

Genomic DNA was extracted from a minimum of 1.5×10^6 cells per sample (to maintain 500x coverage) using the DNeasy Blood and Tissue Kit. The sgRNA regions were PCR-amplified with NEBNext High-Fidelity 2X PCR Master Mix, and the resulting amplicons were subjected to high-throughput sequencing by Novogene across three biological replicates. sgRNA read counts were analyzed with MAGeCK v0.5.9 software.

2.3 Gene Ablation Assays

2.3.1 Establishment of knockout cell lines

2.3.1.1 Lentiviral packaging and transduction

For lentiviral packaging and transduction, viral particles were generated by transfecting HEK293FT cells (maintained in complete DMEM) with the lentiviral construct alongside the packaging plasmid psPAX2 and the envelope plasmid pMD2.G, utilizing Lipofectamine 3000 (Thermo Fisher). The transfection medium was refreshed after 6–12 hours. Viral supernatant was harvested 48 hours later by centrifugation at 3,000 rpm for a duration of 15 minutes.

2.3.1.2 Generation of RIL-175 and PLC/PRF/5 sublines

Stable Cas9-expressing cell lines for RIL-175 and PLC/PRF/5 were established by lentiviral transduction to integrate the Cas9 coding sequence into the cellular genome. Successful Cas9 protein expression was subsequently verified by western blotting using a Cas9-specific antibody (Cell Signaling #14697; dilution 1:1000). For *Ikbkb* or IKBKB knockout, sgRNAs targeting the respective coding sequences were introduced via lentiviral overexpression in the corresponding RIL-175-Cas9 or PLC/PRF/5-Cas9 cells. Following 48 hours of transduction, transduced cells were selected using puromycin at 12 μg/ml for RIL-175 or 10 μg/ml for PLC/PRF/5, applied for 2 to 3 days. A stable knockout subline was then generated by isolating single-cell clones via serial dilution in 96-well plates. The resulting KO sublines were validated through confirmation of depletion at both the mRNA and protein levels. The sgRNA sequences targeting *Ikbkb* or IKBKB were obtained from either the Brie library or the Human CRISPR

Knockout Pooled Library (GeCKO v2). The sRNA sequences used are listed as follows: sg*Ikbkb*: 5′- GAAGCCAGTGATGCACTCGA -3′, sg*IKBKB*: 5′- GCCATGGAGTACTGCCAAGG -3′.

2.3.2 Validation of gene depletion

2.3.2.1 RT-qPCR

Total RNA was isolated with the RNAiso reagent (Takara), and reverse transcribed to cDNA using the PrimeScript RT Reagent Kit (Takara) in strict accordance with the manufacturer's protocol. Quantitative real-time PCR (qRT-PCR) was then performed for quantifying gene expression using SYBR Green qPCR Master Mix (Applied Biosystems) on a QuantStudio™ 7 Flex Real-Time PCR System. The ΔΔCT method was used to analyze the relative expression of each transcript normalized to mouse *GAPDH* or human *HPRT*. Primer sequences are listed as follows: Mouse *Ikbkb*: F' TGCATCACTGGCTTCCG, R' CTTCACTAACAACGATGTCCACT; Human *IKBKB*: F' CCCTGCTGGCCATGGAGTA, R' GCAGGACGATGTTTTCTGGC.

2.3.2.2 Western blotting

Protein was lysed in samples using RIPA buffer containing phosphatase and protease inhibitors. The supernatant was collected following centrifugation at 13,000 rpm for 15 minutes at 4°C, and protein concentration was measured by Bradford assay. Equal protein amounts (30–40 μg) were separated by SDS-PAGE on 10% gels and transferred to PVDF membranes. The membranes were blocked with 5% BSA or non-fat milk in TBST and then incubated with primary antibodies overnight at 4°C. Following TBST washes, membranes were incubated with HRP-conjugated secondary antibodies. Signal detection was performed using an ECL substrate. Antibodies used for specific detection included anti-IKKβ, anti-phospho-IKKα/β, and anti-β-actin as a loading control.

2.3.2.3 Immunohistochemistry (IHC) analysis

Formalin-fixed, paraffin-embedded (FFPE) tumor sections were deparaffinized by heating to 85°C for 5–10 min, then cleared in xylene (Anaqua) and rehydrated through a graded ethanol

series (Anaqua). Antigen retrieval was carried out via microwave treatment in either citrate buffer (pH 6.0) or Tris-EDTA buffer (pH 9.0) (both from Dako, Agilent) using the following cycle: 1 min at 1000 W, followed by three pulses of 10 s at 1000 W and three 5-min incubations at 100 W. After cooling, slides were rinsed in Tris-buffered saline with Tween-20 (TBST). Endogenous peroxidase activity was quenched with 3% H_2O_2 for 10–30 min, and non-specific binding was blocked with a protein-blocking solution for 30–60 min. Sections were incubated overnight at 4°C with primary antibodies diluted in antibody diluent (S3022, Dako, Agilent). Following a TBST wash, slides were incubated for 1 h at room temperature with an HRP-conjugated secondary antibody (K5007, Dako, Agilent). Signal was developed using a 3,3'-diaminobenzidine (DAB) substrate system (K5007, Dako, Agilent) diluted 1:50 in substrate buffer. Sections were counterstained with hematoxylin (Biognost), differentiated in 0.5% acid alcohol (Biognost), blued in Scott's water (Biognost), and dehydrated through graded ethanol and xylene (Anaqua). Coverslips were applied with an organic mounting medium (Biomount, Biognost), and slides were examined under bright-field microscopy.

2.4 Phagocytosis assay

2.4.1 In vitro phagocytosis assays

The described in vitro phagocytosis assays utilized fluorescently tagged macrophages (RAW264.7 and THP-1 lines) and cancer cells (RIL-175 and PLC/PRF/5). Macrophages were detached with TrypLE Express and labeled by incubating with 2µM CellTrace™ CFSE dye in PBS at 37°C for 20 minutes. Following a 5-minute incubation in complete DMEM (10% FBS), they were washed twice with PBS. Cancer cells were plated overnight, allowed to attach, and then stained with 1.67µM CellTracker™ Red CMTPX dye in serum-free medium overnight. After trypsinization, the cancer cells were also washed twice with PBS.

For the phagocytosis assay, macrophages and target cells were co-cultured at a 2:1 ratio for 16 hours in serum-free medium within a 37°C, 5% CO_2 incubator. Two methods were used to quantify phagocytosis. In the flow cytometry-based assay, cells were harvested with TrypLE Express and analyzed on a BD Accuri™ C6 Flow Cytometer. Phagocytosis was quantified as the percentage of double-positive (CFSE+ CMTPX+) cells among the total macrophage (CFSE+) population.

For the microscopy-based assay, co-cultures were imaged using a Nikon Eclipse Ti2-E Live-cell Fluorescence Imaging System. The phagocytic index was calculated as the number of macrophages that had engulfed tumor cells (CFSE+ CMTPX+) per 100 total macrophages (CFSE+).For the competitive phagocytosis experiment, RIL-175-NTC (or PLC/PRF/5-NTC) cells were labelled with CellTrace™ CFSE dye with the procedure as described above, and mix with RIL-175-sg*Ikbkb* (or PLC/PRF/5-sg*IKBKB*) cells which were labelled with CellTracker™ Red CMTPX Dye with the procedure mentioned, at 1:1 ratio. The target cells then co-cultured with macrophages at 1:2 effector:target ratio. The wells were imaged with the Fluorescence Imaging System. The phagocytic index was calculated as the percentage of macrophages that had enguled tumor cells per 100 macrophages.

2.4.2 In vivo phagocytosis assays

For tumor establishment, BALB/c nude mice (4–6 weeks old) were subcutaneously injected with murine HCC cells (1×10^4 RIL-175-NTC or RIL-175-sg*Ikbkb* cells) expressing GFP suspended in 100µl PBS, or human HCC cells (8×10^5 PLC/PRF/5-NTC or PLC/PRF/5-sg*Ikbkb* cells) expressing GFP suspended in 100µl mix of serum-free medium and Matrigel, Then, tumors are allowed to grow for 21 days and 49 days, respectively, until reaching a volume of approximately 300-400 mm^3. Tumors are excised, minced, and dissociated with gentleMACS™ Dissociator (Miltenyi Biotec) in dissociation buffer containing 10% collagenase IV (Gibco™), DNase I (Roche) to single cell suspension according to the manufacturer's protocol. The single cell suspension was resuspended in 40% Percoll and gently layered on top of 80% Percoll, and was centrifuged at 1,200 x g, 25 minutes with the centrifuge brake off to ensure gentle gradient formation. The immune cell layer was then subjected to red cell lysis using ACK lysis buffer (Invitrogen™) Cells were incubated in an Fc receptor blocking agent (BD Biosciences) in FACS buffer, followed by staining with surface marker anti-CD45-APC (BD Pharmingen, #559864), anti-CD11b-BV421 (BioLegend, #101235), anti-F4/80- APC/Cy7 (BioLegend, #123117), and Zombie Yellow™ Fixable Viability Dye (BioLegend, #423103). Phagocytosis was quantified by measuring the percentage of GFP-positive cells within live, $CD45^+$, $CD11b^+$, and $F4/80^+$ tumor-associated macrophages (TAMs). Flow cytometry was performed on a BD FACSymphony A3 Cell Analyzer, and data were analyzed using FlowJo™ software (BD Biosciences).

2.5 Cell viability assay

To validate the growth inhibition effects brought by the *Ikbkb* (or *IKBKB*) KO, MTT and in vitro cell proliferation assays were applied. For the MTT assay, the cells were seeded at 8-10% confluence in a 96-well plate. Cell viability was then determined at 48 and 72 hours by performing an MTT assay according to the manufacturer's protocol. Absorbance was measured at 570 nm by spectrophotometry. For *in vitro* cell proliferation assays, cells were plated at 10-15% confluence in 24-well plates, and cell proliferation was measured with Nikon microscopy every 24 hours for 3 days. The percentage of confluence after cell growth was measured by ImageJ software. For the assessment of cell proliferation *in vivo*, the FFPE section was processed as described and was stained overnight at 4°C with anti-Ki-67 monoclonal antibody (Origene, 1:100 dilution). The immunofluorescence image was taken using Nikon Eclipse Ti2-E Live-cell Fluorescence Imaging System, and Ki-67^{+} cells were quantified using ImageJ software.

2.6 NF-kB pathway signaling

2.6.1. Nuclear and Cytoplasmic Fractionation

For NF-κB pathway activation studies, cells were added with 10 ng/mL or 20 ng/mL recombinant TNFα (R&D system, 210-TA) for RIL-175 cells and PLC/PRF/5 cells, respectively, for defined timepoints (0, 15, 30, 45, 60 mins). Cells were harvested and fractionated at specific time points using the hypotonic solution (10mM Tris-Cl, pH 7.8, 5mM MgCl2, 10mM KCl, 0.1mM EDTA, 300mM sucrose, 5mM β-glycerol phosphate), and the cytoplasmic fraction was collected by centrifugation (800 × g, 10 min). Then, cells were washed with 0.9% NaCl, and the nuclear pellet was lysed in RIPR buffer containing inhibitors of protease and phosphatase. Nuclear and cytoplasmic fractions were collected for Western Blot analysis. The following primary antibodies were incubated overnight at 4°C with gentle agitation: mouse anti-phospho-IκBα (Ser32/36) (Cell Signaling Technology, #9246; 1:250), mouse anti-phospho-NF-κB p65 (Ser536) (Cell Signaling Technology, #3036; 1:250), rabbit anti-NF-κB p65 (Santa Cruz, #sc372; 1:1000), rabbit anti-phospho-IKK alpha/beta (Ser176/180) (Cell Signaling Technology, #2697; 1:1000), rabbit anti-sp1 (Santa Cruz, #sc59; 1:500; nuclear loading control), and GAPDH (GenScript #A00192; 1:2000; cytoplasmic loading control). After washing, membranes were incubated with HRP-conjugated anti-mouse

or anti-rabbit secondary antibodies (Cytiva; 1:1000) for 1 hour at room temperature. Chemiluminescent detection was then performed.

2.6.2 Immunofluorescence (IF) Microscopy and IHC analysis for p65 nuclear localization

For immunofluorescence (IF) analysis, cells were grown on coverslips and subjected to a 30-minute stimulation as specified. Following fixation with 4% paraformaldehyde (15 minutes) and permeabilization with 0.3% Triton X-100 in PBS (15 minutes), non-specific binding was blocked using 5% BSA in PBS for one hour. Cells were subsequently incubated overnight at 4°C with primary antibodies targeting phospho-NF-κB p65 (Ser536), total NF-κB p65, or a normal rabbit IgG control. After washing, samples were incubated for one hour with an Alexa Fluor 488-conjugated anti-rabbit secondary antibody. Coverslips were mounted with an antifade medium containing DAPI. Imaging was performed on a confocal microscope, and the nuclear translocation of p65 was quantified by calculating the nuclear-to-cytoplasmic fluorescence intensity ratio using ImageJ software, with analysis encompassing at least three fields from three separate experiments.

2.6.3. NF-κB Reporter Assay

Cells were plated at 12 well-plates and transfected with 1 μg of the NF-κB luciferase reporter plasmid (Stratagene) and 50ng of the pRL-CMV Renilla luciferase control vector (Promega) using Lipofectamine 2000 (Invitrogen) according to the manufacturer's instructions. After 16 hours, cells were stimulated as indicated for 6 hours. Luciferase activity was measured using the Dual-Luciferase Reporter Assay System (Promega, #E1910). Measurements were performed on a CLARIOstar Plus microplate reader and normalized to Renilla luciferase activity.

2.6.4 CD47 and PDL1 expression

2.6.4.1 Surface staining by flow cytometry

Cells were seeded at 1×10^5 in 12-well plates overnight, followed by stimulation with TNFα as described for 24 hours. The next days, the cells are trypinized and stained with BV-786 anti-CD47 (BD Pharmingen #740975) or AF488 anti-PDL1 (BD Pharmingen #568304) at 4°C for

30 mins and then washed with 3ml PBS. And the surface marker expression was measured by the C6 Flow Cytometer. For tumor harvest from the mouse model, the tumor pellet was collected by centrifugation at 50xg for 10 mins following tumor mincing, followed by red cell lysis and stained with anti-CD47 or anti-PDL1 for 45mins on ice. the surface marker expression was measured by BD FACSymphony A3 Cell Analyzer, and data were analyzed using FlowJo™ software (BD Biosciences).

2.6.4.2 qPCR

Total RNA was extracted with RNAios Plus (TakaRa #9109) and reverse transcribed by (). qPCR was performed as described previously. Primers for murine genes were as follows: Cd47 F' 5'-TGCGGTTCAGCTCAACTACTG-3', R' 5'-GCTTTGCGCCTCCACATTAC-3'; Pdl1 F' 5'-GACGCAGGCGTTTACTGCT-3', R' 5'-GCGGTATGGGGCATTGACTTT-3'. Primers for murine genes were as follows: CD47 F' 5'-TCCGGTGGTATGGATGAGAAA, R' 5'-ACCAAGGCCAGTAGCATTCTT-3'; PD-L1 F' 5'-TGGCATTTGCTGAACGCATTT-3', R' 5'-TGCAGCCAGGTCTAATTGTTTT-3'. Relative gene expression was calculated using the 2-ΔΔCt method with *Gapdh* or HPRT as the endogenous control.

2.6.4.3 Reporter assays

Luciferase reporter assays were conducted in PLC/PRF/5 cells using pGL3 2kb prom. CD274 (Addgene, #107003) and pGL3-CD47 were synthesized by cloning of CD47 promoter region into the pGL3-basic vector (GenScript). The plasmid co-transfection and stimulation with TNFα were performed as described for 6 hours, and measurement of reporter activity was conducted as described. GFP reporter assays were conducted in RIL-175 cells for measuring promoter activity using pGL3-Cd47-EGFP or pGL3-Pdl1-EGFP (both generated by GenScript by cloning). The plasmid transfection was conducted using 0.75 μg plasmid in 6-well plates, followed by stimulation with TNFα as described for 6 hours, and measurement of reporter activity was conducted using BD Accuri™ C6 Flow Cytometer.

2.7 Immune cell analysis

2.7.1. Macrophage infiltration and activation in the TME

For the assessment of macrophage presence and state, multiplex immunohistochemistry (IHC) was performed on paraffin-embedded HCC tissue sections. The procedure utilized a tyramide signal amplification (TSA) approach with a four-color detection kit. Tissue sections were prepared through deparaffinization, rehydration, and antigen retrieval using a target retrieval buffer. Endogenous peroxidase activity was quenched with a 10-minute incubation in 3% hydrogen peroxide. After blocking, sections were incubated overnight at 4°C with primary antibodies against CD86 or CD68. Following this, a polymer-based horseradish peroxidase (HRP) conjugate was applied, and detection was achieved using Opal fluorophores. Nuclei were counterstained with DAPI. Stained slides were visualized with a confocal microscope, and fluorescence signal intensity was measured for quantification.

2.7.2. Immune profiling

After tumor processing and single cell isolation as described earlier, around 1 x10e^6 cells were incubated in an Fc receptor blocking agent (BD Biosciences) in FACS buffer, followed by staining with surface marker antibody cocktail (see Table 2.1) for 45 minutes on ice covered with aluminum foil. For intracellular targets, cells were subsequently fixed, permeabilized, washed, and stained with the antibodies. The samples were analyzed on a BD FACSymphony A3 Cell Analyzer (BD Biosciences). Data analysis was performed using the FlowJo software.

Table 2.1 Panel of antibodies for surface and intracellular markers of immune cells

Panel 1: Broad Immunophenotyping Panel				
Markers	Fluorochrome	Ratio	Cell types	Manufacturer
CD8	BUV395	1:20	$CD8^+$ T-cells	BioLegend®
Live/dead	FSV440UV	1:200	Viability	BD Biosciences
MHCII	BUV496	1:200	Antigen-presenting cells, M1 macrophages	BioLegend®
CD11c	BUV615	1:20	Dendritic cells (DCs)	BioLegend®
CD3	BUV661	1:200	T-cells	BioLegend®
CD45	APC	1:200	Leukocytes	BioLegend®

CD11b	BV421	1:125	Myeloid cells	BioLegend®
Ki-67	BV480	1:200	Proliferation	BioLegend®
Ly6G	BV650	1:20	Neutrophils	BioLegend®
Siglec H	BV711	1:200	pDCs	BioLegend®
CD49b	BV750	1:200	Natural killer (NK) cells	BioLegend®
CD103	BV786	1:200	cDC1	BioLegend®
Ly6C	AF488	1:20	$Ly6C^+$ monocytes	BioLegend®
F4/80	RB705	1:200	Mouse macrophage	BioLegend®
FoxP3	PE	1:200	Regulatory T-cells (Tregs)	BioLegend®
γδ-TCR	PE-CF594	1:125	γδ-T-cells	BioLegend®
CD19	PE-Cy7	1:125	B cells	BioLegend®
CD206	R718	1:40	M2 macrophages	BioLegend®
CD4	APC-H7	1:200	$CD4^+$ T-cells	BioLegend®

Panel 2: T-cell differentiation and exhaustion				
Markers	Fluorochrome	Ratio	Cell types	Manufacturer
CD8	BUV395	1:20	$CD8^+$ T-cells	BioLegend®
Live/dead	FSV440UV	1:200	Viability	BD Biosciences
CD44	BUV737	1:40	Effector memory T-cell (Tem); central memory T-cell (Tcm)	BioLegend®
CD45	APC	1:200	Leukocytes	BioLegend®
Ki-67	BV480	1:200	Proliferation	BioLegend®
TIGIT	BV650	1:20	Co-inhibitory marker	BioLegend®
TIM3	BV750	1:20	Co-inhibitory marker	BioLegend®
CD3	BV786	1:125	T-cells	BioLegend®
PD-1	BB515	1:200	Co-inhibitory marker	BioLegend®
Tbet	RB705	1:200	T helper 1 (Th1) cells	BioLegend®
FoxP3	PE	1:200	Tregs	BioLegend®
Anti-GATA	PE-CF594	1:40	T helper 2 (Th2) cells	BioLegend®
CTLA4	APC	1:200	Co-inhibitory marker	BioLegend®
RORγt	R718	1:200	T helper 17 (Th17) cells	BioLegend®
CD4	APC-H7	1:200	$CD4^+$ T-cells	BioLegend®

Panel 5: Macrophage infiltration and activation				
Markers	Fluorochrome	Ratio	Cell types	Manufacturer
CD45	APC	1:200	Leukocytes	BioLegend®
Live/dead	FSV440UV	0.125	Viability	BD Biosciences
CD11b	BV421	1:125	Myeloid cells	BioLegend®
F4/80	RB705	1:200	Mouse macrophage	BioLegend®
MHCII	BUV496	1:200	Antigen-presenting cells, M1 macrophages	BioLegend®
MHCI	FITC	1:100	Antigen-presenting cells	BioLegend®
CD86	PE	1:100	Proliferation	BioLegend®
CD206	R718	1:40	M2 macrophages	BioLegend®

2.8 Inhibition of *IKBKB* with peptide

Peptide targeting *IKBKB* were used for studying the effect on cancer cell phagocytosis by macrophage. IKKβ-targeting TAT-NEMO^{ActPep} peptide ($TAT^{YGRKKRRQRRR}$-GG-LSSPLALPSQRRSPPEE) or control TAT-NEMO$^{ActPep\ 6G}$ peptide ($TAT^{YGRKKRRQRRR}$-GG-LSSPLALPSGGGGGGEE) (MotifBiotech) was incubated in RIL-175 or PLC/PRF/5 cells at 100µM for 24 hours in serum-free condition prior to co-incubation with respective macrophages for 16hours for assays phagocytosis rate.

2.9 Clinical data analyses

Patient clinical data were sourced from The Cancer Genome Atlas (TCGA) via the cBioPortal database (https://www.cbioportal.org/datasets). Corresponding gene mRNA expression data were obtained from the GDAC Firehose (https://gdac.broadinstitute.org/). Expression profiles, gene dependency scores, and lists of essential genes were downloaded from the Cancer Cell Line Encyclopedia (CCLE) through the DepMap data portal (https://depmap.org/portal/download/). Expression datasets for the cohorts ICGC-LIRI-JP and LICA-FR were acquired from the ICGC data portal (https://dcc.icgc.org). The GSE36376 expression dataset was retrieved from the HCCDB database (http://lifeome.net/database/hccdb/home.html).

For pan cancer analysis, gene expression of tumoral samples was compared to that of normal samples using an unpaired T-test with Welch's correction. Pathway and immune infiltration

analyses were performed between the high expressor group (Top 25 percentile; transcript per million, TPM) *vs.* the low expressor group (bottom 25 percentile; TPM).

2.10 Statistical analysis and graphing software

All values are expressed as the mean ± standard error of the mean (SEM). Statistical significance between two independent groups was assessed using an unpaired t-test with Welch's correction, unless noted otherwise. For comparisons of paired samples, such as tumor versus adjacent normal tissue mRNA expression, a paired t-test was employed. All statistical analyses were conducted with GraphPad Prism software (version 9.0c).

CHAPTER 3 CRISPR KO screen identifies *Ikbkb* as a regulator of phagocytic evasion in HCC

3.1 Introduction

CRISPR knockout screening

In recent years, the advent of CRISPR (Clustered Regularly Interspaced Short Palindromic Repeats) library screening has allowed the systematic and genome-wide interrogation of gene function, enabling the unbiased discovery of new therapeutic targets and synthetic lethal interactions (Dhanjal & Radhakrishnan, 2021; Shalem et al., 2014). The core of the technology is the single-guide RNA (sgRNA) that directs the Cas9 nuclease to a specific target site in the genome and generates a double-strand break (Tan et al., 2013). Human cells repair this break via a process known as non-homologous end joining (NHEJ), which is an error-prone process that often results in frameshift mutation, leading to effective knockout of the target gene (Mali et al., 2013). In a pooled CRISPR knockout screen, a library of thousands of unique sgRNAs, typically 4 to 6 guide RNA per gene for statistical robustness, is designed to simultaneously knockout hundreds or thousands of genes in the genome within a population of cancer cells, which are then subjected to positive and negative selection screens to identify which genes are essential for fitness under various conditions, and thus provide a comprehensive, functional map of gene-phenotype relationships (Doench et al., 2016; Sanson et al., 2018).

A CRISPR knockout screen usually follows a core pipeline of library transduction, positive or negative selection of cell population, and deconvolution by sequencing (Joung et al., 2017). For library transduction, a complex pool of lentiviral vectors, each encoding a unique sgRNA targeting a specific gene, is transduced into cancer cells at a low multiplicity of infection. This ensures that each cell receives only one gRNA, generating a heterogeneous population of knockout mutants (Shalem et al., 2014). Several types of selective pressures are generally used for CRISPR screens, including viability or proliferation, therapeutic stress, and pathway-specific challenges. Viability screen identifies genes essential for basal survival in a cell line (Hat et al., 2015**).** Therapeutic screen identifies genes whose knockout confers resistance or sensitivity to chemotherapies, targeted therapies, or immunotherapies. Pathway-specific screen identifies genes crucial for survival under hypoxia conditions, nutrient deprivation, or metastatic pressure (Shalem et al., 2014). Following the selection, sgRNAs that give cells a fitness advantage become enriched, while those causing a disadvantage are depleted. The final phase is deconvolution by next-generation sequencing. During this phase, genomic DNA is harvested from the selected population and a reference control, then the integrated sgRNA sequences are amplified and sequenced (Shalem et al., 2014). Finally, bioinformatic algorithms

such as MAGeCK statistically compare sgRNA abundance between selected and control samples to identify genes whose perturbation drives the phenotype (Li et al., 2014).

In the past decade, CRISPR screens have been instrumental in delineating cancer dependencies. Several genome-wide screens, such as Cancer Dependency Map (DepMap) have been conducted across hundreds of cancer cell lines, uncovering a vast landscape of pan-essential genes or context-dependent essential genes (Tsherniak et al., 2017). Research studies have also focused on deciphering synthetic lethal interactions for cancer treatment, and one prominent example is the synthetic lethality between PARP inhibitors and defects in homologous recombination genes, i.e., BRCA1/2 (Lord & Ashworth, 2017). This approach has also been utilized to unravel the mechanisms underlying resistance and sensitivity to cancer treatments, as well as mapping immune evasion and immunotherapy (Manguso et al., 2017). Recently, kinase inhibitors, apart from their direct cytotoxic effects, have been shown to induce anti-cancer immunity by enhancing tumor immunogenicity and reprogramming the TME (Werner-Klein et al., 2021). In 2017, Manguso et al. reported that MAPK inhibitors have been shown to induce a conserved inflammatory response in cancer cells, leading to increased influx of T cells into the tumor, particularly less exhausted T-cells with higher cytolytic activity. In non-small cell lung cancer, Epidermal Growth Factor Receptor (EGFR) inhibitors, gefitinib and erlotinib, have been shown to upregulate MHCI and II molecules on the cancer cell surface, increasing their visibility for T cell recognition (Werner-Klein et al., 2022). Meanwhile, these drugs possess immunomodulatory effects, including reducing the immunosuppressive Tregs and M2 macrophages in the TME while increasing the abundance and cytotoxic function of Tc cells (Werner-Klein et al., 2022). Multikinase inhibitor H89 has been demonstrated to promote CD8+ T cells activation and reduce Treg infiltration in colorectal cancer models (Li et al. 2022). These examples illustrate that kinase inhibitors can shift the TME from immunosuppressive to immunogenic by modulating cancer cell properties and immune cell functions.

3.2 Method

In vitro CRISPR KO screen with mouse kinome library for identifying kinases crucial for evasion of phagocytosis in HCC cells

In this study, we performed a CRISPR-Cas9 KO screen to identify genes essential for evading macrophage-mediated phagocytosis, i.e., antiphagocytic genes, in HCC. The mouse HCC cell line, RIL-175, which exhibits a high proliferation rate, was used as an *in vitro* model for Cas9 overexpression and library transduction (Figure 3.1A & 3.2A). The mouse kinome knockout Brie library, consisting of 2,852 unique single-guide RNAs (sgRNAs) targeting 713 mouse kinase genes, was transduced into RIL-175-Cas9 cells to generate a mutant cell pool (Figure 3.1A). We then co-incubated the mutant cell pool with mouse macrophages RAW264.7 and performed two sequential rounds of phagocytosis (Figure 3.1A). We posit that KO of anti-phagocytic genes sensitizes HCC cells to phagocytic clearance by macrophages. In other words, RIL-175-Cas9 cells with the depletion of antiphagocytic genes were negatively screened in the resultant cell pool, and the absence of their respective sgRNAs in the library can be determined by next-generation sequencing (Figure 3.1A). In the co-culture of HCC cells with macrophages, we found that RAW264.7 cells exhibited an approximately 30% phagocytosis rate on RIL-175 cells, suggesting an effective negative selection pressure (Figure 3.1B). After co-incubation, we achieved around 500x coverage of the library, which is considered sufficient for CRISPR library screening (Figure 3.2B). Moreover, the control sgRNA was evenly distributed between the initial sample and the co-cultured group, suggesting that the complexity of the library was maintained throughout the screen (Figure 3.2B). Using the MAGeCK algorithm, we identified a subset of sgRNAs targeting 5 genes that were significantly depleted ($P < 0.01$, fold change < -1.5) in the co-cultured cells as compared to those in the untreated control, indicating that these genes could be potential anti-phagocytic genes in HCC (Figure 3.2D & 3.2F).

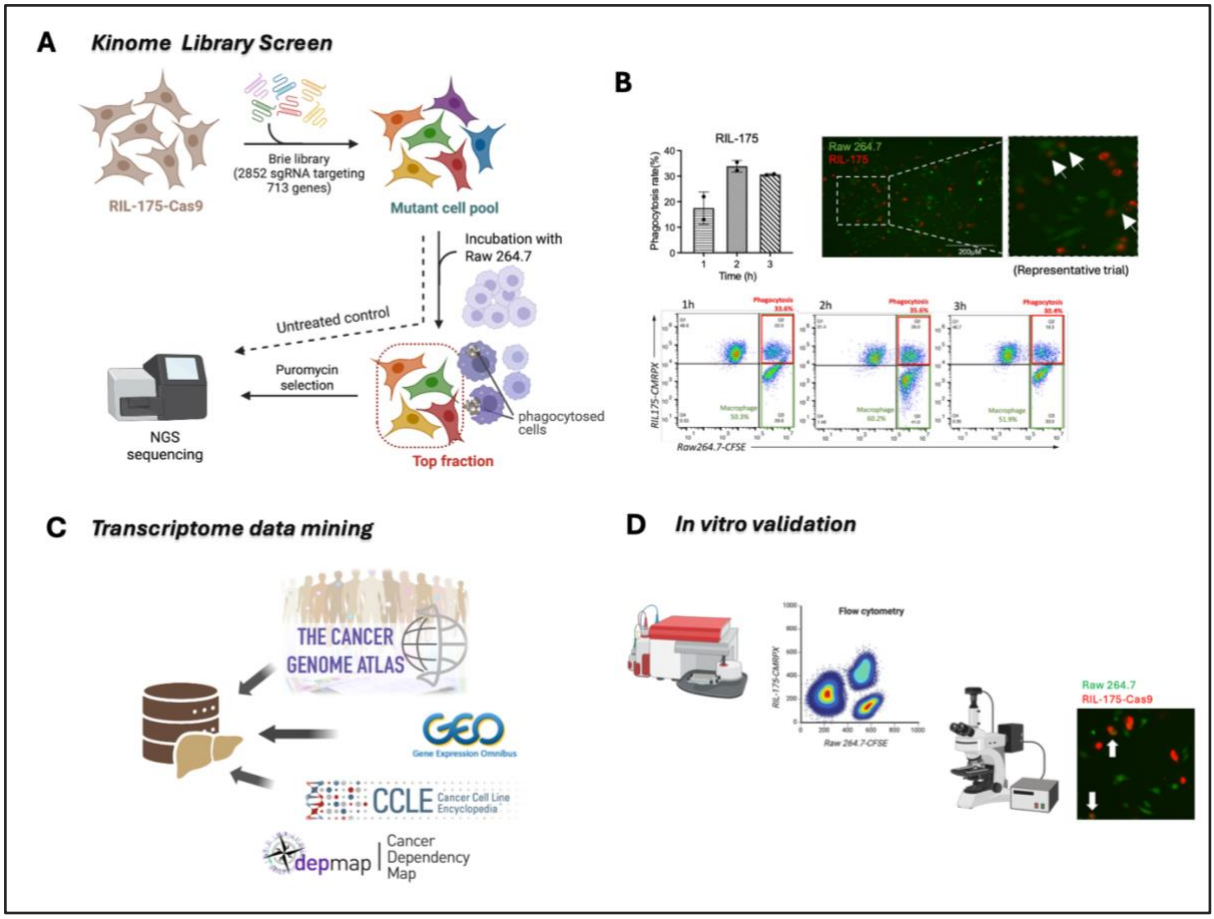

Figure 3.1 CRISPR KO screen in murine RIL-175 cells and validation strategies for identifying genes governing phagocytic evasion. (A) Graphical illustration of the schedule of the CRISPR/Cas9 knockout library screening. The Mouse Kinome CRISPR KO Library (Brie) was infected into RIL-175-Cas9 cells at low multiplicity of infection (MOI). And puromycin was applied for 2 days to select the mutant cell pool. The mutant cells were then cultured with or without mouse macrophages RAW264.7 in SFM for 16h, followed by elimination of phagocytosed cells and macrophages by isolating the top fraction and puromycin selection. The cells were allowed to recover for 2 days, followed by a second round of co-culturing with macrophages. Genomic DNA (gDNA) from untreated control mutant cells and co-cultured mutant cells was extracted, and gRNAs were amplified by PCR. (B) Phagocytosis rate of Raw264.7 cells on RIL-175 cells. (C) Examination of candidate(s) clinical relevance by transcriptome data mining of public clinical datasets. (D) Methods employed for *in vitro* validation of the screen hit(s).

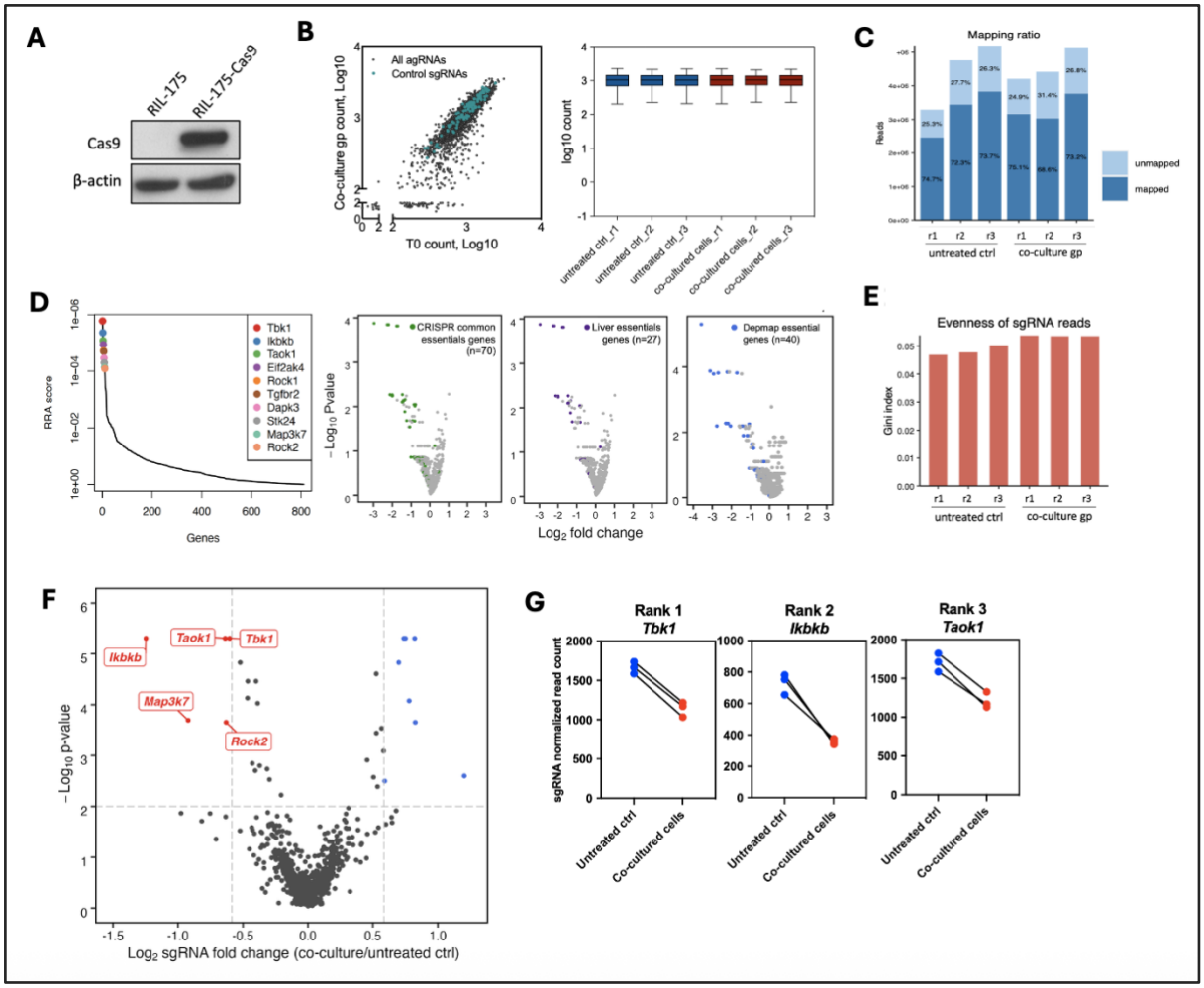

Figure 3.2 Screening quality and results. (A) Western blot analysis showing Cas9 overexpression in RIL-175 cells. (B) Distribution of normalized read counts for each sample of the CRISPR/Cas9 KO library screening (left). Sequencing counts of 2,852 sgRNAs in a T0 (initial cell) sample and a co-culture group sample (black dots) from the screen showing the most negative control sgRNA (green dots) are not enriched or dis-enriched between the two groups. (C) Mapping the rate of each sample. (D) Robust rank aggregation (RRA) score of the top-ranked depleted genes in the screen (left). Essential gene depletion in the initial cell pool was transduced with the Brie library (right). E) Gini Index of the untreated control group and co-culture group. (F) Volcano plot highlighting top-ranked screen hits in the screen that are negatively depleted in the co-culture group compared to the untreated control group (red dots; the significant depleted genes are labeled). (G) Line chart showing the average normalized read counts of four gRNAs in triplicate samples of top sensitizing hits in the library screen.

3.3 *Ikbkb* as a targetable top sensitizing hit that demonstrates clinical relevance and targetability

Among the top sensitizing hits, *inhibitor of nuclear factor kappa B kinase subunit beta* (*Ikbkb*) was found to be most dramatically depleted upon macrophage co-incubation, indicating that the loss of *Ikbkb* might potentiate phagocytic clearance by macrophages (Figure 3.2D). *Ikbkb* is implicated in diverse functions, including apoptosis, inflammation and angiogenesis; however, its role in cancer development remains controversial and it has not been previously implicated in the regulation of phagocytosis. To investigate if *Ikbkb* inhibition has potential therapeutic value for HCC, we first analyzed whether *Ikbkb* expression is differentially expressed in HCC tumors and associated with patient clinical outcomes. Analysis of multiple hepatocellular carcinoma (HCC) clinical datasets, The Cancer Genome Atlas Liver Hepatocellular Carcinoma (TCGA-LIHC), International Cancer Genome Consortium Liver Cancer - RIKEN, Japan (ICGC-LIRI-JP), and GSE36376, showed increased IKBKB mRNA expression in tumor tissue compared to adjacent non-tumor liver tissue (Figures 3.1C & 3.3A-B). Further examination of TCGA-LIHC data indicated that IKBKB levels were markedly elevated in advanced-stage tumors relative to early-stage tumors and normal samples, suggesting a potential role for *IKBKB* in disease progression (Figure 3.3C). Notably, IKBKB upregulation was more widespread across tumor samples than increases in established innate immune checkpoints such as CD24 and CD274 (Figure 3.3D). Although *IKBKB* is universally expressed across cell lines in the Cancer Cell Line Encyclopedia, data from DepMap indicate it is not essential for the growth of any of the 789 profiled lines under standard culture conditions, implying that targeting *IKBKB* may not cause broad cytotoxic effects (Figures 3.1C & 3.3E). To evaluate the role of *IKBKB* in macrophage-mediated antitumor immunity, we grouped HCC tumors based on *IKBKB* expression levels and performed Gene Ontology enrichment analysis on the resulting differentially expressed genes. This analysis revealed a significant association between high *IKBKB* expression and gene sets related to phagocytic processes (Figure 3.3F). Using the same stratification to analyze the immune cell infiltration levels by CIBERSORT-Absolute and ImmunCellAI databases, we observed that *IKBKB* expression was associated with reduced monocyte infiltration, suggesting a possible immunomodulatory role of *IKBKB* in HCC (Figure 3.3G).

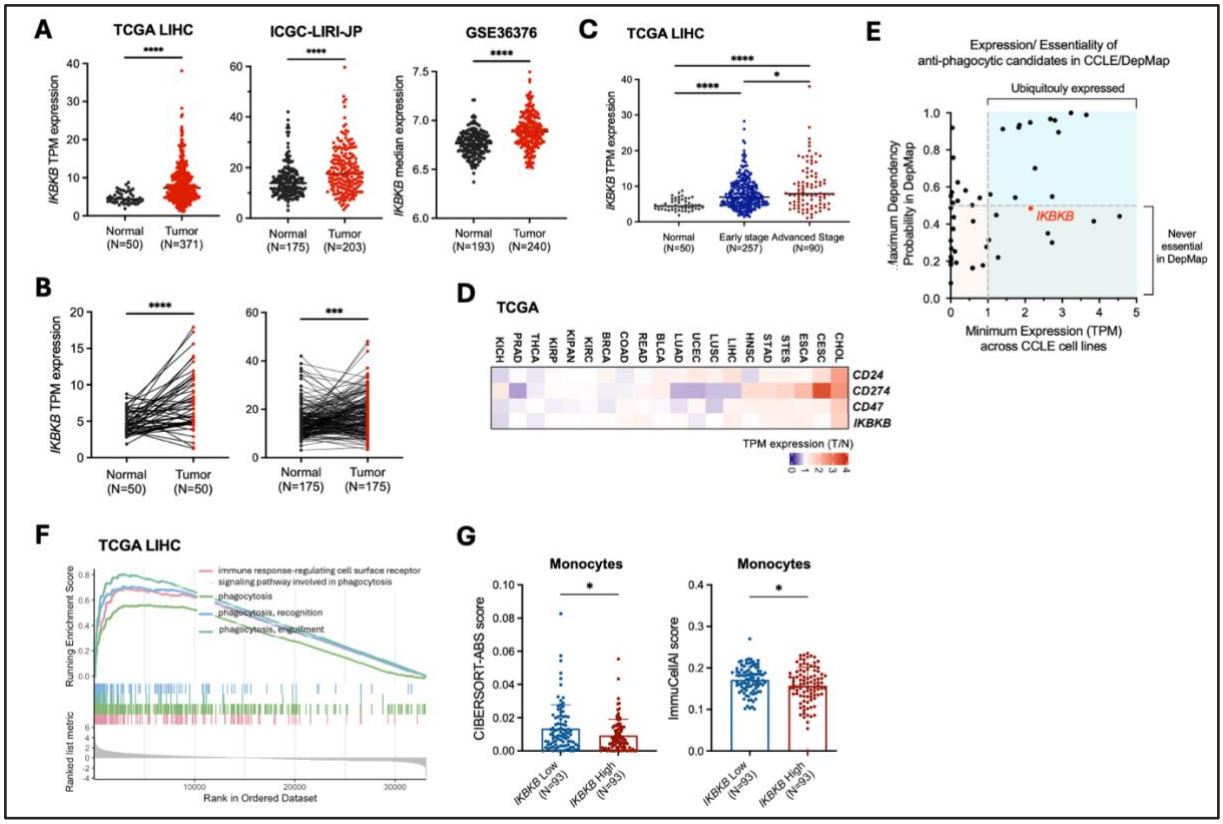

Figure 3.3 Clinical relevance of *IKBKB*. (A) High expression of *IKBKB* (TPM, transcript per million) was detected in HCC tumor samples compared to nontumor tissue. Data was extracted from The Cancer Genome Atlas Liver Hepatocellular Carcinoma (TCGA-LIHC), International Cancer Genome Consortium Liver Cancer - RIKEN, JP (ICGC-LIRI-JP) and GSE36376 databases. (B)The paired HCC tumor and tumor-adjacent normal tissues of corresponding dataset were plotted in the bottom. (C) Analysis of *IKBKB* expression in normal tissue and across HCC samples in early and late stage. (D) Heatmap of differential expression for *IKBKB* and known immune checkpoints in tumor samples compared to normal tissues in 20 tumor types. (E) For the negatively depleted genes identified in figure 3.1F, a scatter plot was generated comparing each gene's minimum expression level (in Transcripts Per Million, TPM) across all Cancer Cell Line Encyclopedia (CCLE) cell lines against its highest probability of being essential for cell survival from the DepMap dataset. Data are shown as the mean ± SEM (*p < 0.05, **p < 0.01, ***p <0.001,****p <0.0001; unpaired t-test with Welch's correction).

3.4 Depletion of *Ikbkb* enhances phagocytosis of HCC cells

To validate the role of *Ikbkb* in inhibiting cancer cell phagocytosis, we generated a stable *Ikbkb* KO subclone using the sgRNAs from the original screening library in RIL-175 cells, the cell line used in our 'discovery panel' (Figure 3.1D & 3.4A-B). Co-culture of the subline with mouse macrophages indicated that in the absence of additional stimulation, deletion of *Ikbkb* was sufficient to significantly enhance spontaneous phagocytosis compared to the non-targeting control, based on the results from FACS-based and microscopy-based measurements (Figure 3.4C). We further validated our results by a competitive phagocytosis assay. We co-incubated mouse macrophages with a mixture of RIL-175-NTC cells and RIL-175-sg*Ikbkb* cells labelled with different dyes. Subsequent fluorescence microscopy analysis and quantification of phagocytosis showed that *Ikbkb* KO induced preferential phagocytosis of RIL-175 cells, which further showed that the elimination of *Ikbkb* was sufficient to induce the phagocytosis of HCC cells *in vitro* (Figure 3.4C). To examine whether the phagocytic regulatory effect of *Ikbkb* can be recapitulated in human HCC cells, we engineered a stable *IKBKB* KO subline in PLC/PRF/5 cells using the CRISPR-Cas9 system with additional independent sgRNA (Figure 3.4A-B). Using *in vitro* phagocytosis assays, we validated that knockout of *IKBKB* in human HCC cells led to increased phagocytic clearance by human macrophages, THP-1, collaborating with our findings in the mouse cell model and confirming the role of *Ikbkb* in inhibiting phagocytosis (Figure 3.4D). It is important to note that the sublines assessed above had no measurable cell-autonomous differences in proliferation, indicating that the observed potentiation of phagocytosis by *Ikbkb* depletion was not attributed to increased uptake of dying cells by human or mouse macrophages (Figure 3.4E).

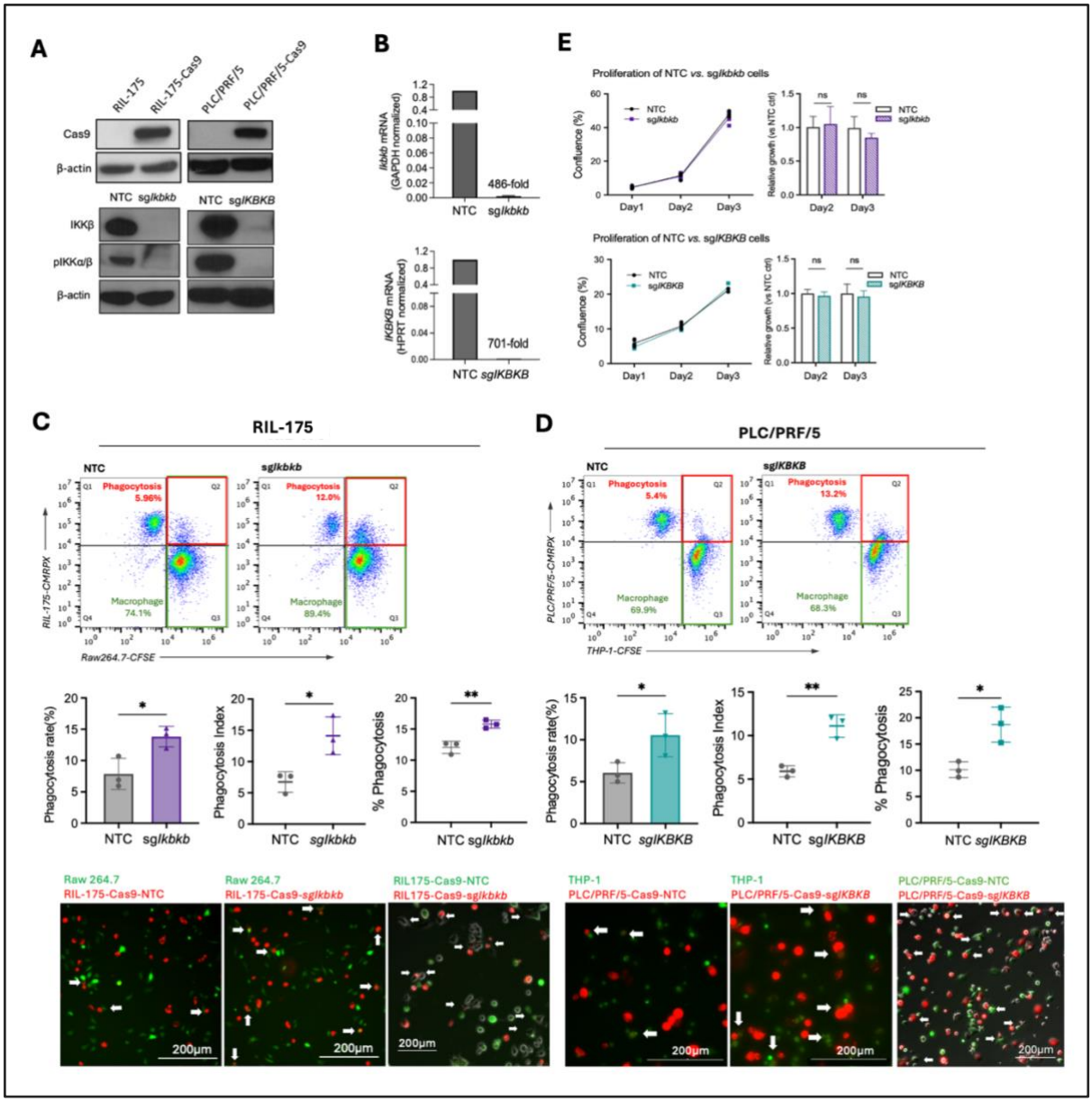

Figure 3.4 *In vitro* validation of phagocytic regulatory role of *Ikbkb* (A,B) *Ikbkb* expression levels upon gene depletion in RIL-175 cells and PLC/PRF/5 cells by Western Blot analysis (A) and qPCR (B). (C,D; top) Representative FACS plots showing phagocytosis rate in RIL175-NTC cells *vs*. sg*Ikbkb* cells (C) or PLC/PRF/5-NTC *vs*. -sgI*KBKB* cells (D). (C, D; middle) Bar chart showing phagocytosis rate determined by flow cytometry (N=3). Dot plot showing phagocytosis index and competitive phagocytosis rate determined by microscopy-based phagocytosis assay (N=3, n=3, respectively). (C, D; bottom) Representative fluorescence microscopic images of three independent experiments; Arrows indicated the macrophages (double colors) that phagocytosed cancer cells. (E) Cancer cell proliferation measured by light microscope (left) and MTT assay (right) (n=4; ns, not significant; two-tailed Student's t-test).

3.5 Discussion

Our CRISPR knockout screen has uncovered five anti-phagocytic candidates that could serve as targets for re-potentiating macrophage antitumor immunity. Inhibitor of nuclear factor kappa B kinase subunit beta (IKKβ, encoded by *IKBKB)* represents one of the top sensitizing hits. The screening result was further confirmed by *in vitro* validation that genetic ablation of *IKBKB* robustly enhanced phagocytosis in both mouse and human HCC models, independent of its effects on cell proliferation. Clinical bioinformatic analyses support the translational potential of this target. The upregulation of *IKBKB* in HCC tumors compared to normal tissue, its association with advanced disease stage, and its broader overexpression across cancers relative to established immune checkpoints like PD-L1 position it as a potential oncogenic driver. Critically, the observation that *IKBKB* is not a common essential gene in DepMap suggests its therapeutic targeting may have a favourable toxicity profile, potentially sparing normal tissue while specifically targeting a key survival mechanism in cancer cells. This concept of targeting context-dependent vulnerabilities, rather than pan-essential genes, represents a central tenet of cancer therapeutic development.

Our hypothesis posits that targeting IKKβ in HCC could activate macrophage-mediated clearance of tumor cells and suppress tumor progression. Nonetheless, this hypothesis encounters the well-documented and context-dependent paradox of IKKβ signaling in liver cancer (Luedde & Schwabe, 2011). For instance, Maeda et al. (2005) reported that *IKBKB* depletion in murine hepatocytes increases hepatocarcinogenesis in a diethylnitrosamine (DEN) model. Their mechanistic work revealed that hepatocyte-specific IKKβ loss increases reactive oxygen species (ROS) production and Jun N-terminal kinase (JNK) activation, leading to enhanced hepatocyte death and compensatory proliferation of surviving hepatocytes, and this drives tumor initiation. Conversely, other studies have presented opposing evidence. For example, systemic or Kupffer cell-specific inhibition of IKKβ was shown to slow hepatocarcinogenesis and decrease tumor incidence in HCC and colitis-associated cancer (Greten et al., 2004; Shiha et al., 2019). In the chemical hepatocarcinogenesis model, it was shown that *IKBKB* targeting in hepatocytes and Kupffer cells reduced hepatocyte regeneration and suppressed hepatomitogen induction. While our *in vitro* data show that IKKβ loss in cancer cells enhances phagocytic clearance, its role in macrophages is also important. Hagemann et al. (2008) have demonstrated that myeloid-specific depletion of IKKβ polarizes macrophages toward an antitumor M1 subtype, with enhanced release of interleukin-12 (IL-12) and potent antigen presentation ability. Therefore, a systemic IKKβ inhibitor might deliver a dual

therapeutic benefit: sensitizing the cancer cells to phagocytosis while simultaneously stimulating the macrophage effector.

Given that cell line models lack of tumor microenvironment with stroma, immune cells, and blood vessels, it is imperative to study the role of IKKβ in controlling cancer cell phagocytosis *in vivo.* Our observation that I*KBKB* genetic depletion does not affect cancer cell proliferation in the HCC cell model makes it crucial to examine its effect on tumor growth *in vivo*. Furthermore, while our bioinformatic analysis of the TCGA-LIHC dataset found that high *IKBKB* was associated with reduced monocyte infiltration but not a significant change in total macrophage infiltration, it is essential to investigate how IKKβ expression in cancer cells alters macrophage function, such as polarization or activation state. Taken together, several key questions remain: Does cancer cell-specific IKKβ suppression suffice to suppress tumor growth *in vivo* via enhanced phagocytosis? Does systemic inhibition offer superior efficacy by co-targeting the macrophage compartment? Answering these questions will determine whether IKKβ inhibition represents a viable strategy to overcome phagocytosis evasion in HCC.

An important finding from out screen was the identification of five candidate genes in cancer cells that appear to suppress phagocytosis. Among them, three genes (i.e. *Ikbkb*, *Tak1* and *Tbk1*) are known to function as positive regulators of the canonical NF-κB signaling pathway. *Ikbkb* serves as the main catalytic subunit of the IKK complex, which is the central regulatory hub of the axis, and its involvement will be further discussed in the subsequent chapter. Transforming growth factor beta-activated kinase 1 (*Tak1*) functions upstream by activating *Ikbkb* through phosphorylation in response to signal such as IL-1 or TNFα (Takaesu et al., 2003). Meanwhile, TRAF Family Member Associated NFKB Activator-binding kinase 1 (*Tbk1*) contributes to pathway activation by directly phosphorylating both the activation loop of Ikbkb and p65 subunit of p65, particularly in contexts like innate immunity and oncogenic transformation (Runde et al., 2022). Together, these highlight the critical role of canonical NF-κB signaling in modulation phagocytosis and suggest targeting *Ikbkb*, a core component of the pathway, could be promising strategy to restore the phagocytic elimination of cancer cells.

CHAPTER 4 *Ikbkb* augments HCC tumor growth by suppressing macrophage-mediated phagocytosis

4.1 Introduction

Unleashing macrophage phagocytic ability for tumoral control

Among the immune populations in the TME, macrophages represent the most abundant immune cell type in most types of malignancies, and studies have illustrated the clinical utility of inducing macrophage phagocytosis, mostly via ADCP, in anticancer therapies. Monoclonal antibodies, such as trastuzumab, rituximab, and daratumumab, have been shown to rely on ADCP for effective tumor killing in breast cancer, lymphoma, and multiple myeloma in mouse models (Sawa-Wejksza & Kandefer-Szerszeń, 2017; Cao et al., 2022; Phipps et al., 2015). In a non-Hodgkin lymphoma patient biopsy, it was observed that the macrophage abundance is associated with the clinical efficacy of rituximab (Vaughan et al., 2024). These findings highlight the importance of macrophage phagocytosis in tumor control across multiple cancer types. Nonetheless, the use of these approaches has been shown to have limited clinical benefits owing to the fact that inadequate monoclonal antibodies could be administered via the current administration routes to reach the local threshold to effectively induce ADCP. Several combination regimens have been investigated to lower the threshold for ADCP or potentiate macrophage phagocytic capabilities. For example, cyclophosphamide, an alkylating drug, stimulates macrophage phagocytosis and suppresses lymphoma tumor cell growth when administered in combination with the anti-CD52 monoclonal antibody alemtuzumab (Lossos et al., 2019). A Toll-like receptor agonist, CpG oligodeoxynucleotide, also demonstrated a macrophage stimulatory effect by downregulating anti-phagocytic signals and increasing phagocytosis of pancreatic ductal adenocarcinoma cells (Liu et al., 2019). Paclitaxel, a commonly used chemotherapy for multiple malignancies, has been found to effectively enhance ADCP of lymphoma cells and colorectal cancer cells in xenograft and PDX models when combined with rituximab or cetuximab. The authors illustrated that paclitaxel could enhance the phagocytic ability of macrophages via CSF1R suppression, which might account for the ameliorated anticancer effect observed in the combination treatment (Cao et al., 2022).

As discussed previously, strategies that aim to “re-educate” macrophages from pro-tumorigenic to tumoricidal states are under active investigation. Promising results from late-stage clinical trials, such as those combining CD40 or TLR agonists with standard treatments for advanced pancreatic and head and neck cancers, confirm the potential of macrophage activity as a central strategy for cancer immunotherapy. In the present study, we aimed to

restore the phagocytic ability of macrophages by targeting cancer cells, specifically by dampening the “don't eat me” signal on cancer cells and rendering them susceptible to phagocytic clearance. Using the CRISPR KO screen, we identified *Ikbkb* as the top hit for conferring an antiphagocytic effect in HCC cells. In this study, we examined the *in vivo* role of *Ikbkb* in tumor growth and how it mediates the interplay between macrophages and tumor cells using a gene knockout approach.

4.2 Method

Subcutaneous mouse models for examining the role of Ikbkb in phagocytic evasion and tumoral control

The role of IKKβ in tumor control was first examined by subcutaneously implanting modified HCC cells, that is, RIL-175 or PLC/PRF/5 cells with or without IKKβ loss, into T cell-deficient nude mice to assess tumor development, macrophage infiltration, and macrophage functional status (Figure 4.1). To verify the specific contribution of macrophages to this process, we systemically depleted macrophages using clodronate liposomes prior to the implantation of RIL-175 tumor cells and examined the subsequent effect on tumor growth (Figure 4.1). Finally, to determine whether enhanced phagocytosis of *Ikbkb knockout* cells occurs *in vivo*, we fluorescently tagged both murine (RIL-175) and human (PLC/PRF/5) HCC cells, with or without *Ikbkb* knockout, with GFP to directly assess phagocytic clearance (Figure 4.1).

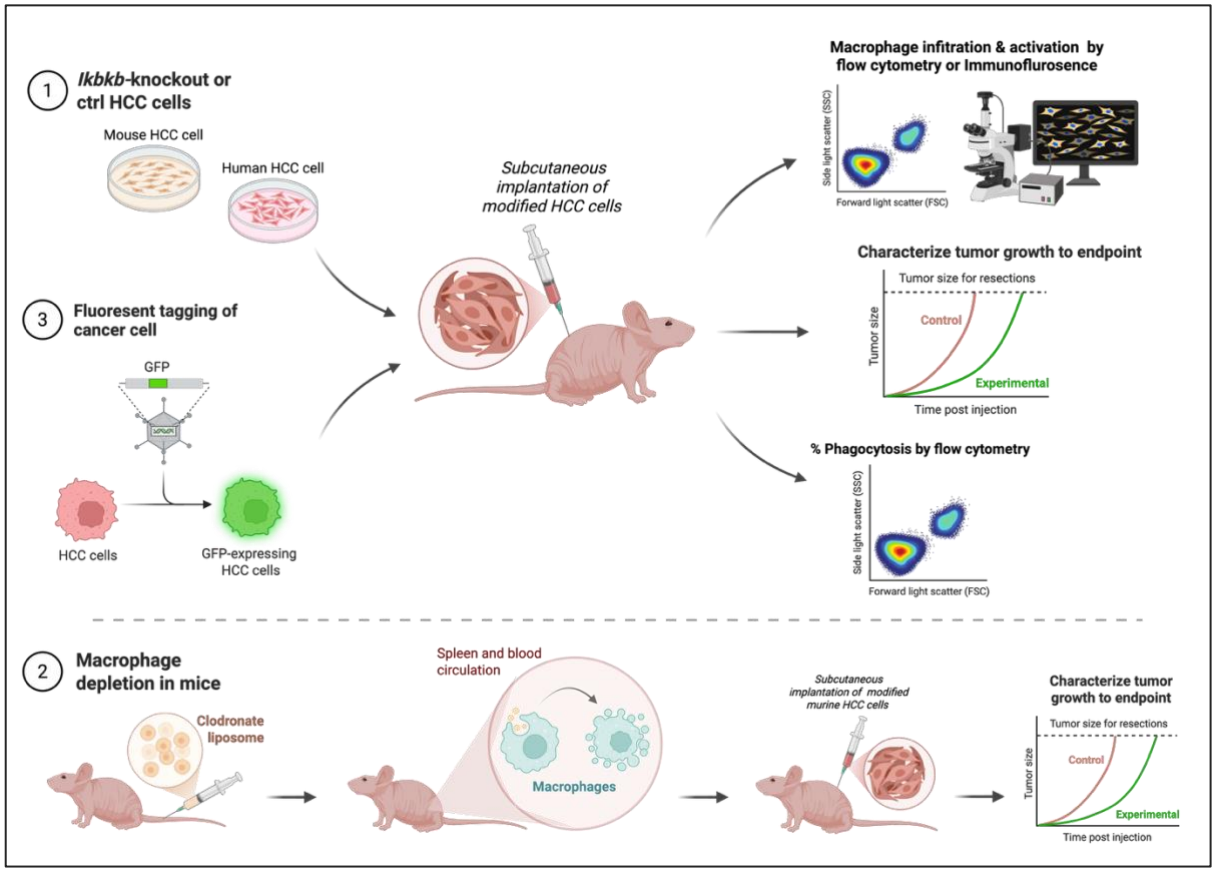

Figure 4.1 Mice model employed to investigate the effect of *Ikbkb* on tumorigenesis, the plausible macrophage-dependencies, and the *in vivo* phagocytosis.

4.3 *Ikbkb* augments HCC tumor growth in syngeneic and xenograft mice models

In this chapter, we first examined the role of *Ikbkb* in HCC tumor growth by subcutaneously injecting stable *Ikbkb* knockout sublines into mice. We successfully confirmed that gene depletion was maintained following tumor establishment (Figure 4.2A). *Ikbkb* knockout drastically diminished tumor burden in both RIL-175 syngeneic and PLC/PRF/5 xenograft models, despite having no observable effect on cell proliferation in the respective cell models (Figure 4.2 B, 3.4E). This discrepancy implies that tumor regression was not caused by a cell-intrinsic effect but was likely facilitated by modulation of the TME. Fluorescence-activated cell sorting (FACS) analysis of *Ikbkb* knockout tumors revealed heightened macrophage infiltration, suggesting that macrophages are potential mediators of the antitumor response (Figure 4.2C-D).

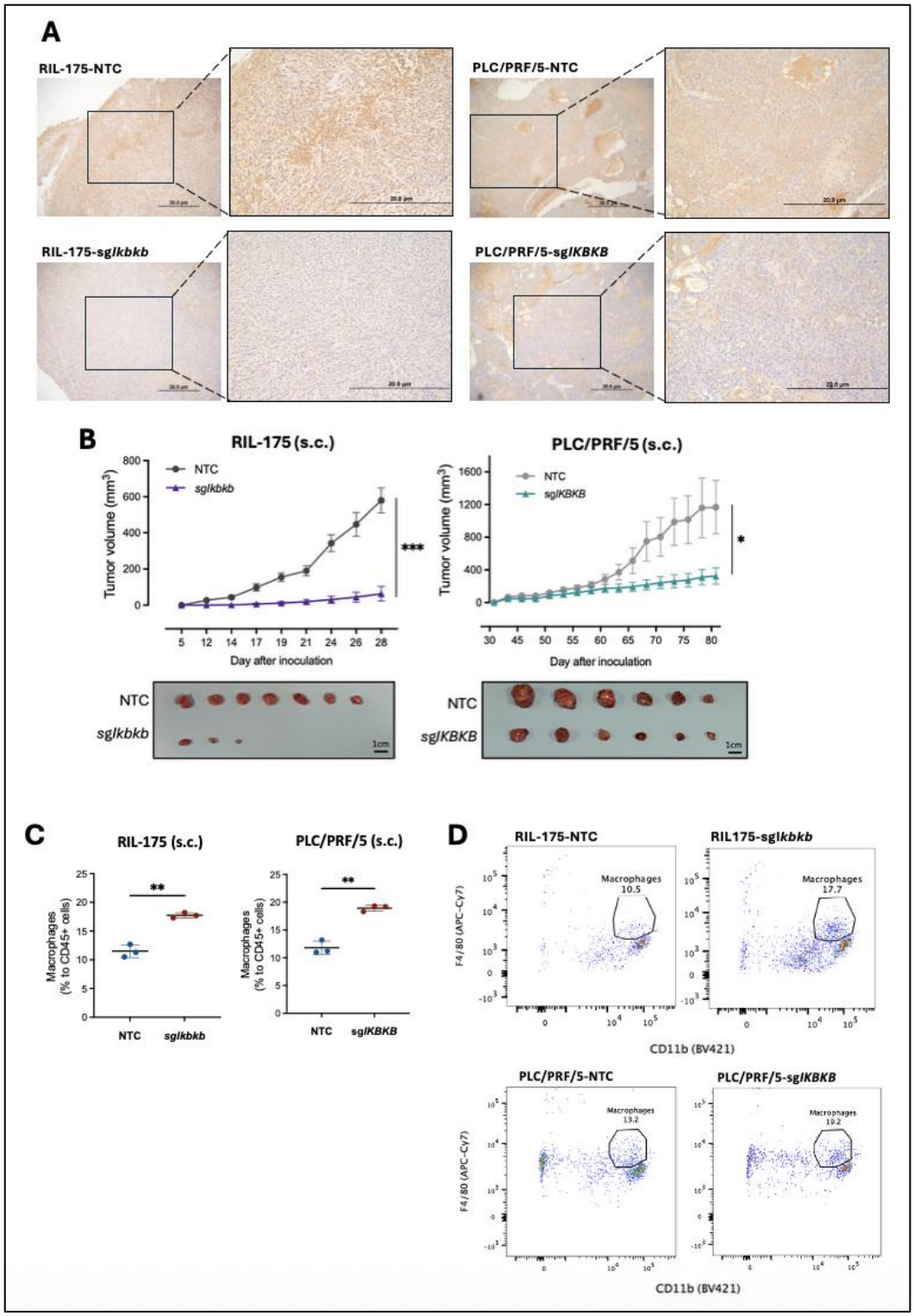

Figure 4.2 *Ikbkb* depletion suppresses HCC tumor growth. (A) Representative IHC images for Ikbkb of syngeneic and xenograft tumors from mice injected with control (NTC) and *Ikbkb* knockout (sg*Ikbkb*) RIL175 cells (top) and PLC/PRF/5 cells (bottom). (B)(Top) *In vivo* tumor growth following subcutaneous injection of RIL175-Cas9-NTC and -sg*Ikbkb* cells (n=4 mice, $1e^4$ cells) (left) or PLC/PRF/5-Cas9-NTC and -sg*IKBKB* cells (n=4 mice, $8e^5$ cells) (right) in

BALB/c nude mice. Tumor volumes were measured by calliper, and the data are shown as the mean ± SEM (*$p < 0.05$, **$p < 0.01$; multiple unpaired t-test). (Bottom) Representative tumor images on day 28 or 80 (for RIL175 cells or PLC/PRF/5 cells, respectively) after engraftment. (C) Percent macrophage infiltration into the syngeneic and xenograft tumors (n=3 replicates). (D) Representative FACS plots showing the percentage of infiltrating macrophages among live immune cells in the tumors.

4.4 *Ikbkb* augments HCC tumor growth by evading macrophage-mediated phagocytosis

To elucidate whether macrophages are the key cell population responsible for tumor clearance in *Ikbkb* knockout tumors, we depleted the mice's macrophages using clodronate liposomes prior to tumor inoculation and assessed tumor growth. The macrophage depletion efficiency was validated to be over 80% in the mouse spleen (Figure 4.3A). Macrophage depletion in mice did not alter the burden of wild-type tumors, whereas depletion largely abolished the reduction in tumor burden in *Ikbkb* knockout tumors, suggesting that increased macrophage-mediated clearance of *Ikbkb* knockout cells causes a reduction in tumor growth (Figure 4.3B). We also observed that either depletion of macrophages or *Ikbkb* did not alter cell proliferation *in vivo*, which is consistent with our previous *in vitro* findings and further validates that the tumor regression was not attributed to cell cell-autonomous effect caused by *Ikbkb* depletion, but rather imposed by macrophage attack (Figure 4.3C, 3.4E).

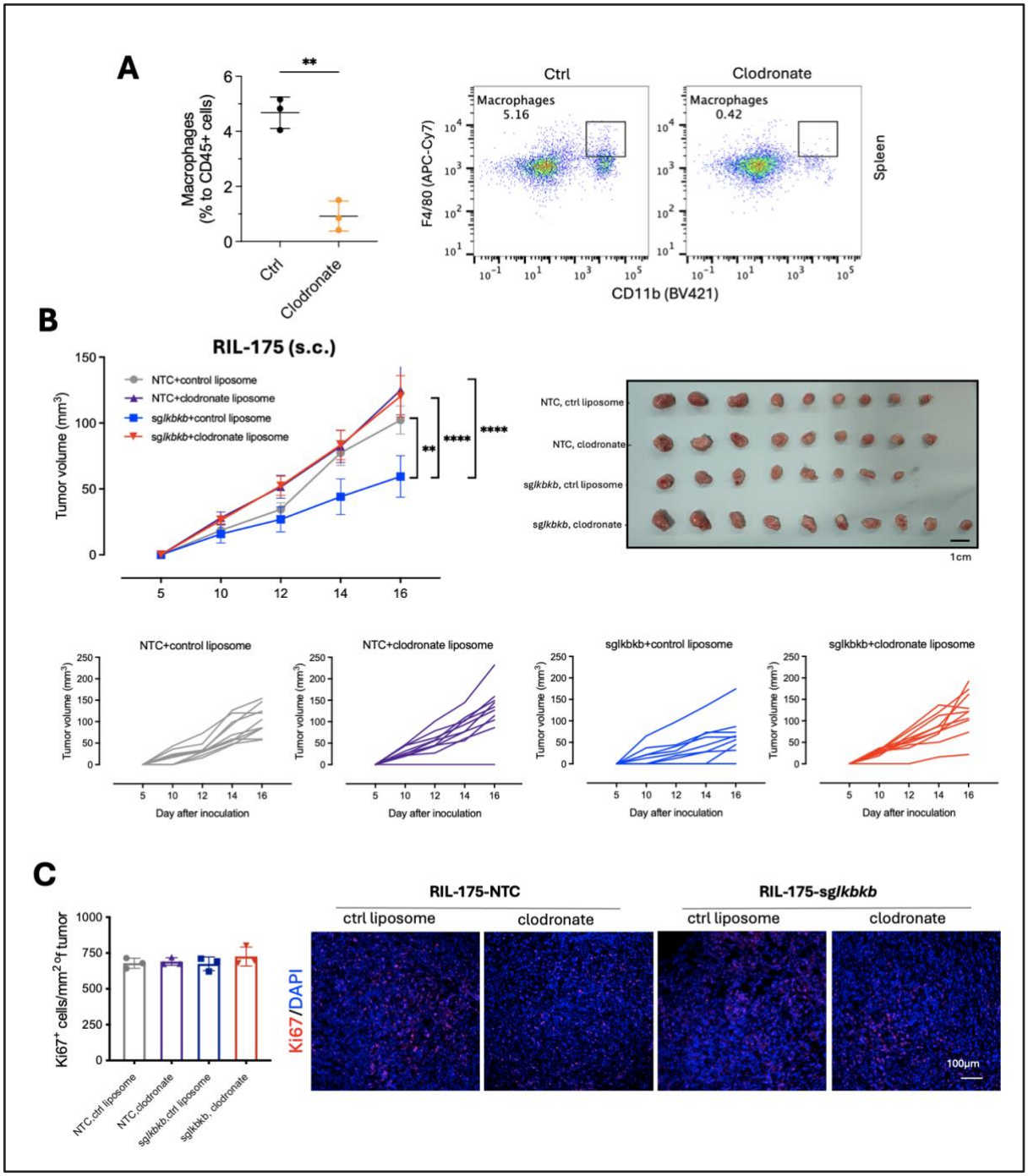

Figure 4.3 *Ikbkb* assists cancer cells to evade macrophage surveillance (A) (Left)Quantitative analysis of splenic macrophage depletion by clodronate liposome. Frequency of CD11b+F4/80+ out of total live immune cells in control liposome-treated mice (n = 3) versus clodronate liposome-treated mice (n=3) as measured by flow cytometry. (Right) Representative FACS staining images showing the splenic macrophage depletion by clodronate liposome. (B) (Top, left) *In vivo* tumor growth following subcutaneous injection of RIL175-Cas9-NTC and -sg*Ikbkb* cells in BALB/c nude mice with control liposome or clodronate liposome (n=5 mice/group, $2e^4$ cells). Control or clodronate liposome administered intravenously

24h prior to RIL-175 cells inoculation, followed by IP injection of liposome twice per week to maintain macrophage depletion. Tumor volumes were measured by calliper, and data are shown as the mean ± SEM (**p < 0.01, ****p <0.0001; 2-way ANOVA followed by Tukey's multiple comparison test). (Top, right) Tumor images obtained on day 18 after engraftment. (Bottom) Tumor growth curves for individual mice. (C) (Left) Quantification of $Ki67^+$ area relative to cell number, Scale bar: 100 μm. Data are mean ± SEM (unpaired t-test). (Right) Representative immunofluorescence (IF) images for cell proliferation (Ki67, red) of syngeneic and xenograft tumors. Nuclei are counterstained with DAPI (blue).

4.5 *Ikbkb* limits phagocytic clearance of HCC tumor cells by macrophages *in vivo*

To verify whether macrophages eliminate *Ikbkb* knockout cells by phagocytosis, we used GFP as a fluorescent tag to track HCC cells and generated GFP-expressing sublines in control and *Ikbkb* knockout cells for engraftment into the mouse model to measure the *in vivo* phagocytosis rate. We confirmed that GFP was stably expressed in both RIL-175 and PLC5/PRF/5 cells, and the tumor-suppressive effect of *Ikbkb* loss was recapitulated in GFP-expressing sublines (Figure 4.4A, B). We found that *Ikbkb*-deficient tumors showed increased macrophage infiltration with elevated levels of *in vivo* phagocytosis by infiltrating macrophages compared to control tumors (Figure 4.4C). This is consistent with our previous *in vitro* results, which indicated that *Ikbkb* knockout results in enhanced phagocytosis in a direct co-culture system of HCC cells and macrophages (Figure 3.4C-D). Notably, Ikbkb expression was enriched in tumors containing a mixture of equal numbers of control and *Ikbkb* KO cells, suggesting that *Ikbkb*-deficient cells are preferentially eliminated in syngeneic and xenograft models (Figure 4.4D). We postulated that the loss of *Ikbkb* facilitates clearance through macrophage engulfment based on our observations that *Ikbkb* depletion increases phagocytosis in both cell and mouse models, as well as the preferential phagocytic elimination of *Ikbkb*-deficient cells in the competitive phagocytosis assay (Figure 3.4C-D).

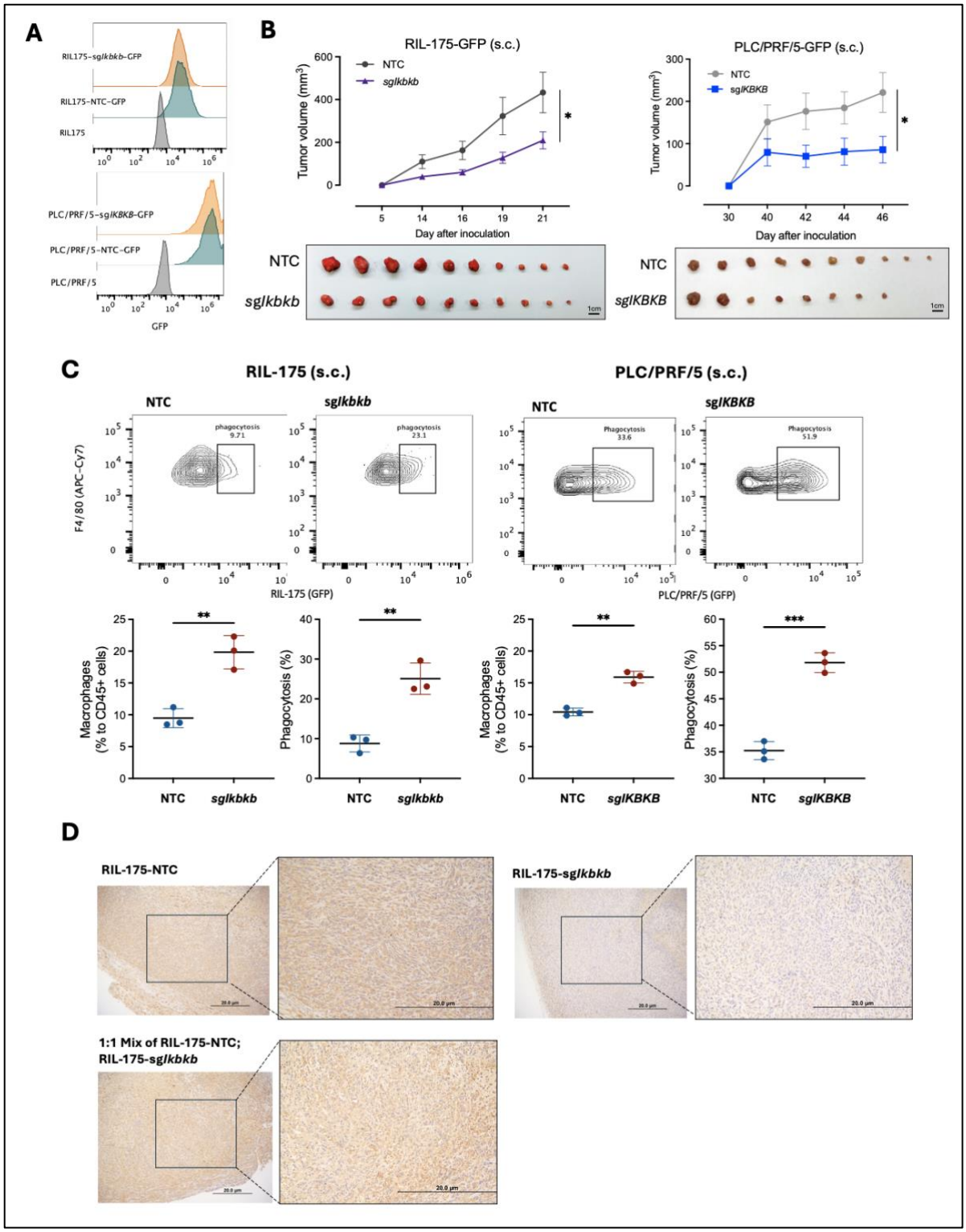

Figure 4.4 Tumor-intrinsic *Ikbkb* inhibits macrophage-mediated phagocytosis *in vivo*. (A) GFP expression in control or *Ikbkb* knockout RIL-175 and PLC/PRF/5 cells as determined by FACS analysis. (B) *In vivo* tumor growth following subcutaneous injection of RIL175-NTC-GFP and -sg*Ikbkb*-GFP cells (n=5 mice, $2e^4$ cells) (left) or PLC/PRF/5-NTC-GFP and -sg*IKBKB*-GFP cells (n=5 mice, $8e^5$ cells) (right) in BALB/c nude mice. Tumor volumes were

measured by calliper, and the data are shown as the mean ± SEM (*$p < 0.05$; multiple unpaired t-test). (Bottom) Representative tumor images on day 21 or 46 (for RIL175 cells or PLC/PRF/5 cells, respectively) after engraftment. (C, Top) Representative FACS staining images showing *in vivo* phagocytosis rate of tumor-infiltrating macrophages of mice engrafted with RIL-175-NTC or -sg*Ikbkb* cells (left, n=5 mice/group, $2e^4$ cells) or with PLC/PRF/5 -NTC or -sg*IKBKB* cells (right, n=5 mice/group, $8e^5$ cells). (C, Bottom) Percent macrophage infiltration (F4/80+CD11b+ cells among live immune cells) and *in vivo* phagocytosis rate of tumor-infiltrating macrophages (GFP+F4/80+CD11b+CD45+ cells) of respective mice models. (D) Representative IHC images for Ikbkb of syngeneic tumors from mice injected with control (NTC), *Ikbkb* knockout (sg*Ikbkb*), or both (at a 1:1 ratio) RIL-175 cells.

4.6 Cancer-intrinsic *Ikbkb* regulates the phenotype of infiltrating macrophages

Next, we explored the immunomodulatory effects of *Ikbkb-targeting* in macrophages. We observed that *Ikbkb*-knockout tumors showed upregulation of CD80 and CD86 expression, which are two macrophage activation markers commonly used to infer the functional state of macrophages (Figure 4.5). This suggests that targeting *Ikbkb* in tumors shifts macrophages towards M1-like states, which possess higher phagocytic and antitumor activities.

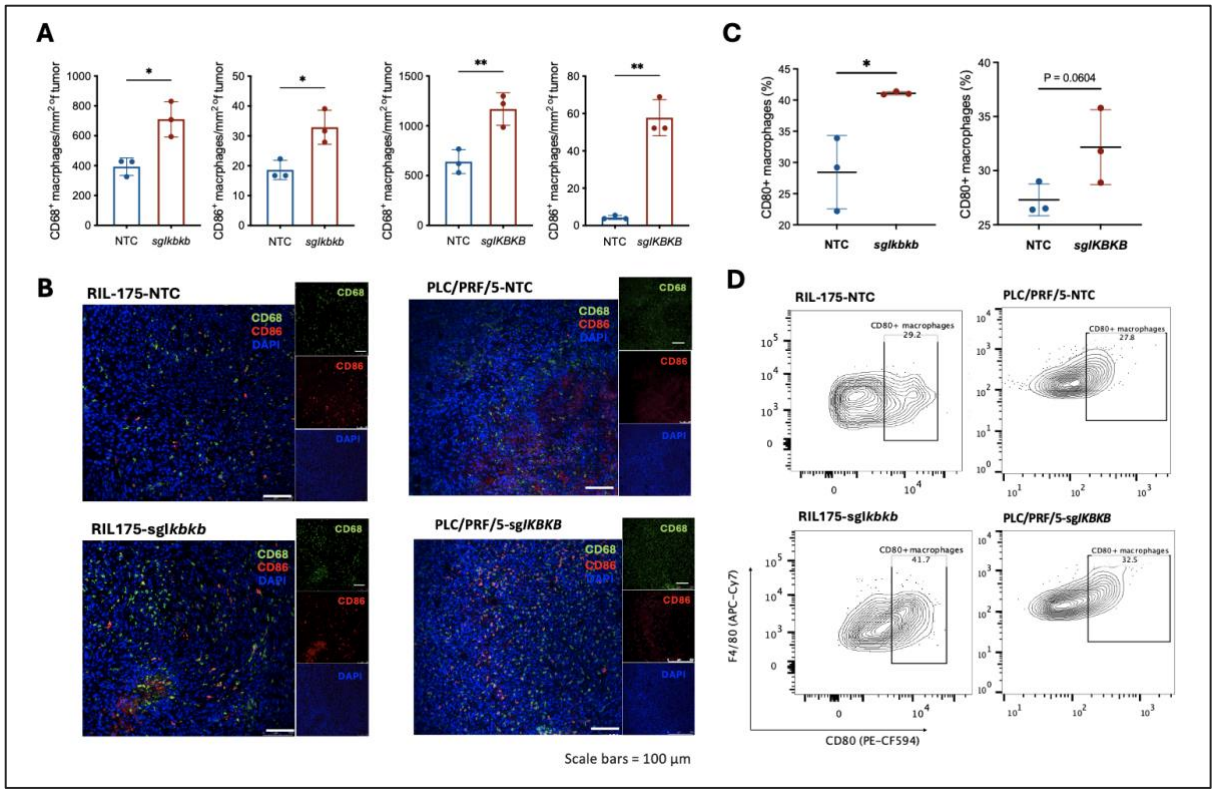

Figure 4.5 Tumor-expressed *Ikbkb* modulates macrophage phenotype (A) Quantification of CD86^{+} and CD68^{+} signal measured by immunofluorescence (IF), Scale bar: 100 µm. (B) Representative IF images for macrophage activation marker and macrophage marker of syngeneic or xenograft tumors. Nuclei are counterstained with DAPI (blue). (C) Quantitative analysis of CD80+ macrophages (among F4/80+CD11b+CD45+ cells) infiltrated into syngeneic or xenograft tumors. (D) Representative FACS staining images showing CD80+tumor tumor-infiltrating macrophages of syngeneic or xenograft models.

4.7 Discussion

As discussed in the previous chapter, the role of *Ikbkb* in tumor development remains controversial. Nevertheless, previous studies have conducted genetic manipulation in normal epithelial cells or myeloid cells to examine the role of *Ikbkb* in tumorigenesis, whereas gene depletion in tumor cells to understand its therapeutic potential has yet to be investigated. Our results showed that loss of *Ikbkb* was sufficient to substantially suppress tumor growth. Notably, potent tumor suppression was not due to the intrinsic proliferative effect caused by *Ikbkb* knockout but was entirely dependent on the presence of macrophages. This aligns with the broader understanding of the TME, where macrophages are among the most abundant immune cells, and their functional state critically dictates antitumor immunity (Palmer et al., 2025). Our *in vivo* phagocytosis experiments provided direct evidence that *Ikbkb* deficiency in cancer cells leads to increased macrophage infiltration and a higher rate of tumor cell engulfment. Importantly, this enhanced phagocytosis correlated with a shift in the infiltrated macrophages toward a more activated phenotype, as indicated by the elevated expression of co-stimulatory molecules CD80 and CD86. This suggests that *Ikbkb* loss in cancer cells does not merely enhance the phagocytic signal in cancer cells but actively reprograms the surrounding immune landscape by promoting the recruitment and M1-like polarization of TAMs. The "re-education" of TAMs towards a more tumoricidal state is a recognized therapeutic goal, as M1 macrophages are associated with enhanced phagocytic activity and tumor cell killing, and repolarization is a major focus in cancer immunotherapy (Palmer et al., 2025). Our data indicate that targeting IKKβ, a single kinase, within cancer cells may achieve this reprogramming *in trans*. These data position IKKβ inhibition as a bifunctional therapeutic strategy: it directly removes a cancer cell's protective shield against phagocytosis while simultaneously altering the TME to foster a more immunostimulatory macrophage population. This hypothesis will be investigated in subsequent chapters in immunocompetent *in vivo* settings.

In the current study, we studied *in vitro* phagocytosis by labelling cancer cells and macrophages with cell tracing or cell tracking dyes and *in vivo* phagocytosis by fluorescently tagging cancer cells. However, these approaches have several constraints. One major limitation is that fluorescent tagging is unable to distinguish between adherence or fluid-phase pinocytosis; that is, macrophages may merely adhere to tumor cell fragments or dying tumor cells or take up free GFP released by dead tumor cells, leading to an overestimation of the actual phagocytic rate (Levin-Konigsberg & Mantegazza, 2020). Another concern is that

GFP protein and cell-tracing dyes are sensitive to proteolytic and acidic degradation, resulting in the quenching of fluorescence signals; thus, these assays may only be able to capture the early phase of phagocytic events (Bogdanov et al., 2002). Despite these limitations, the prominent increase in GFP+ macrophages in *Ikbkb*-knockout tumors, corroborated by our *in vitro* co-culture data, strongly supports the conclusion that Ikbkb depletion enhances phagocytosis. Future studies could employ more definitive approaches, such as pH-sensitive fluorescent tags (to distinguish internalized acidic compartments) or immunohistochemistry for phagosomal markers, such as LAMP-1, LAMP2, and Rab7, in conjunction with tumor cell tags, to further validate and refine these findings Levin-Konigsberg & Mantegazza, 2020).

This chapter establishes that tumor-intrinsic *Ikbkb* expression is a critical regulator of tumor growth by modulating the macrophage activity. Nonetheless, the mechanism by which IKKβ signaling in cancer cells is communicated to macrophages remains unknown. Consequently, a primary objective of our subsequent investigation was to delineate the signaling axis by which tumor cell *Ikbkb* activity is transduced to elicit functional changes in macrophages.

CHAPTER 5 *Ikbkb* evades macrophage-mediated phagocytosis by upregulating ‘don't eat me’ signals through NF-κB signaling

5.1 Introduction

Phagocytic checkpoints and possible regulation by IKK/NF-κB signaling

Macrophage phagocytic ability is dictated by a delicate balance between pro-phagocytic ("eat me") and anti-phagocytic ("don't eat me") signals displayed on cancer cells. Cancer cells evolve to overexpress anti-phagocytosis molecules, including cluster of differentiation 47 (CD47), programmed death-ligand 1 (PD-L1), cluster of differentiation 24 (CD24), the beta-2 microglobulin (β2M) subunit of the major histocompatibility class I complex (MHC-I), Disialoganglioside GD2, and stanniocalcin 1 (STC-1), which engage inhibitory receptors on macrophages to effectively disguise themselves as "self" and thereby avoid macrophage-mediated eradication (Figure 5.1).

The CD47-SIRPα axis is the most prominent and therapeutically targeted "don't eat me" signal. CD47 is widely overexpressed on cancer cells, and its interaction with Signal Regulatory Protein Alpha (SIRPα) on macrophages initiates an intracellular tyrosine phosphatase (SHP-1/2) signal that suppresses myosin IIA accumulation in phagocytic synapses, physically preventing the engulfment of the tumor cell (Cassetta and Pollard, 2018). Nonetheless, the widespread expression of CD47 in normal cells, including platelets and red blood cells, has raised concerns regarding hepatotoxicity, specifically anemia and thrombocytopenia (Liu et al., 2023). Strategies to circumvent this potential toxicity include blocking the interacting receptor SIRPα on phagocytes and using anti-CD47 antibodies with weak cytolytic properties (TTI-621, TTI-622, and ALX148) or bispecific agents targeting both CD47 and tumor-associated antigens (such as EGFR, CD20, PD-L1, and CD19) (Zhuang et al., 2025; Shitara et al., 2025).

While the PD-1/PD-L1 axis is a well-known T-cell immune checkpoint, recent evidence has confirmed that it also directly dampens the phagocytic function of TAMs. In the TME, TAMs showed upregulated PD-1 levels, and the expression was associated with a protumoral, M2-like polarization state (Feng et al., 2019). Phenotypically, these PD-1^+ TAMs exhibited a significantly weakened phagocytic ability compared to PD-1^- subsets (Feng et al., 2019). This study also showed that blocking PD-1/PD-L1 signaling with a PD-L1 inhibitor (HAC; an engineered protein devoid of an Fc domain that unable to induce Fc-mediated phagocytosis), robustly enhanced macrophage-mediated phagocytosis and exerted antitumor effects in T-cell-deficient NOD SCID gamma (NSG) mouse models. This suggests a direct antitumor role for the PD-1/PD-L1 phagocytosis checkpoint.

Recent studies have demonstrated that IKKβ, through its canonical role in activating the NF-κB pathway, directly maintains the expression of CD47 and PD-L1, the two critical phagocytic checkpoint ligands on tumor cells (Betancur et al., 2017; Antonangeli et al., 2020). In light of this, the central focus of this chapter is to elucidate the mechanistic role of IKKβ in modulating these critical immune evasion pathways in the specific context of HCC. Specifically, we investigated how the genetic depletion of IKKβ in HCC cells regulates the expression of CD47 and PD-L1 at the transcriptional and translational levels and whether this regulation is mediated through canonical NF-κB signaling. Understanding this regulatory axis is crucial for revealing the mechanistic basis of how the loss of IKKβ within tumor cells renders them more susceptible to macrophage phagocytosis. It is also crucial to develop novel therapeutic strategies that disrupt the "don't eat me" signal at its transcriptional source, potentially overcoming the limitation of direct antibody blockade (i.e., systemic toxicities).

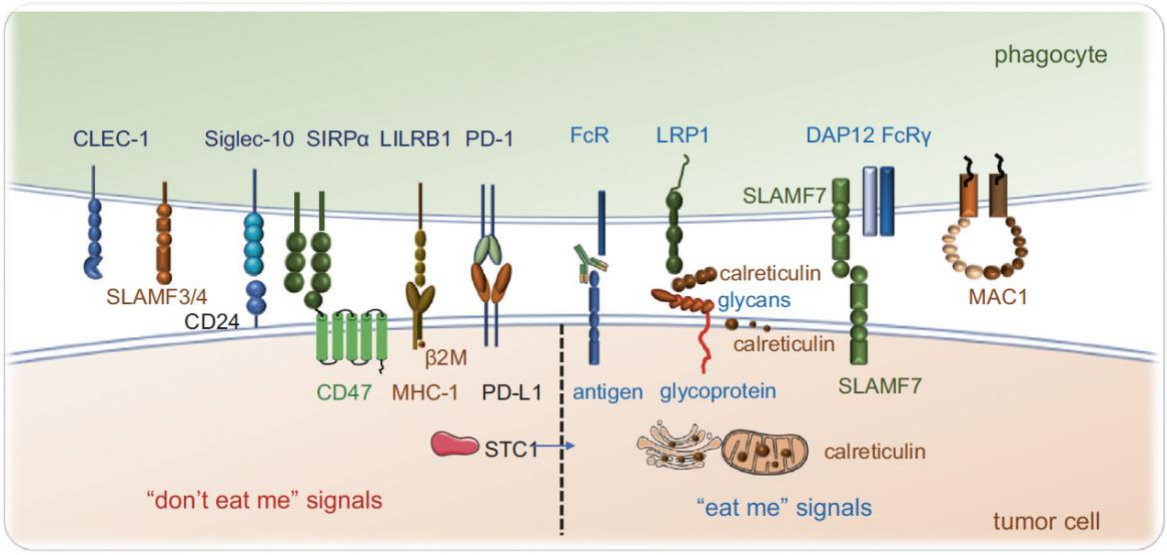

Figure 5.1. The 'eat-me' and 'don't eat me' signals on tumor cells and phagocytes' surface. (C-type lectin-like receptor-1 (CLEC-1), Signaling lymphocytic activation molecule family (SLAMF) receptors, Sialic acid-binding immunoglobulin-type lectins (Siglec), Signal regulatory protein α (SIRPα), leukocyte immunoglobulin-like receptor subfamily B 1 (LILRB1), programmed cell death protein 1 (PD-1), lipoprotein receptor-related protein 1 (LRP1), Macrophage antigen complex-1 (MAC1) (This figure adopted from Liu et al., 2023)

5.2 Method

We first explored the clinical database to examine the association of *IKBKB* with *CD47* and *PD-L1* at the transcriptional level in HCC tumors, as well as the correlation with NF-κB pathway activity inferred from the respective expression data (Figure 5.2). Next, we experimentally investigated the regulatory effect of IKKβ on these phagocytic checkpoints using the established knockout sublines. The influence of IKKβ loss on the surface expression, mRNA expression, and transcriptional activation of CD47 and PD-L1 was examined using flow cytometry, qPCR, and reporter assays, respectively. We also examined whether the control of expression is maintained following tumor establishment by isolating syngeneic and xenograft tumors from mouse models and performing surface marker staining (Figure 5.2). To examine the regulation of canonical NF-κB signaling, the nuclear localization of p65 (RelA) and phospho-p65 Ser536, which indicate pathway activation, was measured by subcellular fractionation followed by western blot analysis for the cell models and by IHC analysis for the syngeneic and xenograft tumors.

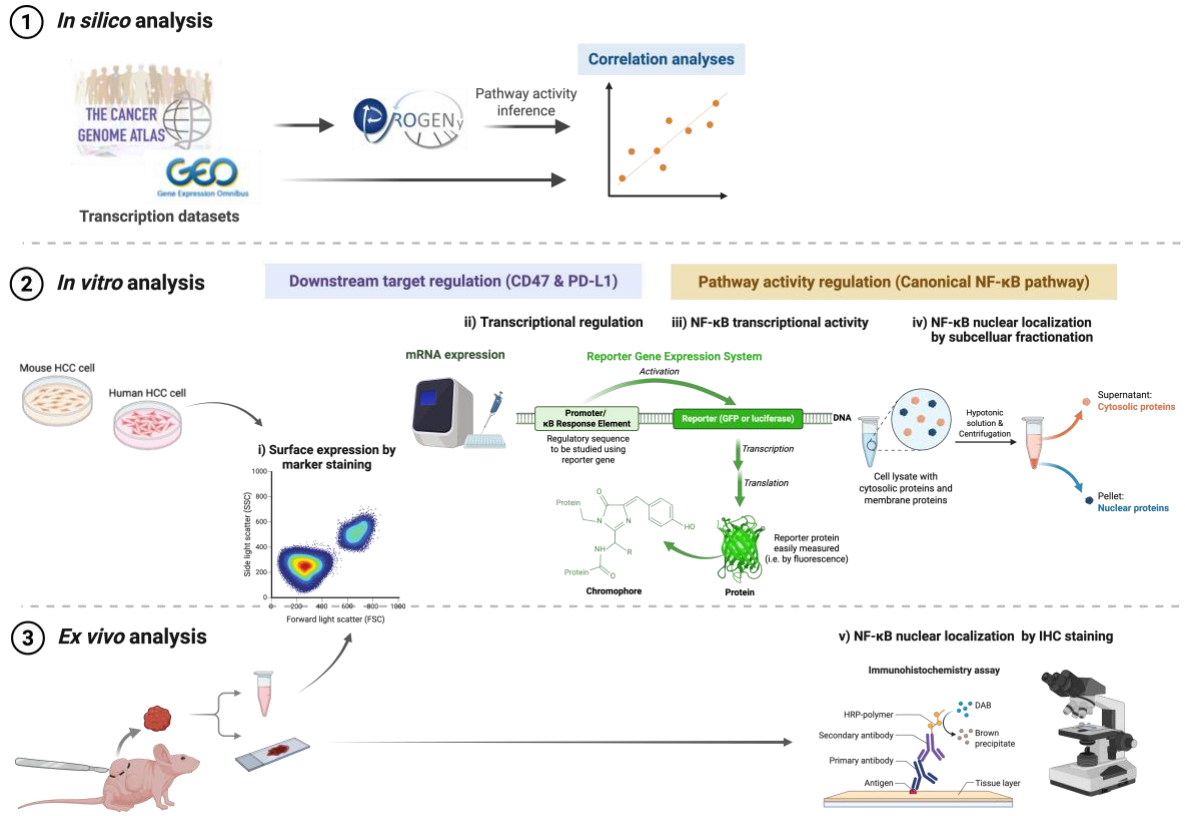

Figure 5.2 Experimental design for investigating the regulation of IKKβ on CD47 and PD-L1 via the NF-κB canonical pathway.

5.3 *Ikbkb* regulates expression of CD47 and PD-L1 in HCC cells

IKBKB is well-known to be a critical kinase responsible for activating the canonical signaling pathway of NF-κB, a master transcriptional regulator that modulates the expression of various genes related to inflammation and immune response, including the anti-phagocytic markers, including *CD47* and *PD-L1,* which are commonly expressed in cancer cells. We first examined whether *IKBKB* expression is associated with NFkB activation and the expression of *CD47* and *PD-L1*. NFkB pathway activity was inferred based on expression data of TCGA-LIHC, ICGC-LIRI-JP, as well as LICA-FR (liver cancer-France) cohorts (or GSE36376) using PROGENy (Pathway RespOnsive GENes), a signature-based method that computes pathway activity based on mRNA levels of perturbation-response genes identified from a large compendium of publicly available perturbation studies. And we found that *IKBKB* mRNA expression was significantly correlated with NFkB pathway activity in the HCC datasets examined and showed comparable strength of association as those of downstream targets (Figure 5.3A). Consistently, *IKBKB* expression was positively correlated with the mRNA expression of *CD47* and *PD-L1* in these cohorts (Figure 5.3A). This association was validated *in vitro,* where *Ikbkb* depletion suppresses the expression of CD47 and PD-L1 at the transcript level (Figure 5.3 B). We then investigated the effect of *Ikbkb* knockout on CD47 and PD-L1 surface expression in PLC/PRF/5 and RIL-175 cell and xenograft models by FACS-based measurement. The results demonstrated a significant reduction in CD47 and PD-L1 expression upon *Ikbkb* depletion (Figure 5.3C, D). These findings support the notion that *Ikbkb* regulates tumor cell expression of CD47 and PD-L1.

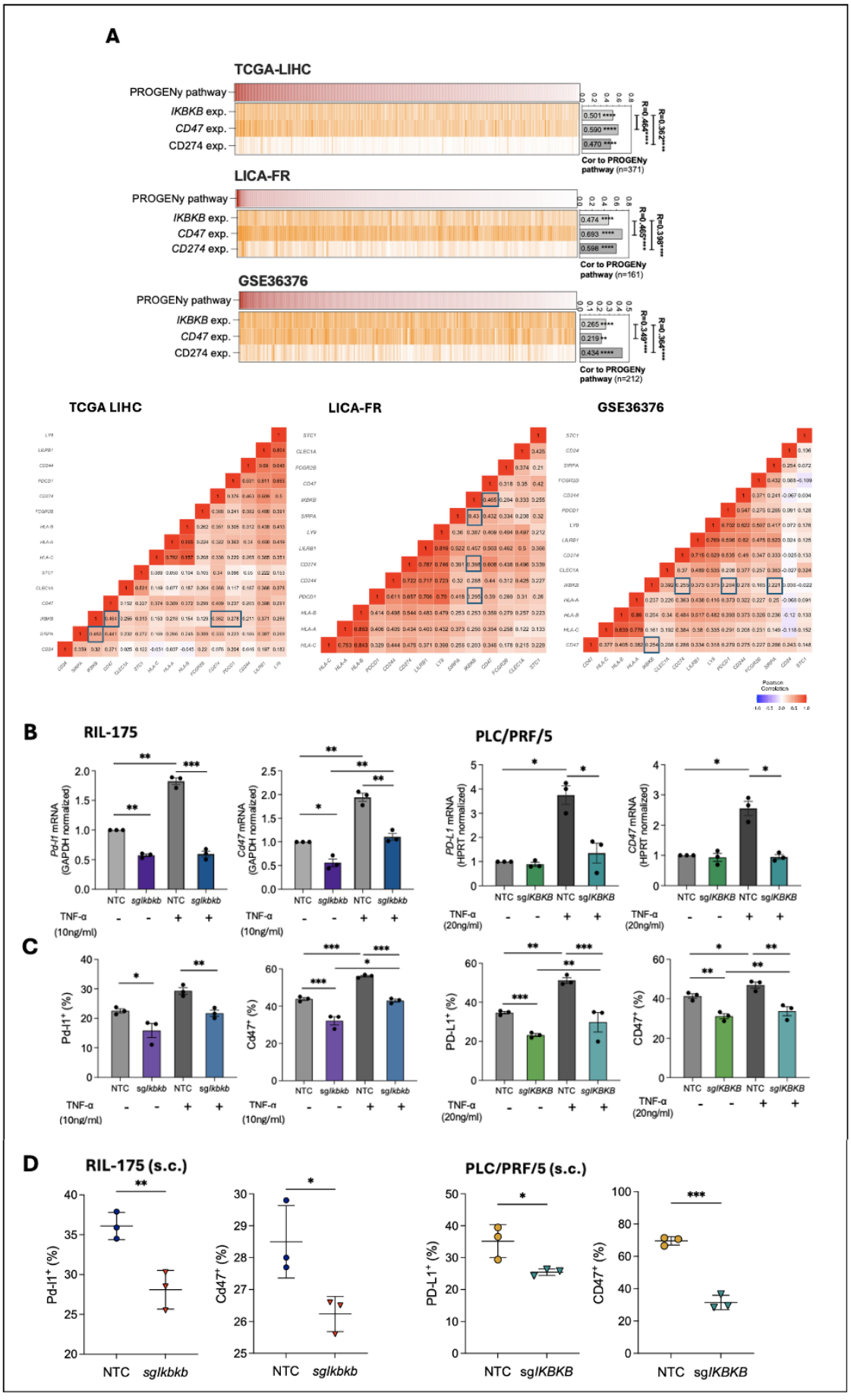
A
TCGA-LIHC
PROGENy pathway
IKBKB exp.
CD47 exp.
CD274 exp.
0.501 ****
0.590 ****
0.470 ****
R=0.464****
R=0.362****
Cor to PROGENy pathway (n=371)
LICA-FR
0.474 ***
0.693 ****
0.598 ****
R=0.465****
R=0.398***
Cor to PROGENy pathway (n=161)
GSE36376
0.265 ***
0.219 **
0.434 ****
R=0.349****
R=0.364***
Cor to PROGENy pathway (n=212)
TCGA LIHC
LICA-FR
GSE36376
Pearson Correlation
B
RIL-175
PLC/PRF/5
Pd-l1 mRNA (GAPDH normalized)
Cd47 mRNA (GAPDH normalized)
PD-L1 mRNA (HPRT normalized)
CD47 mRNA (HPRT normalized)
NTC sgIkbkb NTC sgIkbkb
NTC sgIKBKB NTC sgIKBKB
TNF-α (10ng/ml)
TNF-α (20ng/ml)
C
Pd-l1+ (%)
Cd47+ (%)
PD-L1+ (%)
CD47+ (%)
D
RIL-175 (s.c.)
PLC/PRF/5 (s.c.)
NTC sgIkbkb
NTC sgIKBKB

Figure 5.3 Control of antiphagocytic molecules by *Ikbkb*. (A, top) Pearson correlation of *IKBKB*, *CD47,* and *CD274* gene expression and with NFκB pathway activity (TCGA-LIHC: The Cancer Genome Atlas Liver Hepatocellular Carcinoma, ICGC-LIRI-JP: International Cancer Genome Consortium Liver Cancer - RIKEN, Japan) (***p < 0.01*, *****p <0.0001*). (A, bottom) Pearson Correlation analyses between *IKBKB* and anti-phagocytic genes at transcript levels in HCC cohorts. (B) Relative mRNA expression of PD-L1 and CD47 in RIL-175-NTC–sg*IKBKB* cells (left) or PLC/PRF/5-NTC or –sg*IKBKB* cells (right) in the absence or presence of TNFα stimulation. (C) Percentage of PD-L1 and CD47 surface expression in RIL-175-NTC–sg*IKBKB* cells (left) or PLC/PRF/5-NTC or –sg*IKBKB* cells (right) in the absence or presence of TNFα stimulation as measured by FACS. (C) Percentage of PD-L1 and CD47 surface expression in RIL-175 (left) and PLC/PRF/5 (right) xenografts following subcutaneous engraftment in a mouse model as measured by FACS.

5.4 Ikbkb mediates canonical NF-κB pathway activity

Next, we sought to verify whether *Ikbkb* regulates NF-κB activation in HCC. Using luciferase or GFP reporter assays, we confirmed that *Ikbkb* potentiates NF-κB transcriptional activity in HCC cells, which is consistent with our earlier correlation data (Figure 5.4A). Western blot analysis revealed that *IKBKB* knockout reduced phosphorylated NF-κB p65 (pS536) levels in both cytosolic and nuclear fractions (Figure 5.4B). Notably, without TNF-α stimulation, total p65 was undetectable in the nucleus, suggesting that *IKBKB* depletion may impair basal NF-κB activity in HCC cells (Figure 5.4B). TNF-α stimulation induced the canonical NF-κB signaling cascade, as evidenced by increased cytosolic phospho-IKKα/β and phospho-p65 levels in both PLC/PRF/5 and RIL-175 cells (Figure 5.4C). However, because of the very low baseline levels of total and phospho-p65 in serum-starved RIL-175 cells, we selected the PLC/PRF/5 cell line for subsequent investigations of *IKBKB*'s role in NF-κB signaling (Figure 5.4C).

Subsequent subcellular fractionation analysis confirmed that *IKBKB* knockout attenuates the canonical NF-κB pathway after TNF-α stimulation. This was demonstrated by a marked reduction in the levels of phospho-p65 (at Ser536 and Ser468) and total p65 in both the cytoplasmic and nuclear fractions (Figure 5.4D). This impaired signaling is likely due to reduced IKK activity, as evidenced by the concomitant decline in phosphorylated IKKα/β and IκBα within the cytosolic fraction (Figure 5.4D). In line with this observation, we noticed a

decline in the expression of both total and phospho-levels of p65 in the PLC/PRF/5 xenograft mouse model (Figure 5.4E). These results provide evidence that *IKBKB* positively regulates classical NF-κB signaling in HCC.

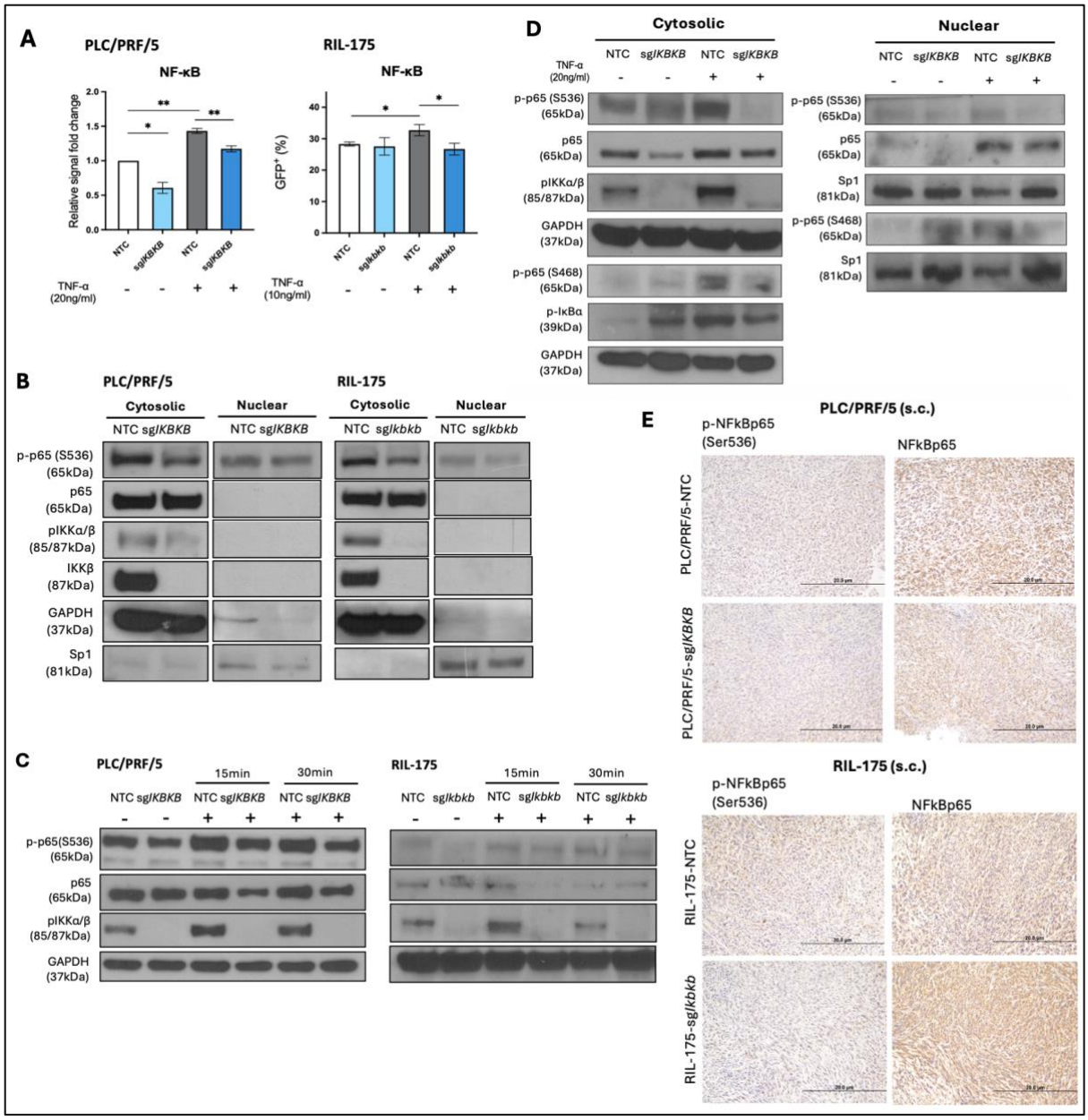

Figure 5.4 *IKBKB* activates transcription factor NF-κB. (A) NF-κB pathway transcriptional activity inferred by luciferase reporter system or GFP reporter system for PLC/PRF/5 or RIL-175 cells, respectively. PLC/PRF/5-NTC and -sg*IKBKB* cells are transfected with the reporter plasmids for 24h and reseeded to 12-well plates O/N. The next day, the cells are incubated in serum-free conditions in the absence or presence of 20ng/ml TNFα for 6 hours and are collected for determining the luciferase or GFP activity. (B) Western blot analysis for the cytosolic and nuclear fractions of PLC/PRF/5 or RIL-175 cells. (C) Western blot analysis for cytosolic

fractions of PLC/PRF/5 or RIL-175 cells. (D) NF-κB pathway activation was assessed by subcellular fractionation using a hypotonic solution in the presence or absence of TNFα stimulation. PLC/PRF/5-NTC and -sg*IKBKB* cells are seeded at 60mm dishes O/N and reach 80% confluence the next day. The cells are then stimulated with 20ng/ml TNFα for 30 minutes to stimulate the canonical NF-κB pathway. (E) Representative IHC images for phospho- or total-p65 of xenograft tumors from mice injected with PLC/PRF/5-NTC and -sg*IKBKB* cells. Scale bar, 20 μm.

5.5 Ikbkb controls the transcriptional activities of CD47 and PD-L1

Next, we aimed to determine whether *IKBKB* regulates the expression of immune checkpoint molecules CD47 and PD-L1 specifically through the NF-κB signaling axis. First, we performed an *in silico* analysis using the Gene Transcription Regulation Database (GTRD), which revealed multiple high-probability NF-κB binding motifs within the promoter regions of both CD*47* and *PD-L1* (Figure 5.5A, B). This bioinformatic evidence provides a structural basis for our hypothesis, suggesting that these genes are direct transcriptional targets of NF-κB. To functionally validate this finding, we performed a luciferase reporter assay. Consistent with previous findings, genetic depletion of *IKBKB* significantly reduced the transcriptional activities of both the *CD47* and PD-L1 promoters. This result demonstrates that *IKBKB* is a crucial upstream regulator required for its expression (Figure 5.5C).

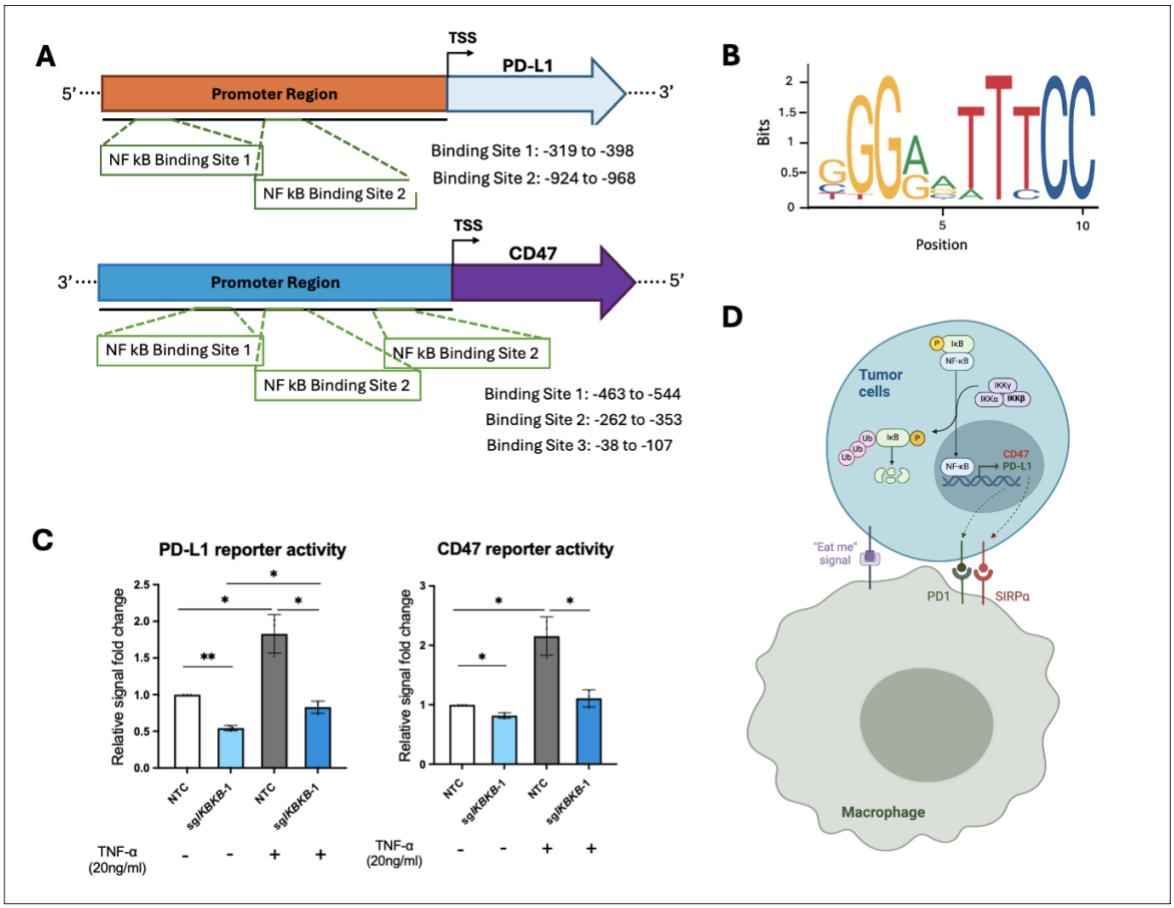

Figure 5.5 *IKBKB* regulates CD47 and PD-L1 transcriptional activation. (A) Predicted NFkB binding sites within promoter regions of CD47 and PD-L1 by GTRD. (B) NFkB-binding motifs predicted by GTRD. (C) Luciferase reporter assay for detecting transcriptional activation of CD47 and PD-L1 triggered by NFkB binding. PLC/PRF/5-NTC and -sg*IKBKB* cells are transfected with the reporter plasmids for 24h and reseeded to 12-well plates O/N. The next day, the cells are incubated in serum-free conditions in the absence or presence of 20ng/ml TNFα for 6 hours and are then collected for determining the luciferase activity. (D) Schematics showing the regulation of *IKBKB* on canonical NFkB pathway activation and the downstream CD47 and PD-L1 expression.

5.6 Discussion

Collectively, these data provide evidence that *IKBKB*-driven NF-κB activation promotes the expression of phagocytic checkpoints, CD47 and PD-L1. Our initial investigations established a strong clinical correlation between *IKBKB* mRNA levels and both NF-κB pathway activity and the expression of *CD47* and *PD-L1* across multiple independent HCC cohorts, suggesting a coordinated regulatory network in human tumors. These findings were validated using our *in vitro* and *in vivo* models, where genetic depletion of *Ikbkb* led to a consistent and significant reduction in both the transcript and surface protein levels of CD47 and PD-L1. These findings indicate *IKBKB* is a key upstream regulator of these critical immune evasion molecules.

We next confirmed that IKBKB acts as a primary activator of the canonical NF-κB pathway in HCC. The observed decline in nuclear p65 and promoter activation upon *IKBKB* knockout, both at baseline and following TNF-α stimulation, demonstrates that *IKBKB* is critical for the nuclear translocation and transcriptional activation of NF-κB. Moreover, we established a molecular connection between IKBKB/NF-κB signaling and the transcriptional control of *CD47* and *PD-L1*. Luciferase reporter assays showed that the loss of *IKBKB* weakened the transcriptional activity of these promoters. This functionally validates that *IKBKB*, via NF-κB, is a direct transcriptional regulator of both genes.

Our data establish *IKBKB* as a master regulator of immune checkpoint expression in HCC, revealing a key mechanism for the upregulation of ' do not eat me' signals. Yet, direct rescue experiments are required to conclusively prove that the phagocytic inhibition by *IKBKB* is mechanistically dependent on the CD47/PD-L1 axis and NF-κB signaling. Moreover, it is important to note that NF-κB plays vital physiological roles in cell survival, immunity, and inflammation, and systemic inhibition inevitably disrupts these processes, leading to a range of adverse effects. NF-κB is essential for innate immunity, that is, for the production of pro-inflammatory cytokines like TNFα, IL-1, IL-6, and adhesion molecules, and the function of B cells, T cells, and dendritic cells (Pasparakis, M., 2009). And targeting may result in immune suppression and severe Infections. Hepatotoxicity and gastrointestinal toxicity have also been reported for NF-κB targeting. Elevated liver transaminases and drug-induced liver injury are observed in patients administered with IKK/NF-κB inhibitors in clinical trials. And this is probably because NF-κB confers a survival signal to hepatocytes, and inhibition leads to TNFα-induced apoptosis. Colitis and diarrhea are observed in the clinical setting for NF-κB targeting. Physiologically, NF-κB maintains the integrity of the gut epithelium and regulates

the immune response to commensal bacteria. Its inhibition leads to increased intestinal permeability and inflammation. It is therefore of paramount importance to assess the systemic effect and toxicities of *IKBKB* targeting in preclinical models, which will be further discussed in the next chapter. We would examine the therapeutic efficacies of *IKBKB* targeting and combination with immunotherapy in treating HCC.

CHAPTER 6 Targeting Ikkβ to Overcome Immunosuppression in HCC

6.1 Introduction

Macrophages orchestrate immune dysfunction in HCC

HCC typically arises from a background of chronic inflammatory liver disease, a condition that cultivates a highly immunosuppressive TME favoring tumor growth, metastasis, and treatment resistance (Llovet et al., 2021). Within this complex TME, TAMs emerge as a dominant and pivotal immune component, comprising 20-40% of the infiltration immune cell population, and were found to be a major driver of the hostile TME (Zheng et al., 2023; Liu et al., 2025). TAMs primarily shaped this hostile TME through matrix remodelling and engaging in extensive crosstalk with other immune populations to suppress antitumor immunity and foster a permissive environment for tumor growth. Immunosuppressive TAMs release VEGF and MMPs, which stimulate tumor proliferation, angiogenesis, invasion, and intravasation. Through interactions with hepatic stellate cells, TAMs drive the progression of liver fibrosis, a key risk factor of HCC development (Affo et al., 2017). Critically, several subsets of TAM have been shown to suppress cytotoxic T lymphocytes. For instance, TREM2+ macrophages impair CD8+ T cells infiltration and function by releasing galectin-1, which upregulates PD-L1 on endothelial cells, and the abundance of this subtype is associated with poor clinical prognosis. SPP1+ macrophages were demonstrated to inhibit T cell proliferation and were associated with an unfavorable patient response. Furthermore, TAMs have also been reported to promote Treg recruitment and expansion. By releasing chemokines such as CCL17, CCL20, and CCL22, TAMs attract Tregs into the tumor core, where they further dampen the activity of neighboring Tc cells and NK cells, thereby perpetuating the immunosuppressive network (Kuang et al., 2009). The net effect of this TAM-mediated immunoregulation is a strong correlation with poor clinical outcomes and higher recurrence rates in patients (Liu et al., 2025; Ye et al., 2018). High density of immunosuppressive TAMs within HCC tumors is consistently associated with aggressive tumor phenotypes, including enhanced venous invasion, metastasis, as well as resistance to standard therapy like sorafenib (Zhou et al., 2017).

The imperative to examine macrophage-driven crosstalk in HCC is also attributed to the fact that it primarily contributes to the limited efficacy of current immunotherapies, particularly immune checkpoint inhibitors (ICIs). While revolutionary, ICIs yield sustained responses in only a subset of HCC patients, with objective response rates typically below 30% (Sangro et al., 2021). This therapeutic resistance is largely orchestrated by TAMs, which establish and maintain a profoundly immunosuppressive TME. Specific subsets of TAMs, such as TREM2+

or SPP1+ macrophages, directly impair cytotoxic cell function and infiltration. TAMs recruit and activate immunosuppressive populations, including Tregs and MDSCs, thereby reinforcing an immune-excluded or “cold” tumor state that is inherently resistant to T cell therapies (Zhu et al., 2021). By “re-educating” TAMs, it may be possible to intercept this suppressive communication, potentially converting the TME from immunosuppressive to immunostimulatory and resensitizing tumors to existing treatment regimens.

Building on our previous findings that targeting Ikkβ can stimulate macrophage phagocytosis and antitumor activity, the current chapter has two central aims. First, we will delineate the general role of TAMs within the HCC TME, with a specific focus on their interactions with crucial T cell subsets, Tc and Treg cells. Secondly, we will investigate the specific immunoregulatory function of Ikkβ in this context. A key question is whether Ikkβ activity exacerbates the hostile TME, and conversely, whether its inhibition can reverse the immunosuppression. Furthermore, given the canonical role of macrophages in bridging innate and adaptive immunity via antigen presentation, either on MHC II to helper T cells or on MHC I for cross-presentation to cytotoxic T cells, we will examine if enhanced phagocytosis via Ikkβ targeting leads to improved antigen presentation, infiltration, and subsequent activation of Tc or Th lymphocytes.

6.2 Method

We first explored publicly available single-cell sequencing datasets to infer the immunomodulatory role of TAMs within the HCC TME (Figure 6.1). Single-cell sequencing data from GSE189903 were downloaded from Gene Expression Omnibus and processed using the Scanpy package in Python. This involves quality control to filter out low-quality cells and counts, normalization, scaling, and identification of highly variable genes. Principal component analysis and graph-based clustering with the Leiden algorithm were then applied to identify the major cell populations. Cell types were annotated using canonical marker genes. Immune subsets were further annotated using subclustering analysis, following the same procedure. To investigate potential interactions, CellPhoneDB was employed, and the strength of the interaction between macrophages and T cell subsets was compared between adjacent normal and tumor core samples.

Next, we employed the hydrodynamic tail vein injection (HTVI) model to delineate the role of Ikkβ in hepatocarcinogenesis and immune regulation (Figure 6.1). The impact of hepatocyte-specific *Ikbkb* overexpression on tumorigenesis was examined using bioluminescent imaging. Flow cytometry analysis was used to evaluate changes in macrophage abundance, functional state, and antigen presentation capacity. This immune profiling was extended to other immune populations, including dendritic cells, neutrophils, NK cells, B cells, and T cells, with a particular focus on T cell subset infiltration, given their critical interaction with macrophages in the TME.

To further investigate the influence of Ikkβ expression on antigen presentation and tumor control, we utilized an orthotopic implantation model. RIL-175-NTC and RIL-175-sg*Ikbkb* cells engineered to express ovalbumin (OVA) were used to generate isogenic sublines (Figure 6.1). These cells were implanted into the murine liver to establish tumors in the liver. Tumor progression was monitored, and the functional competence of TAMs, specifically their antigen presentation capacities, was assessed. Specifically, we measured the presentation of the tumor-derived SIINFEKL peptide (from OVA) by H-2Kb molecules on macrophages from the liver and spleen. These analyses were integrated with an evaluation of broader immune landscape alterations, including shifts in major immune populations and T cell subsets, to determine the systemic immunoregulatory effects of modulating Ikkβ signaling.

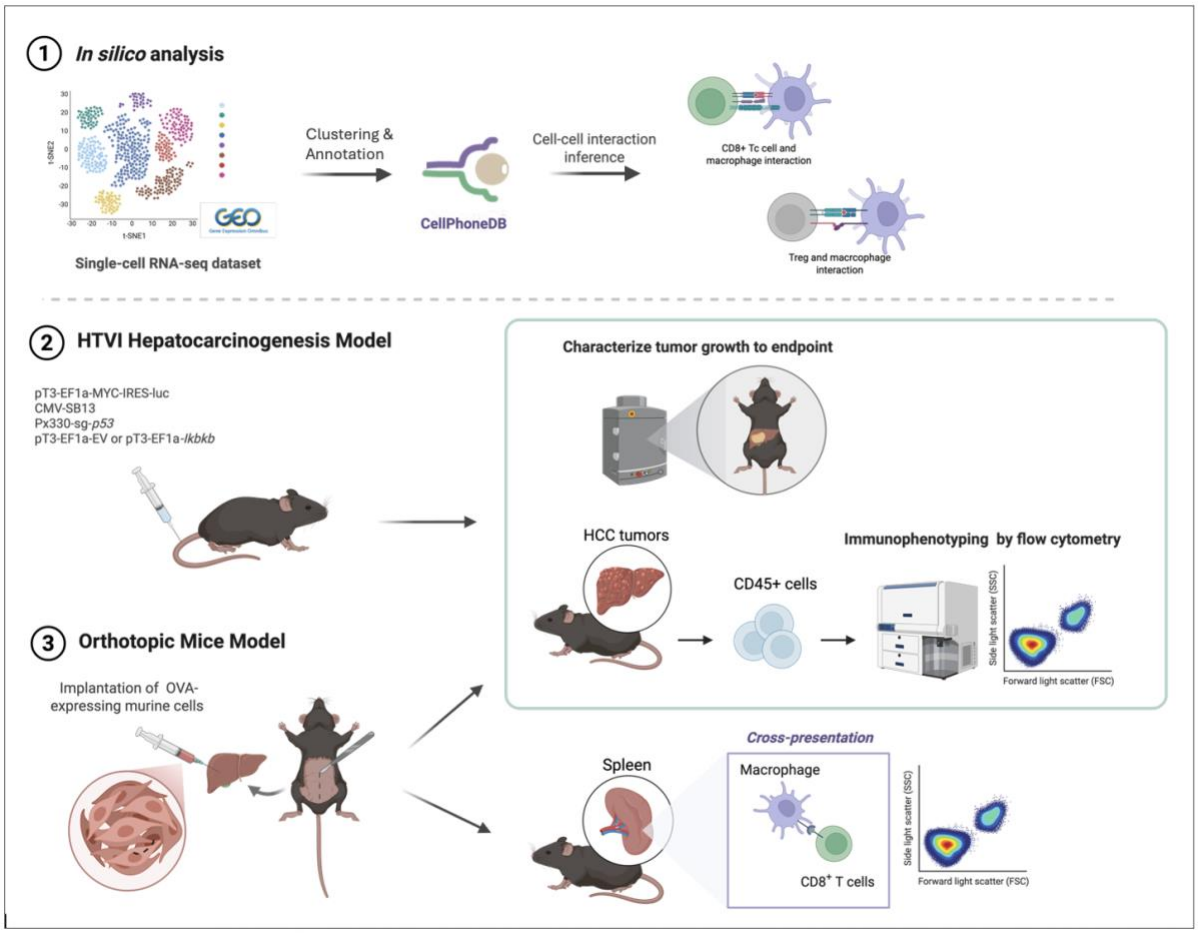

Figure 6.1 Experimental design for investigating the role of TAMs and IKKβ on immune regulation.

6.3 The immunosuppressive crosstalk of TAMs with Tc and Treg cells

To build a comprehensive atlas of TME, we employed Scanpy for cell classification and marker gene detection, and revealed 11 distinct clusters, which we defined and displayed (Figure 6.2A). Non-immune compartments were mainly composed of cancer-associated fibroblast (CAFs; markers COL1A2, DCN, COL3A1, COL6A1), endothelial cells (markers VWF, CDH5, PECAM1), hepatocytes (markers AMBP, APOA1, APOH, ALB), and cholangiocytes (markers CD24, KRT19) (Figure 6.2B). The immune cell populations we characterized consisted of myeloid-derived cells (expressing AIF1, CD14), T cells (with IL17R, CD3G, CD3D), memory B cells (marked by CD19, MS4A1), plasma cells (with CD38, TNFRSF17), NK cells (displaying PRF1, KLRD1, KLRF1) and pDCs (marked by IL3RA, CLEC4C) (Fig 6.2B). Subsequent unsupervised clustering of myeloid cells revealed 10 distinct clusters within the myeloid compartment. These comprise four macrophage subsets (Macro1-Macro3 and Kupffer cells), three monocyte clusters (Mono1-Mono3), and three dendritic cell groups (DC1-DC3) (Figure 6.2C). We identified macrophages based on high expression of the CD68 marker (Figure 6.2D). Established marker genes like FCGR3A (for M1) and CD163 (for M2) did not clearly separate M1 and M2 subsets, as both are co-expressed, which is consistent with earlier research (Figure 6.2D). Clustering of T cells revealed 10 subclusters, regulatory T cells (Tregs) expressed characteristic markers such as CTLA-4, FOXP3, and ICOS, and cytotoxic T cells (Tc) displayed high expression of cytotoxic genes (GZMK, GZMA, and NKG7) and the low expression of checkpoint genes, consistent with a precursor cytotoxic phenotype (Figure 6.2 E-F).

To decipher receptor-ligand interactions within the normal and tumor ecosystems, we conducted a cell-cell interaction analysis using CellPhoneDB. We focused on macrophage-T cell interactions, a crosstalk known for its immunosuppressive role in HCC progression. We observed increased interactions of key immune checkpoint receptor-ligand pairs in the tumor core compared to normal tissue, including SPP1:CD44, CD58:CD2, HBEGF:CD44, and SIRPA:CD47 (Figure 6.2G-H). The SPP1:CD44 interaction is of particular relevance, as recent studies have shown that this axis is crucial for TAM-induced T-cell exhaustion and immune suppression. Consistent with their immunosuppressive role, macrophages in the tumor core expressed higher levels of critical interaction partners (e.g., SPP1, CD58, and SIRPA) and immunomodulatory signaling molecules, including HBEGF, MIF, and GRN (Figure 6.2I). These data suggest that TAMs engage in immunoinhibitory crosstalk with both cytotoxic and regulatory T cells within the HCC microenvironment.

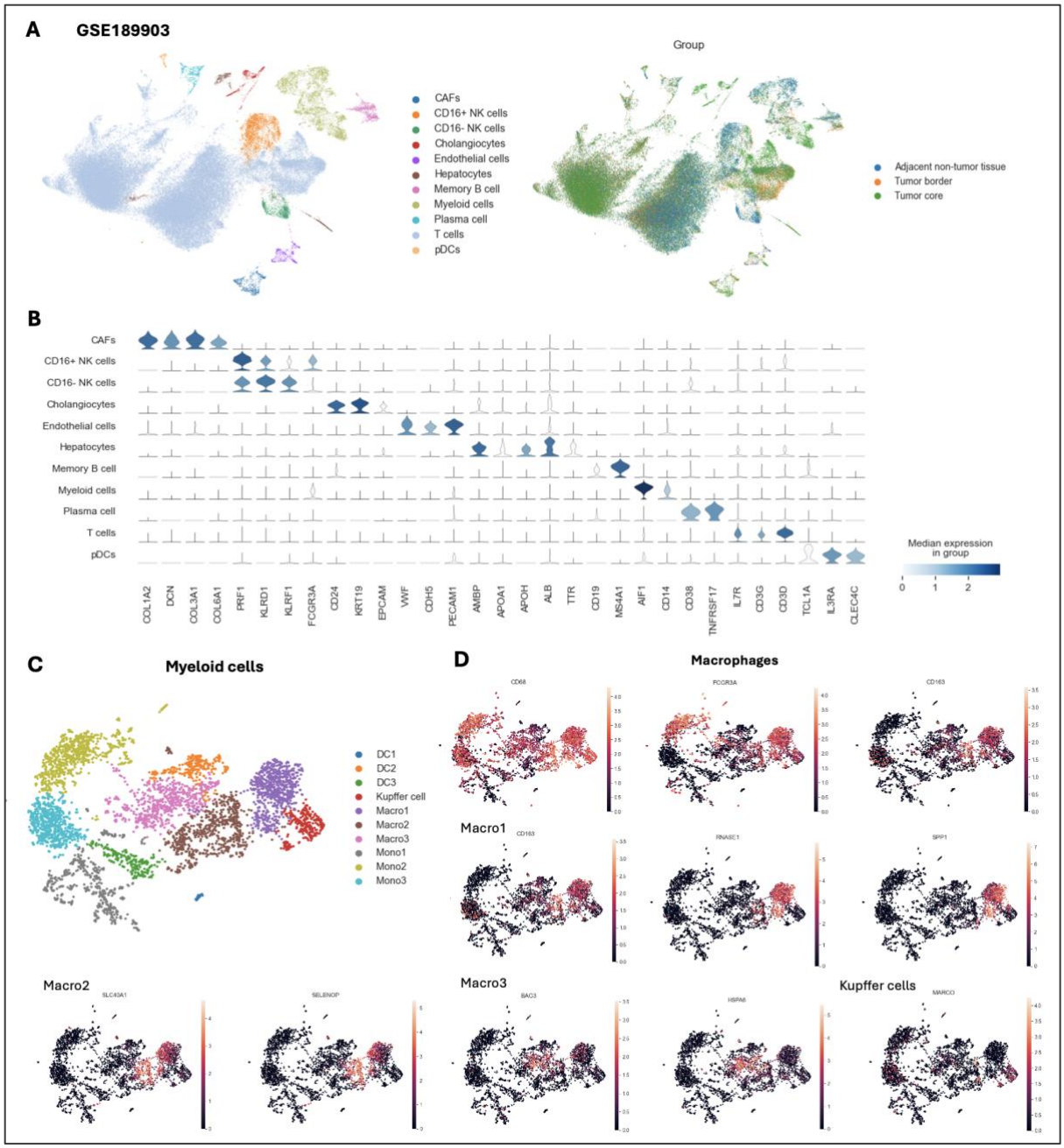

Figure 6.2 Immunosuppressive crosstalk between macrophage and T cell subsets as revealed by a single-cell RNA-seq dataset. (A) UMAP plot showing the annotation of cell and sample types. (B) Violin plot showing marker genes expression in the annotated cell types. (C) UMPA showing the subtypes of myeloid-derived cells. Each cluster is color-code based on the cell type. (D) UMAP showing expression of markers genes of selected cell types.

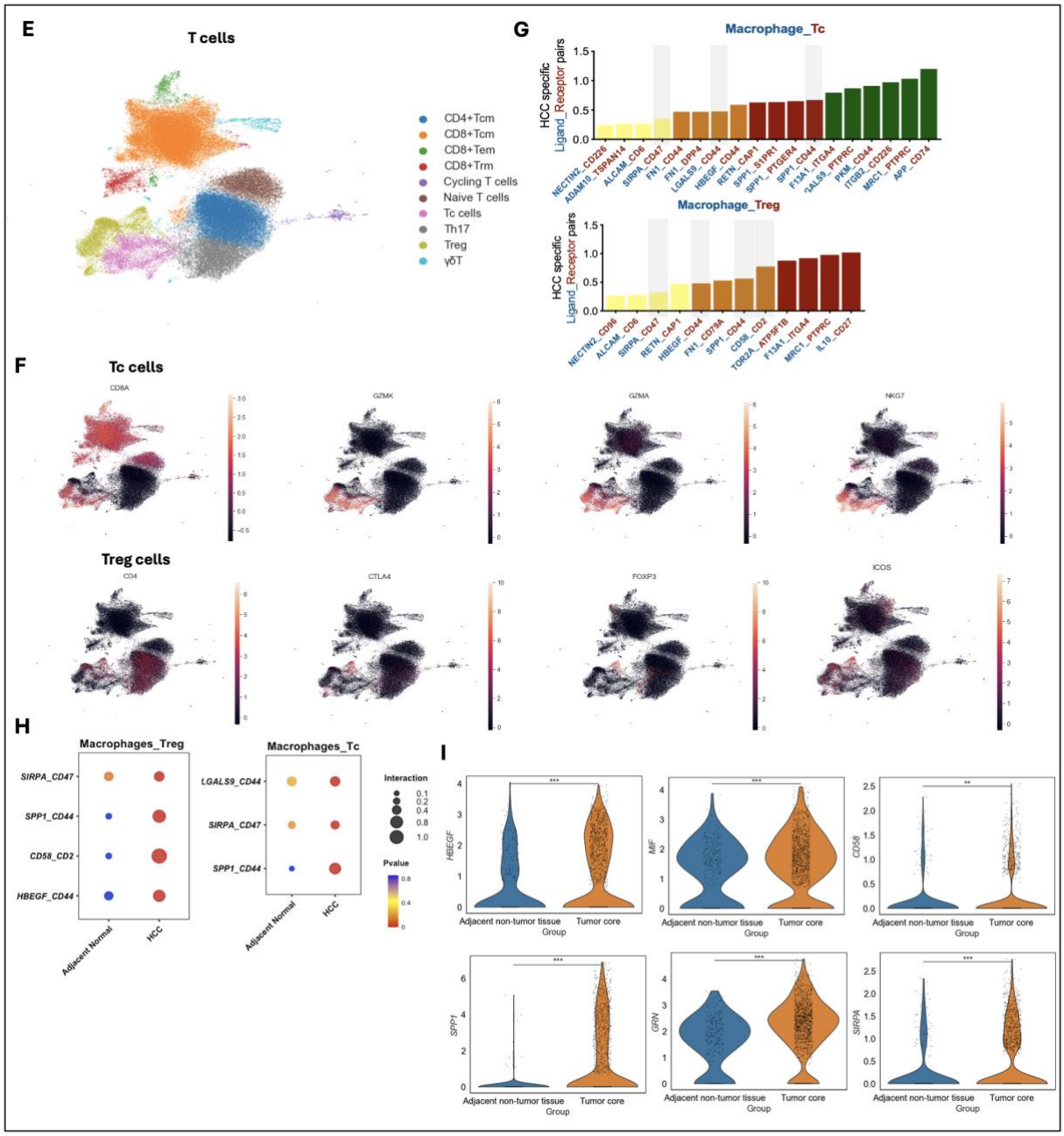

Figure 6.2 Immunosuppressive crosstalk between macrophage and T cell subsets as revealed by single-cell RNA-seq dataset (cont'). (E) UMPA showing T cells subtypes. (F) UMAP showing expressions of markers genes for selected cell types. (G) HCC-specific ligand-receptor pairs. (H) Dot plot showing interactions between macrophages and Treg or Tc cells. (I) Expression of immunosuppressive ligands or cytokines in macrophages (Welch's independent t test, ***p< 0.001, **p<0.01, *p<0.05)

6.4 Ikbkb overexpression promotes tumor development with increased populations of immunosuppressive TAMs

We next sought to explore the role of Ikkβ in hepatocarcinogenesis and immune regulation. Hydrodynamic injection of px330-sg-*p53,* MYC-luc and CMV-SB13 plasmids, together with pT3-EF1a-EV or pT3-EF1a-*Ikbkb* into 8-week-old male CD57BL/6 mice resulted in comparable levels of luciferase expression in the liver at day 6, as measured by bioluminescence imaging (Figure 6.3A-B). This confirmed equivalent injection efficiency and transgene expression between the two groups. Notably, on day 36 post-injection, a sharp increase in luciferase signal was observed specifically in the or pT3-EF1a-*Ikbkb* mice, suggestive of the tumor-promoting role of *Ikbkb* (Figure 6.3A-B). At the time of euthanasia, we observed a concordant increase in both tumor volume and mass in the mice where *Ikbkb* was overexpressed (Figure 6.3C). To infer the plausible involvement of macrophages in mediating the pro-tumoral response, we assessed the relative abundance of macrophages and functional status within the tumors. In mice overexpressing *Ikbkb,* there was a reduction in macrophage infiltration, accompanied by diminished anti-tumor and antigen presentation capacities, as indicated by reduced F4/80+CD11b+ macrophage population, as well as lower expression of activation marker CD86 and the antigen-presenting molecules MHCI+ or MHCII+, respectively (Figure 6.3D-E).

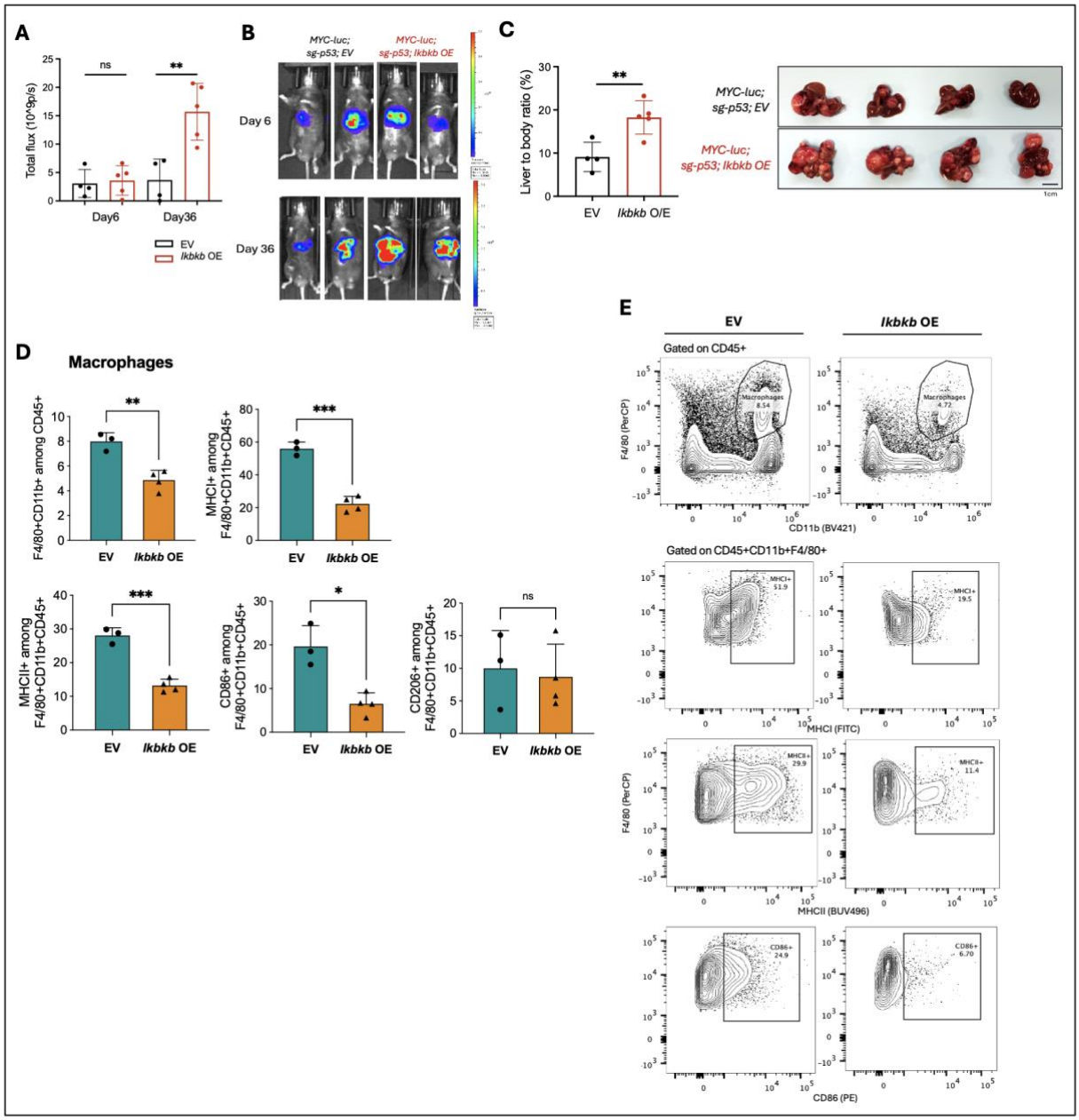

Figure 6.3 Tumorigenic and immune tolerogenic effects of *Ikbkb* in the HTVI mouse model. (A-B) Quantification of normalized luciferase signal (A) and representative bioluminescence images (B) 6 and 36 days after injection of vectors into C57BL/6 mice (n=4 for EV group, n=5 for *Ikbkb* OE group). (C) Liver-to-body ratio of the mice models (left). Representative tumor images on day 37 after engraftment (right). (D) Percent macrophage infiltration and expression of MHC molecules, co-stimulatory or inhibitory markers in the macrophage population (n=3 for EV group, n=4 for *Ikbkb* OE group). (E) Representative FACS plots showing the percentage of abundance of total macrophage and macrophage subsets.

6.5 *Ikbkb* overexpression dampens innate and adaptive anti-tumor immunity

Next, we examined whether Ikkβ expression alteration exhibited a broader immune regulatory effect in the TME. Profiling of immune cell infiltration revealed a significant impairment of the innate immune compartment in *Ikbkb*-overexpressing tumors. This is indicated by a pronounced reduction in key innate cell populations: conventional type 2 dendritic cells (cDC2s), their antigen-presenting MHCII+ subset, and neutrophils (Figure 6.4A-B). In contrast, the overall abundance of adaptive immune cells (T and B lymphocytes) was not significantly altered (Figure 6.4A-B). We also showed that in this broader immunophenotyping panel, *Ikbkb* overexpression diminished macrophage recruitment and activity, which is in concordance with our previous observation (Figure 6.4A-B).

Given the indispensable role of macrophages in mediating T-cell antitumor immunity, we next performed a detailed characterization of the T cell subsets. Using a T-cell-specific immunophenotyping panel, we found that *Ikbkb* overexpression functionally impaired cytotoxic CD8+ T cells, as evidenced by the significantly reduced expression of the early activation marker CD69 (Figure 6.4A-B). However, the proportion of exhausted or memory CD8+ T cell populations remained unchanged (Figure 6.4A-B). For the CD4+ T repertoire, we observed a marked reduction in the levels of pro-inflammatory T helper 1 (Th1) and T helper 17 (Th17) cells, which are crucial for driving effective antitumor adaptive response (Figure 6.4A-B). Notably, the abundance of Tregs was not diminished, indicating a net shift towards tolerance upon *Ikbkb* overexpression.

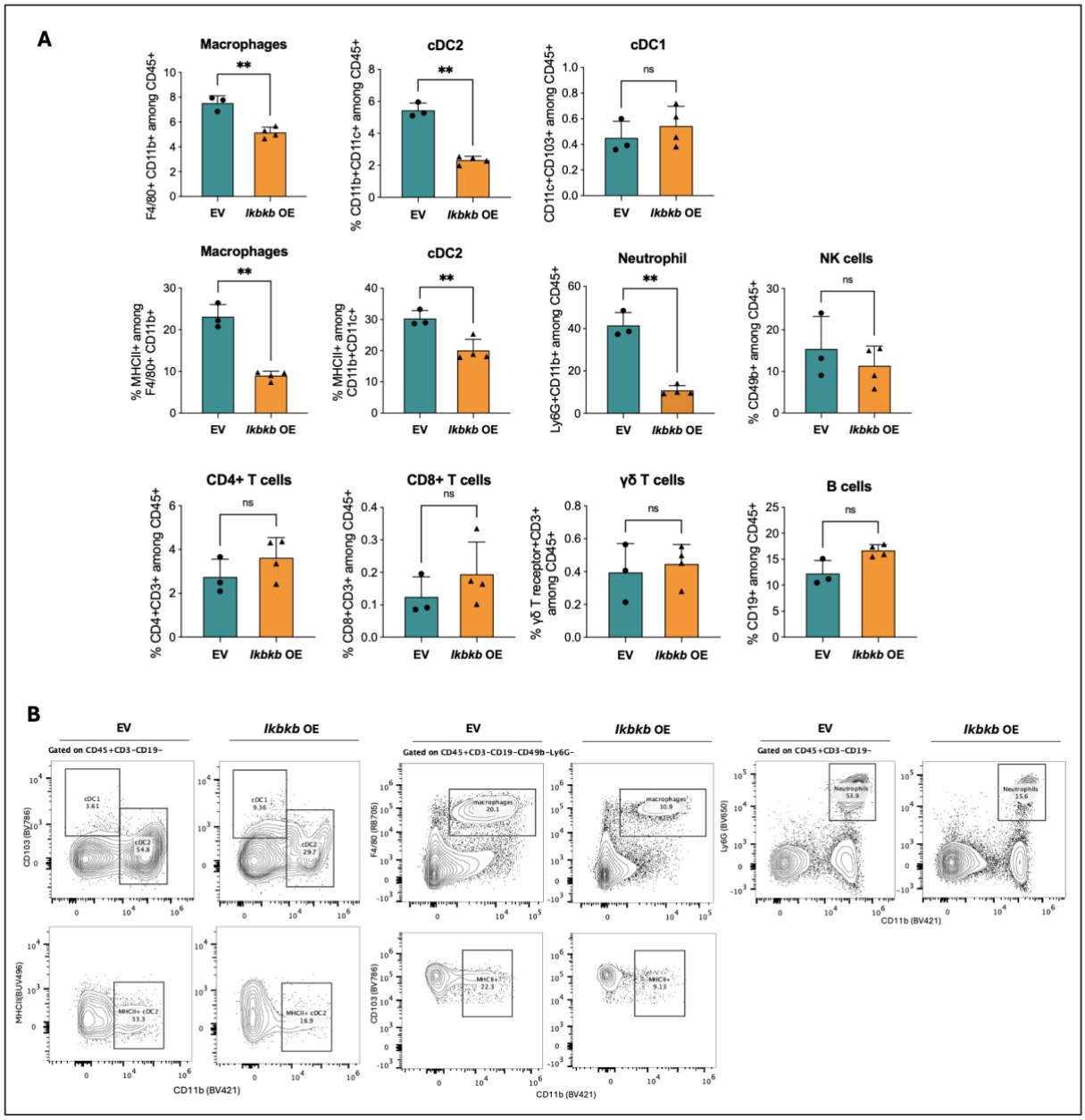

Figure 6.4 Inhibitory effects of *Ikbkb* on innate immune cell infiltration and activation. (A) Percent immune cells infiltration in HCC TME (n=3 for EV group, n=4 for *Ikbkb* OE group). (B) Representative FACS plots showing the percentage of abundance of immune infiltrates.

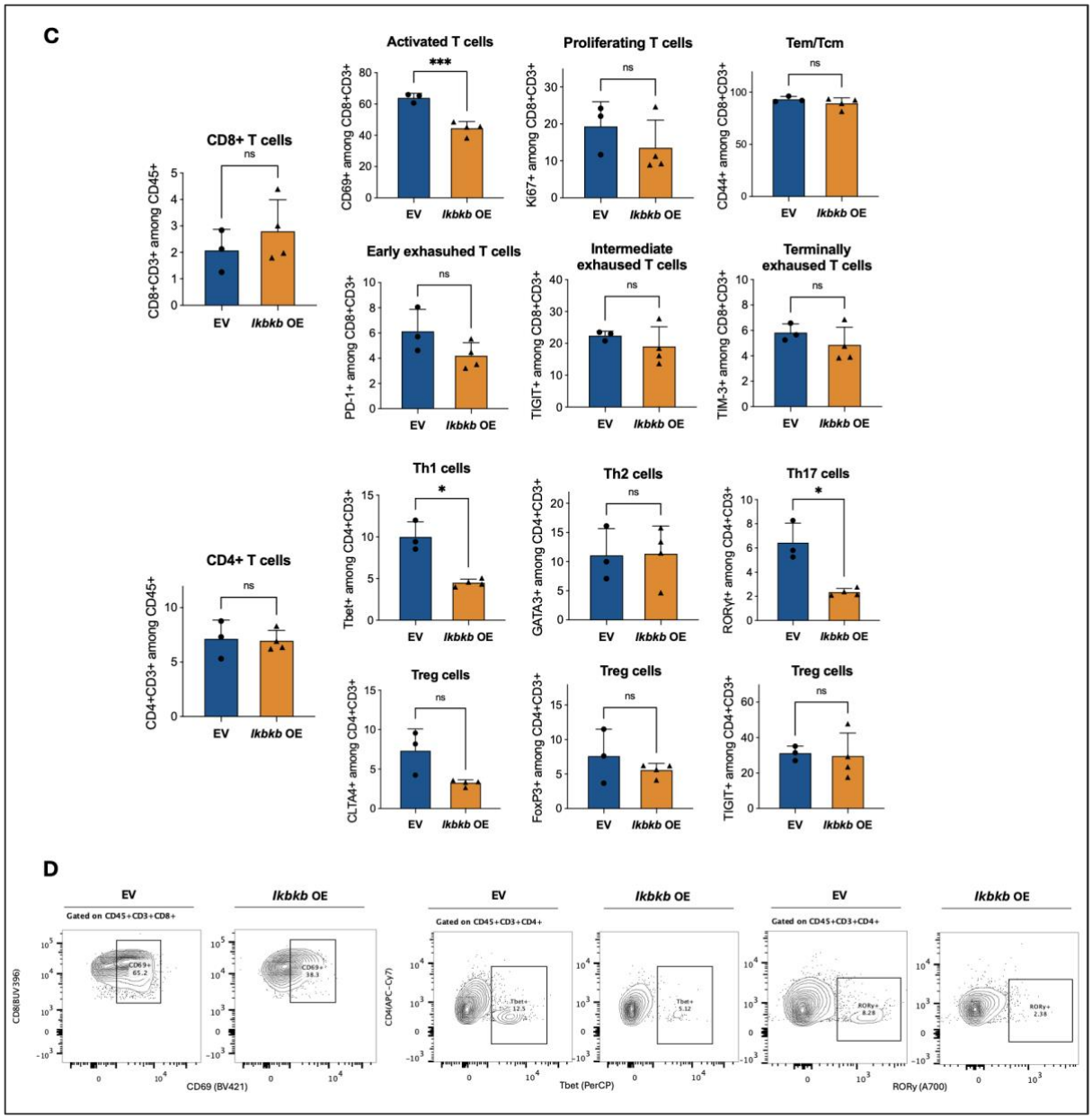

Figure 6.4 Inhibitory effects of *Ikbkb* on adaptive immune cell infiltration and activation (cont'). (C) Percent T cell subsets infiltration in HCC TME (n=3 for EV group, n=4 for *Ikbkb* OE group). (D) Representative FACS plots showing the percentage of abundance of immune infiltrates.

6.6 *Ikbkb* loss diminishes tumorigenesis with enhanced antigen presentation capacities of macrophages

To elucidate the functional link between phagocytosis and antigen-presentation, and the T cell activation, we conducted orthotopic implantation of OVA-expressing RIL-175 cells that harbour intact *Ikbkb* or with *Ikbkb* depletion. The stable expression of OVA antigen in the engineered RIL-175 sublines was first confirmed by Western Blot analysis (Figure 6.5A). Subsequent monitoring of tumor growth revealed a dramatic reduction in both tumor burden and incidence in the group receiving OVA-expressing, *Ikbkb*-depleted cells (Figure 6.5B-D). This finding indicated that loss of *Ikbkb* enhances immune-mediated elimination of antigen-expressing tumor cells. To interrogate the involvement of macrophages in mediating the elimination of antigen-expressing tumor cells, we profiled the macrophage phenotype as previously described, and in particular, we measured the expression of SIINFEKL/H-2Kb complex on the macrophages isolated from both the tumor and spleen. This measurement also provides crucial evidence for determining whether the *Ikbkb* loss in HCC cells enhances the ability of macrophages to cross-present tumor antigen and thereby activate the T cell immunity. Immunophenotyping analysis of the TME revealed that the abundance of macrophages and their antigen-presenting (i.e., MHCII+ or MHCI+) subset is significantly increased, whereas the level of SIINFEKL/H-2Kb complex on the macrophages' surface is not markedly altered (Figure 6.5E-F, G). Intriguingly, we observed a prominent increase in SIINFEKL/H-2Kb complex expression on macrophages in the spleen, which is indicative of systemic, priming phase of the immune response (Figure 6.5E-F). Concordant with this finding, T cell activity was shown to be higher in *Ikbkb* knockout tumors as indicated by increased abundance of Ki67+ proliferating T cells and Th17 cells in the tumor (Figure 6.5G).

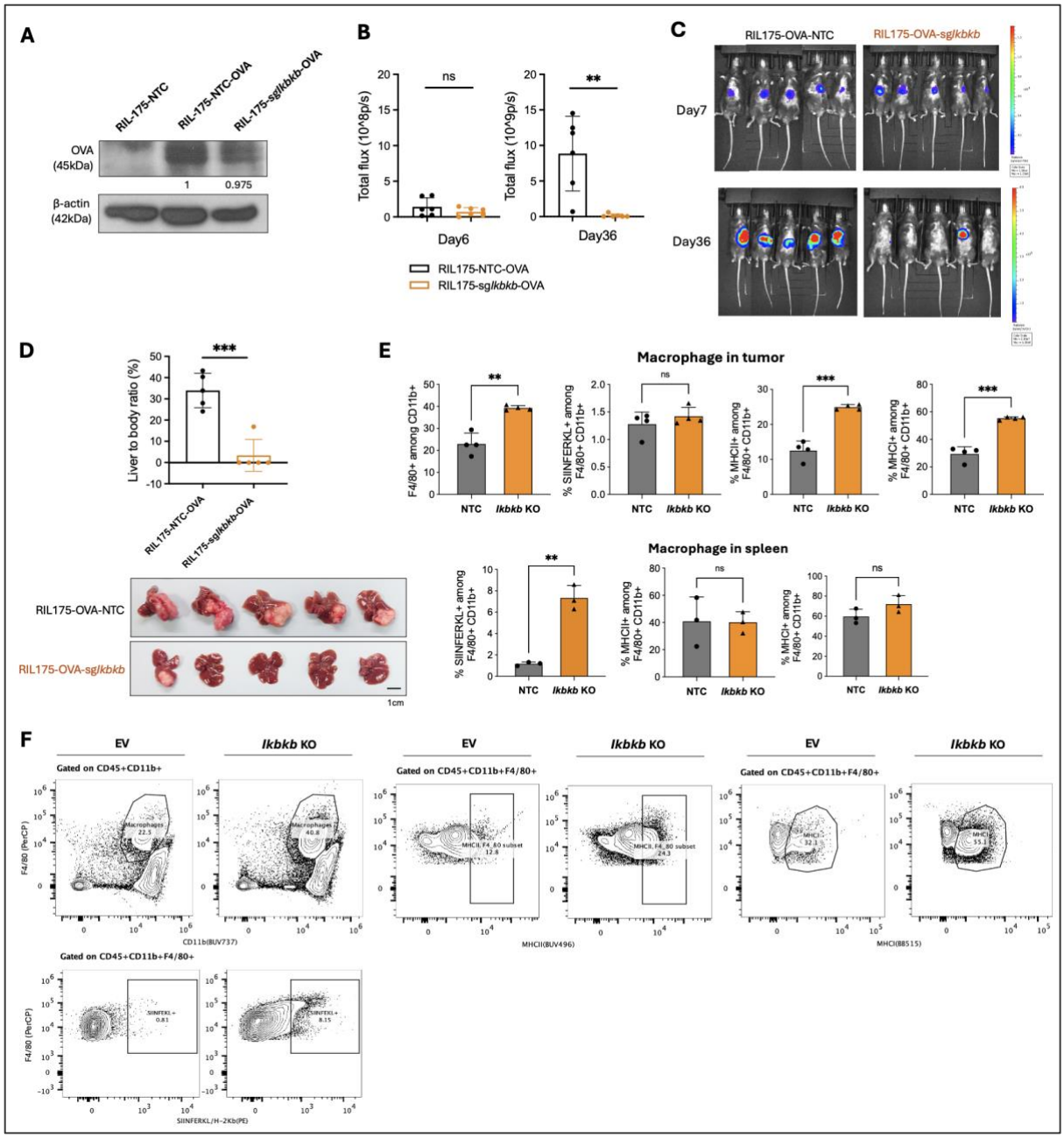

Figure 6.5 *Ikbkb* targeting results in tumor eradication and activation of macrophage and T cells in the OVA mice model. (A) OVA antigen expression in RIL-175 sublines. Quantification of normalized luciferase signal (B) and representative bioluminescence images (C) 6 and 36 days after orthotopic implantation of OVA-expressing cells into C57BL/6 mice (n=6 per group). (D) Liver-to-body ratio of the mice models (top). Representative tumor images on day 37 after engraftment (bottom). (E) Percent macrophage infiltration and expression of MHC molecules and SIINFERKL/H-2Kb complex on the macrophage population (n=4 per group for tumor, n=3 per group for spleen). (F) Representative FACS plots showing the percentage of abundance of total macrophage and macrophage subsets.

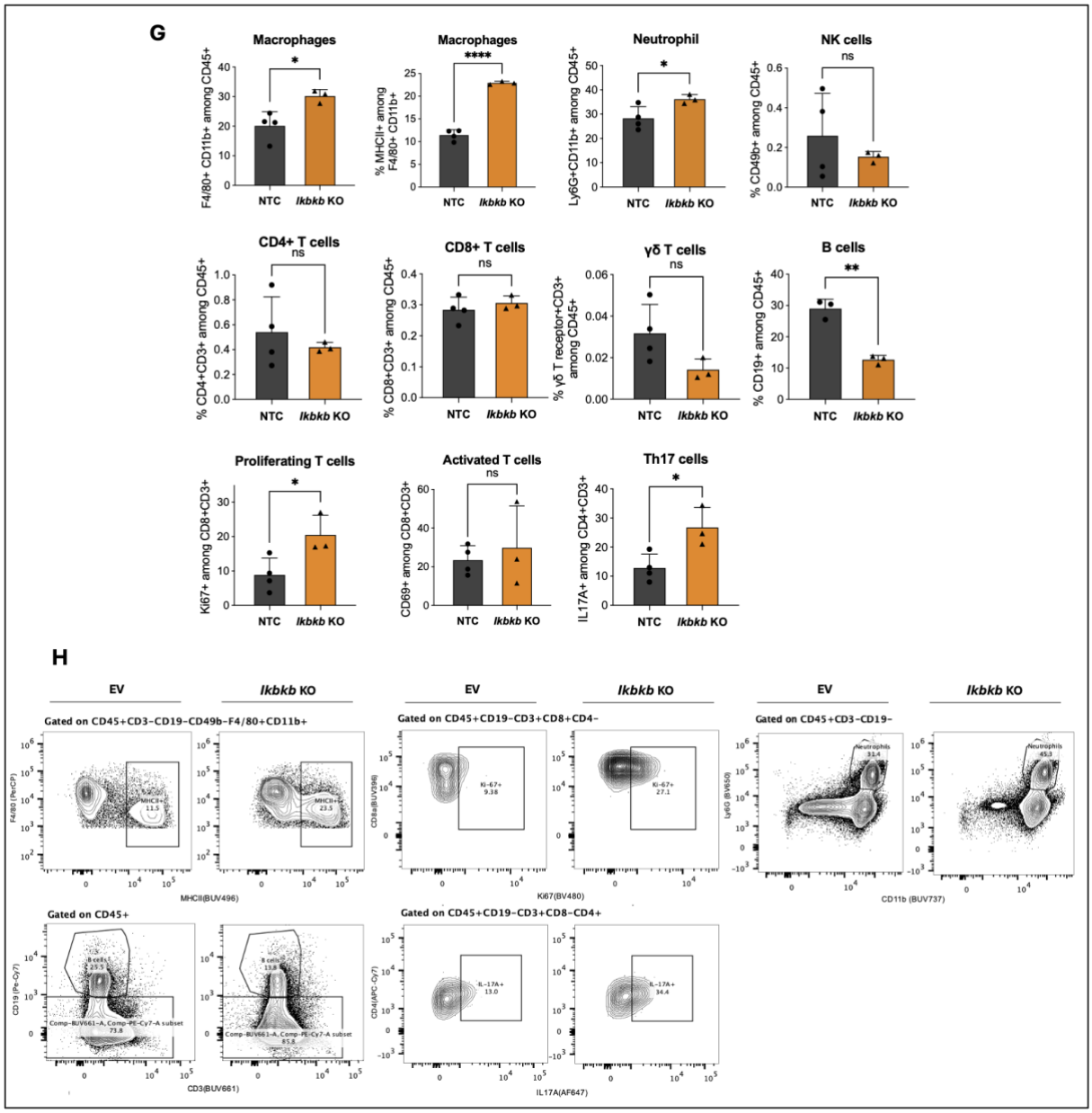

Figure 6.5 *Ikbkb* targeting results in tumor eradication and activation of macrophage and T cells in OVA mice model (cont'). (G) Percent infiltration of immune cells into the HCC tumors (n=4 for NTC and n=3 for *Ikbkb* KO tumors). (F) Representative FACS plots showing the percentage of abundance of immune infiltrates.

6.7 Discussion

Our integrated immunophenotyping and functional study established an indispensable role of Ikkβ in orchestrating an immunosuppressive or tolerogenic TME in HCC, with TAMs serving as pivotal mediators. We showed that hepatocyte-specific *Ikbkb* overexpression drives hepatocarcinogenesis and actively generates an immunologically "cold" TME, characterized by the loss of antitumor innate repertoire and functional inactivation of adaptive T cell immunity. Conversely, *Ikbkb* depletion in tumor reprograms the TME towards immunogenicity, triggering local and systemic antitumor immunity and enhancing tumor clearance.

Our HTVI model revealed that *Ikbkb* overexpression in hepatocytes suppressed antitumor immunity across both the innate and adaptive arms. The observed dramatic reduction in cDC2s is particularly significant, as cDC2s are essential for initiating and sustaining antitumor responses through the priming of CD4+ T helper cells, and their paucity in *Ikbkb*-overexpressing tumors may account for the concurrent reduction of Th1 and Th17 lineages. Meanwhile, overall macrophage infiltration was reduced, and the remaining population of *Ikbkb*-overexpressing tumors exhibited a profoundly tolerogenic phenotype, with diminished expression of antigen-presentation machinery (MHCI/II) and co-stimulatory molecules such as CD86. Impaired CD8+ T cell activation, as evidenced by CD69 expression, also accounted for the enhanced tumor burden in the *Ikbkb*-overexpressing group. However, an open and crucial question is whether this Tc dysfunction is primarily a downstream consequence of failed CD4+ T cell help, a result of direct immunosuppressive signaling from tolerogenic macrophages, or a combination of both mechanisms.

The functional consequences of targeting Ikkβ were demonstrated in our OVA model. Gene depletion not only eases the tumor burden but also enables extensive immune-mediated eradication. This striking outcome might be attributed to a shift in the macrophage phenotype to an immunogenic state. The prominent increase in macrophages, particularly the MHCII+ subset, within the TME, indicates enhanced recruitment and activation. Notably, the SIINFEKL/H-2Kb complex levels were markedly elevated in splenic macrophages, indicating that these splenic phagocytes acquired and cross-presented the tumor-derived OVA antigen, and demonstrated that *Ikbkb* loss triggered systemic antigen spread and potentially immune priming. This process of antigen transport and distant priming explains the antitumor immunity and potent systemic response observed in this study. The resultant influx of proliferating Ki-67+ CD8+ T cells and Th17-polarized T cells into the tumor signifies the active immune

surveillance of the adaptive arm. Nonetheless, the mechanism by which the antigen is transported to the secondary lymphoid organ (here the spleen), whether it involves antigen handoff from macrophages to migratory cells, such as dendritic cells or monocytes, or by other mechanisms, remains an open and critical question for future investigation.

CHAPTER 7 Therapeutic potential of Ikkβ targeting in HCC

7.1 Introduction

Limitations of current treatment modalities and macrophage-based therapies in HCC

HCC presents a formidable therapeutic challenge, as a substantial proportion of patients show poor response or develop acquired resistance to the current standard-of-care treatments, including TKIs such as sorafenib and Lenvatinib, and increasingly, immune checkpoint blockade therapy (Llovet et al., 2022). Even first-line immunotherapy combinations yield durable benefits in a minority of patients, underscoring the critical need to develop alternative combination regimens for HCC treatment. Within the TME of HCC, TAMs represent a major immune infiltrate and are recognized as a central orchestrator of immunosuppression, angiogenesis, and tumor progression. While clinical studies have illustrated the utility of macrophage-targeting approaches in some cancer types, such as PDACs, head and neck cancer, and melanoma, their use has yet to be extensively investigated in HCC. It also remains to be studied how to optimally integrate them with existing therapies to achieve effective and durable responses (Bian et al., 2020; Zhu et al., 2019).

Building upon our previous finding that *IKBKB* regulates the tumoral expression of PD-L1, a molecule known to function as a 'do not eat me' signal or anti-phagocytic protein, we tested the synergistic potential of co-targeting these nodes. We hypothesized that concurrent inhibition of the *IKBKB*/NF-κB pathway and downstream PD-1/PD-L1 interactions would enhance macrophage-mediated phagocytosis of HCC cells, thus cooperatively disrupting the tumor's capacity to evade immune evasion. This hypothesis was tested using *in vitro* and *in vivo* assays. We first determined whether concurrent blockade of PD-L1 binding on tumor cells could further enhance the pro-phagocytic effects of *IKBKB* depletion *in vitro* (Figure 7.1). Next, we tested whether IKKβ pharmacological targeting yields the same phagocytic stimulatory effect as genetic depletion, using a recently developed cell-permeable peptide, TAT-NEMO^{Actpep} (Ko et al., 2022; Figure 7.1). This peptide is derived from a specific region of NEMO (Nuclear Factor-kappa B Essential Modulator; amino acids 384-389, sequence QRRSPP) that binds to IKKβ in a ubiquitin-dependent manner for its full activation (Ko et al., 2022). And it acts as a competitive antagonist to disrupt this secondary and inducible interaction and thereby inhibits downstream canonical NF-κB signaling. The sequence specificity of TAT-NEMO^{Actpep} was illustrated by *in vitro* pull down assays which demonstrated dose-dependent inhibition on the interaction, whereas the control peptide TAT-NEMO$^{Actpep\ 6G}$ (key 384-389 residues mutated to glycine) displayed no effect (Ko et al., 2022).

In terms of it signaling regulation, TAT-NEMO^{Actpep} was shown to specifically suppress canonical NF-κB signaling and impose no effect on non-canonical NF-κB signaling or other parallel inflammatory pathways. This was illustrated by its potent inhibition in IKKβ activation loop phosphorylation, subsequent IκBα degradation, and NF-κB nuclear translocation or DNA binding and lack of effect on p100 processing as well as phosphorylation of MAP kinases JNK, Erk2, and p38 (Ko et al., 2022). Finally, we will translate these findings to an *in vivo* setting by investigating the antitumor effects of TAT-NEMO^{Actpep} monotherapy and its combinatorial efficacy with an anti-PD1 mAb in an HTVI-induced liver cancer model (Figure 7.1). This model will also allow us to assess the specific remodelling of the TME, including changes in TAM, T cells, and innate cell populations, providing a comprehensive evaluation of the immunomodulatory potential of our combination strategy.

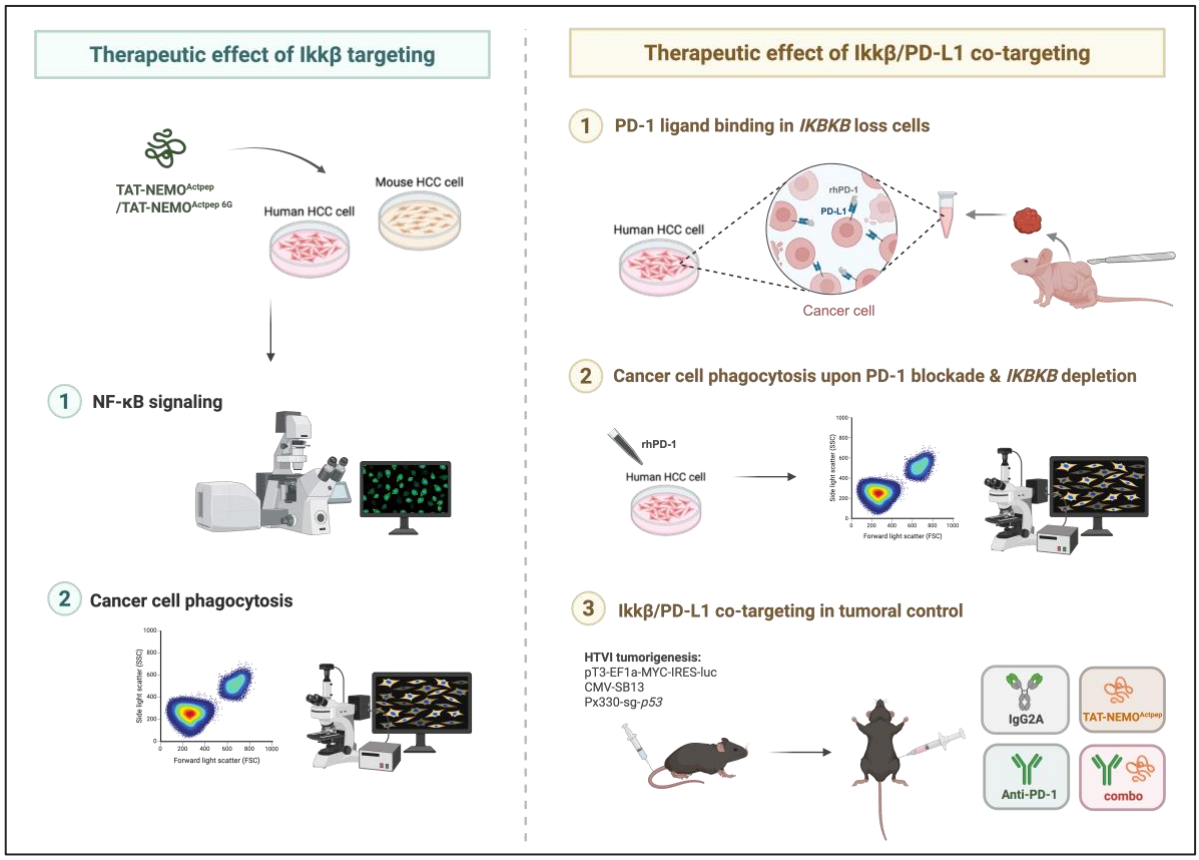

Figure 7.1 Experimental design for investigating therapeutic targeting of IKKβ in HCC.

7.3 Blockade of PD-L1 binding further enhances the pro-phagocytic effect of *IKBKB* depletion

First, to functionally verify that the genetic depletion of *IKBKB* leads to a reduction in surface PD-L1 capable of engaging its receptor, we employed a recombinant human PD-1 (rhPD-1) protein binding assay. The results confirmed our molecular finding that *IKBKB*-depleted cells exhibited a reduced percentage of cells binding to rhPD-1 *in vitro* (Figure 7.2A-B). This effect was recapitulated in vivo, as flow cytometry analysis of subcutaneous tumors derived from *IKBKB*-deficient cells showed markedly diminished PD-1 ligand-binding capacity, directly correlated with our earlier data demonstrating reduced PD-L1 protein expression upon *IKBKB* loss (Figure 7.2C, 5.2B-D, 5.4C). Subsequently, we tested the functional consequences of PD-L1 blockade with rhPD-1 protein, and from the phagocytosis assays, the combination of intrinsic *IKBKB* depletion and extrinsic PD-1/PD-L1 interaction blockade produced a synergistic effect. Macrophages demonstrated significantly enhanced phagocytic capacity against *IKBKB*-loss cells in the presence of rhPD-1. The potentiation was evident in both flow and microscopy data, showing an increased phagocytosis rate (Figure 7.2D-G).

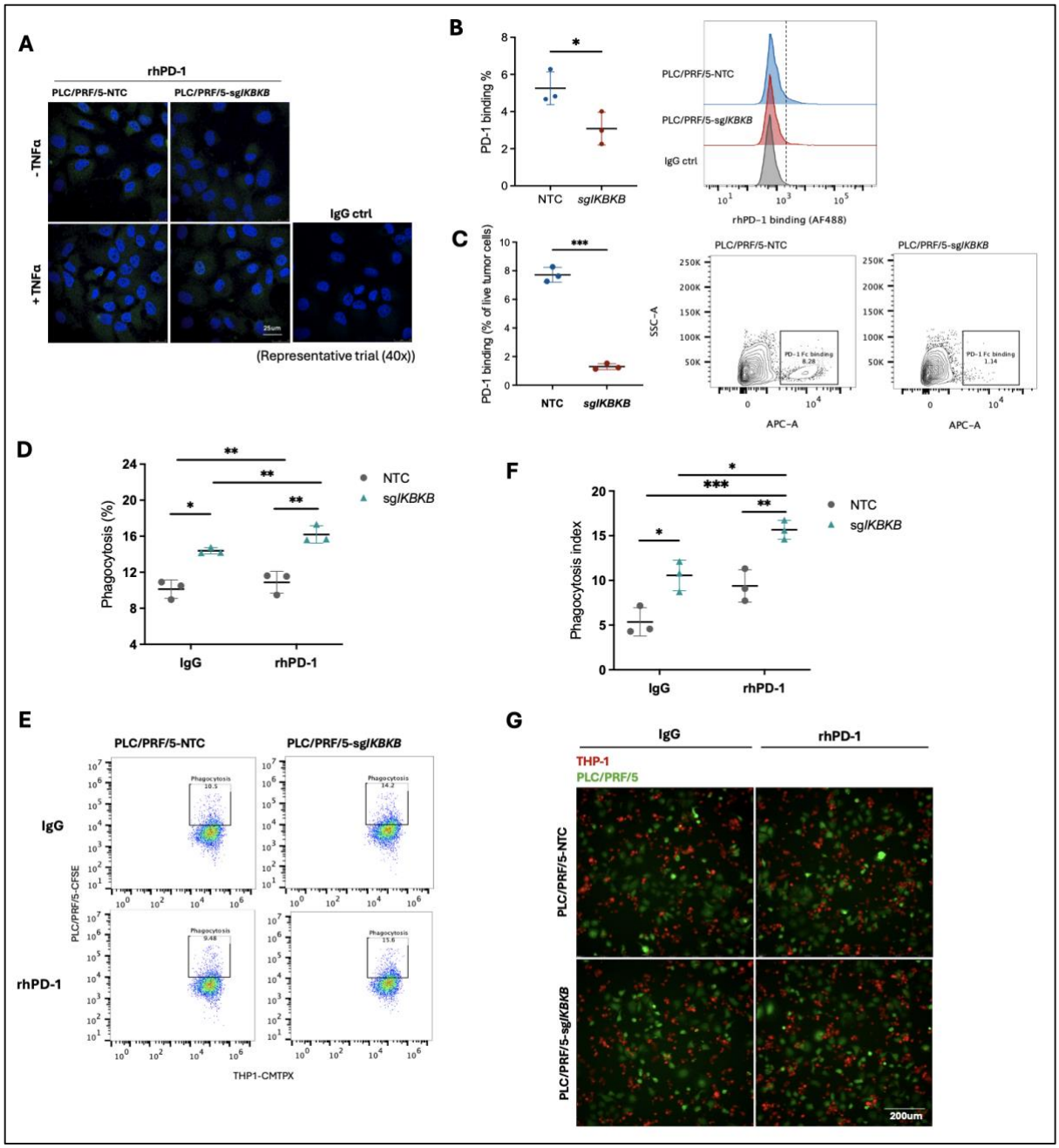

Figure 7.2 *IKBKB* loss weakens PD-1 binding and co-targeting further potentiates HCC cell phagocytosis. (A) Representative immunofluorescence (IF) images for rhPD-1 binding (green) of PLC/PRF/5-NTC and PLC/PRF/5-sg*IKBKB*. Nuclei are counterstained with DAPI (blue). (B) Flow cytometry analysis for rhPD-1 binding of PLC/PRF/5-NTC and PLC/PRF/5-sg*IKBKB*. *(C)* Flow cytometry analysis for rhPD-1 binding of PLC/PRF/5-NTC and PLC/PRF/5-sg*IKBKB tumors. (D)* Dot plot showing phagocytosis rate determined by flow cytometry (N=3). (E) Representative FACS plots showing phagocytosis rate. (F) Dot plot and (G) Representative fluorescence microscopic images of three independent experiments showing phagocytosis index determined by microscopy-based phagocytosis assay.

7.2 Targeting IKKβ suppresses canonical NF-κB signaling and HCC cell phagocytosis

Prior to assessing the systemic effect of PD-L1 and IKKβ targeting in tumoral control *in vivo*, we first sought to characterize the activity of TAT-NEMO^{Actpep}. To determine the optimal dosing parameter for eliciting its potentiation of macrophage phagocytic activity, we conducted flow cytometry-based analysis. We found that 8-hour incubation with TAT-NEMO^{Actpep} 100 μM produced the optimal pro-phagocytic effect (Figure 7.3A). We next validated the peptides' on-target molecular mechanism, which is the inhibition of NF-κB signaling**.** This is assessed by the nuclear localization of phosphorylated p65 and p65. Immunofluorescence analysis confirmed that treatment with TAT-NEMO^{Actpep} effectively suppressed the nuclear localization of both forms of p65, demonstrating robust suppression of the canonical NF-κB pathway using this peptide, and this result aligns with its reported effectiveness in blocking the intended pathway (Figure 7.3B-C). We then performed phagocytosis assays following the peptide incubation and macrophage co-incubation. We found the pharmacological IKKβ targeting stimulates macrophage phagocytosis of HCC cells, recapitulating our previous findings on genetic *Ikbkb* depletion (Figure 7.3D-E).

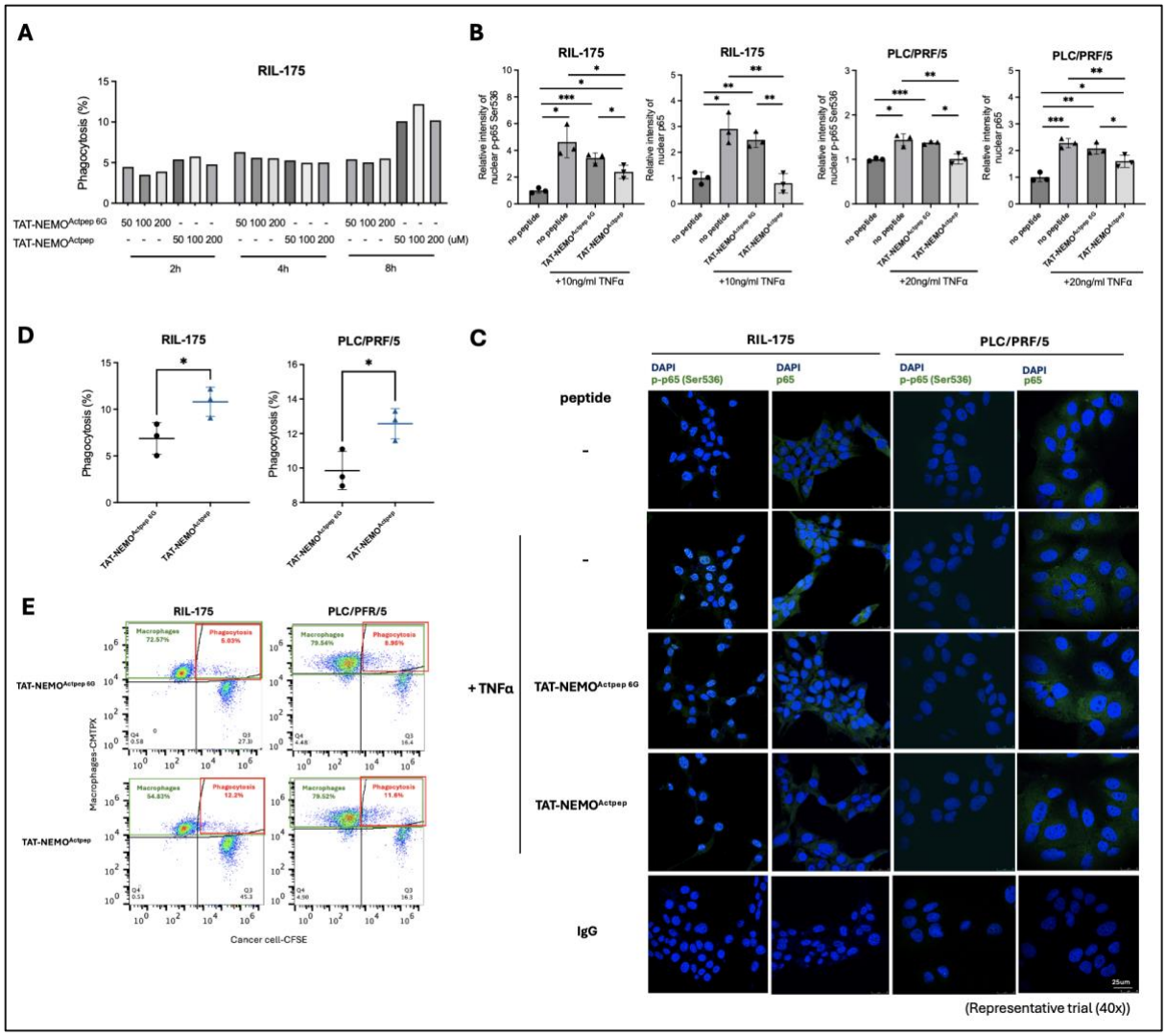

Figure 7.3 Characterization of TAT-NEMO^{Actpep} *in vitro*. (A) Bar chart showing phagocytosis rate of administering various doses of TAT-NEMO peptides with different durations. (B) Quantification of IF images and (C) representative images for phosphor-p65(Ser 536) and p65 nuclear localization. (D-E) Phagocytosis rate for TAT-NEMO peptides treatment in HCC cells.

7.4 IKKβ and PD-1 co-targeting attenuates tumor progression in HCC

To evaluate the systemic antitumor efficacy of IKKβ targeting, both as a single agent and in combination with PD1 blockade, we employed the HTVI model of hepatocarcinogenesis. This model was selected because it generates HCC that recapitulates "immune-cold," or non-inflamed, tumor microenvironment, a phenotype known to be unresponsive to anti-PD-1 monotherapy, thus providing a stringent test for our combination strategy. We initiated tumorigenesis by hydrodynamic injection of px330-sg-*p53-*,MYC-luc, and CMV-SB13 plasmids into 8-week-old male CD57BL/6 mice, which were then randomized into four treatment groups based on bioluminescence signal before treatment initiation (Figure 7.4A). Consistent with a previous report, anti-PD-1 mAb monotherapy was ineffective in tumor control. In contrast, TAT-NEMO^{Actpep} monotherapy showed a trend toward tumor growth suppression, and the combined therapy was effective in reducing the tumor burden (Figure 7.4B-C). Importantly, this enhanced antitumor efficacy was not accompanied by overt systemic toxicity, as evidenced by the insignificant body weight alterations in all treated mice throughout the study period (Figure 7.4D). In line with our previous findings, IKKβ and PD-1 co-targeting resulted in enhanced macrophage recruitment into the HCC TME and stimulated their activation, yet their contribution to the observed tumoral control remains to be studied (Figure 7.4E).

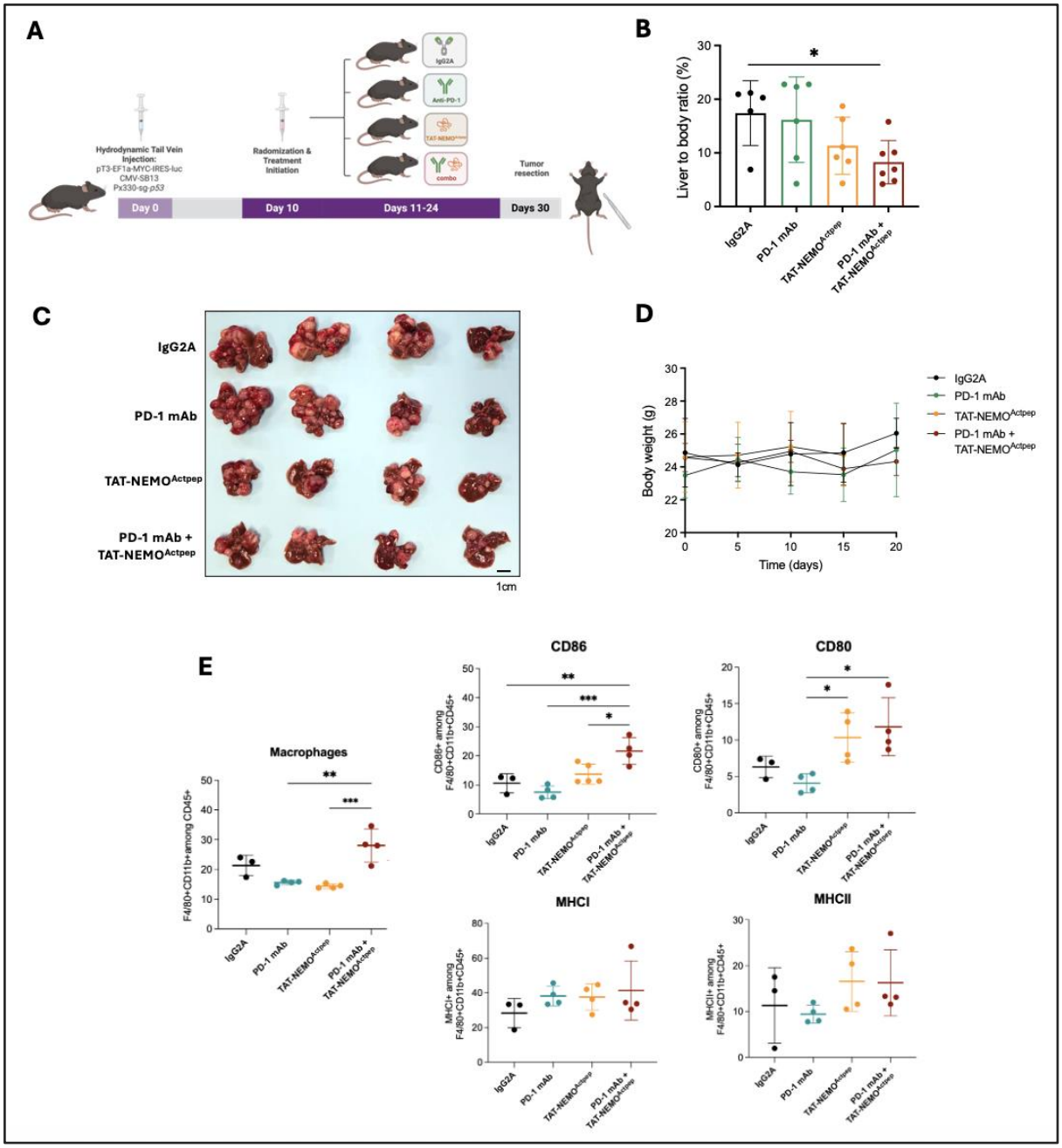

Figure 7.4 Therapeutic potential for IKKβ targeting. (A) Schematics showing the treatment regimens. (B) Liver-to-body ratio for mice receiving different treatments at day 30 after HTVI. (n=5 for IgG2A, n= 6 for TAT-NEMO^{Actpep} and anti-PD-1 mAb, n=7 for combination group). (C) Representative tumor images on day 30 after HTVI. (D) Mice's body weight in different treatment groups. (E) Percent macrophage infiltration and expression of MHC molecules, co-stimulatory markers in the macrophage population (n=3 for IgG2A group, n=4 for the remaining groups). Data are shown as the mean ± SEM (*$p < 0.05$, **$p < 0.01$, ***$p < 0.001$; One way ANOVA followed by Tukey's multiple comparison test).

7.5 Discussion

The results presented in the chapter demonstrated the therapeutic potential of a novel strategy that simultaneously inhibits the IKKβ/ NF-κB pathway and the PD-1/PD-L1 immune checkpoint in HCC. Our data provide evidence, from molecular target validation to functional *in vitro* synergy and to *in vivo* efficacy in an "immune-cold" tumor model. The foundation of this approach lies in our initial finding that depletion of *Ikbkb* downregulates PD-L1 expression in HCC (Chapter 5). In this chapter, we validate the functional link, showing that *Ikbkb*-loss cells exhibit reduced binding for PD-1. Crucially, when this intrinsic reduction in PD-L1 was combined with extrinsic blockade using recombinant PD-1 protein, we observed synergistic enhancement of macrophage phagocytosis, resembling the effect of maximal pathway inhibition. This also aligns with previous studies that PD-L1 functions as a critical anti-phagocytic signal in HCC, and targeting both the upstream regulator, IKKβ, and the downstream receptor-ligand interaction can disrupt this immune evasion mechanism. This also positions our strategy to potentiate both innate (macrophage phagocytosis) and adaptive (T-cell cytotoxicity) immunity.

We then demonstrated that pharmacological inhibition of IKKβ with TAT-NEMO^{Actpep} can potentiate macrophage phagocytic clearance of tumor cells, resembling the effect observed in gene depletion experiments. In a preclinical model, we demonstrated the therapeutic potential of IKKβ targeting with TAT-NEMO^{Actpep}, which is deemed to slow tumor growth in cold tumors. A primary benefit of using peptides rather than kinase inhibitors is their high specificity and affinity for targeted molecules owing to their specific amino acid sequence, which minimizes off-target effects and enhances therapeutic efficacy. Moreover, they are generally less immunogenic than large protein inhibitors and are metabolized into natural amino acids, preventing toxic metabolite accumulation. The third advantage is the cell-penetrable nature of the TAT sequence, which enables cellular uptake by cancer cells to exert its effect intracellularly.

Critically, the combinatorial approach with anti-PD-1 antibody demonstrated significant synergy in tumor control without imposing overt systemic toxicity. These results support our central premise that IKKβ inhibition can remodel the immunosuppressive TME and potentially convert a cold, PD-1-resistant tumor into a responsive state. Taken together with our previous findings, this synergy likely stems from IKKβ inhibition mitigating barriers to immunotherapy, including preventing HCC cell evasion from phagocytosis and enhancing antigen presentation

and T cell responses, thereby allowing PD-1 blockade to more effectively provoke pre-existing or newly primed T-cell responses. Despite these interesting findings, the precise immune subset changes within the TME following combination therapy, particularly the functional status of the T cell repertoire, require deeper characterization by immune phenotyping, which will be conducted subsequently. Furthermore, the long-term durability of the response and potential acquired resistance remains to be investigated. In this pilot study, the peptide was administered every two days and one day prior to anti-PD-1 treatment. Future optimization of the dosing schedule is required to determine whether a combination or sequential therapy regimen yields superior immunostimulatory effects. From clinical development perspective, both agents are amenable to systemic administration. Anti-PD-1 antibodies are routinely delivered through intravenous (IV) infusion using well established dosing schedule, i.e. 240mg every two weeks. TAT-NEMO^{actpep}, as a peptide therapeutic, could similarly be administrated via IV infusion, prior to the checkpoint inhibitor, allowing for systemic exposure and precise dose escalation.

CHAPTER 8 Conclusion & Future Perspectives

The investigation of macrophage targeting in HCC was motivated by its unique therapeutic potential. Their abundance, functional plasticity, and pivotal role in bridging innate and adaptive immunity present a compelling but underexplored area for HCC treatment. This study employed a pooled CRISPR-Cas9 knockout screen targeting the mouse kinome to systematically identify the genes regulating the susceptibility of HCC cells to macrophage-mediated phagocytosis. Our screening and validation experiments identified *Ikbkb* (IKKβ) as the master regulator of phagocytic evasion in HCC. Genetic ablation of *Ikbkb* sensitizes cancer cells to phagocytic clearance in both murine and human cells and mouse models, an effect that translates to significant *in vivo tumor* control. Critically, the *in vivo* reliance on macrophages for tumor clearance was proven by a macrophage-ablation experiment, which completely reversed the therapeutic benefit of the pro-phagocytic phenotype. Mechanistically, we have shown that *Ikbkbs suppresses* cancer cell phagocytosis by supporting surface expression of antiphagocytic proteins, CD47 and PD-L1, potentially through the canonical NF-κB pathway. While IKKβ is frequently reported to promote cancer cell survival, our findings revealed no measurable impact of *Ikbkb* depletion on cell proliferation, both *in vitro* and *in vivo.* This suggests that the potent antitumor effects we observed are not primarily mediated by halting cell division but rather driven by enhanced immune surveillance by macrophages, based on our *in vivo* findings. However, the potential role of IKKβ in regulating cancer stemness, a function well-established for its downstream NF-κB pathway, remains a plausible and important avenue for future investigation.

Following the observation that *Ikbkb* depletion in cancer cells drives a macrophage phenotypic shift towards an antitumor state (marked by increased CD80/86 expression), we examined the broader immunomodulatory consequences of this reprogramming on the TME. In HCC, TAMs possess a profoundly immunosuppressive phenotype that promotes tumor progression and actively inhibits adaptive immunity, particularly T-cell activity, as corroborated by the literature and single-cell dataset analyses. We therefore anticipated that such a phenotypic shift would alleviate this suppressive pressure and thereby potentiate the function of other immune subsets within the TME. We demonstrated that hepatocyte-specific *Ikbkb* overexpression accelerates hepatocarcinogenesis and actively engineers a profoundly immunosuppressive TME, characterized by impaired innate immune cell infiltration and function, alongside a blunted adaptive immunity. Conversely, *Ikbkb* depletion in cancer cells on an immunocompetent, orthotopic model produced a dramatic antitumor effect. This efficacy was underpinned by a remodeled TME featuring increased infiltration of antitumor macrophages

characterized by elevated antigen-presentation or costimulatory molecules (MHCI/II). These changes likely orchestrated the robust recruitment of proliferating T and Th17 cells into the tumor, leading to effective immune-mediated tumor eradication. Our data indicates that cancer cell-intrinsic *Ikbkb depletion* remodels the TME to a more immunogenic state. However, the observed association between antitumor macrophage polarization and enhanced T-cell activity remains correlative. More definitive approaches, like macrophage-ablation experiment, are required to provide causal evidence that macrophage repolarization and adaptive immunity activity. Moreover, our data showed that *Ikbkb* loss potentiated the systemic immune response, leading to enhanced cross-presentation of tumor antigen (OVA) by splenic macrophages. Critical downstream consequences, that is, functional expansion and activation of OVA-specific Tc cells, remain to be quantified and characterized.

The translational potential of this strategy is underscored by the synergistic tumor control achieved by combining the pharmacological IKKβ inhibitor TAT-NEMO^{Actpep} with anti-PD-1 therapy in a model of immunotherapy-resistant HCC. This combination successfully addresses primary resistance to checkpoint blockade by simultaneously dampening the cancer cell's defensive shield and disrupting immunosuppressive interactions in the TME. Despite this observed preclinical efficacy and a favorable initial toxicity profile, given that the IKKβ/NF-κB pathway is a key signaling hub for the function and survival of immune cells, future studies should precisely delineate the immune subset changes induced by the combination approach and investigate its long-term durability. Furthermore, the immune mechanisms of response and resistance require further investigation. While we demonstrated the TAM phenotypic shift and CD8+ T cell response, single-cell RNA sequencing of the TME before and after treatment could reveal a finer shift in macrophage subsets, dendritic cell states, and T cell activation or exhaustion. Understanding these dynamics will help identify compensatory resistance pathways that may emerge or expand in other immunosuppressive subsets. This knowledge can inform the design of rational treatment regimens, potentially adding additional agents to counteract potential escape mechanisms.

Taken together, this study illustrates that IKKβ is a master regulator of immune evasion and positions its inhibition as an effective strategy to reprogram the TME. Future investigations should examine adaptive response potentiation, long-term efficacy, resistance, and rational combinations. By addressing these issues, the promising synergy between IKKβ and PD-1 inhibition can be translated into an efficacious treatment option for patients with advanced, and possibly immunotherapy-resistant, HCC.

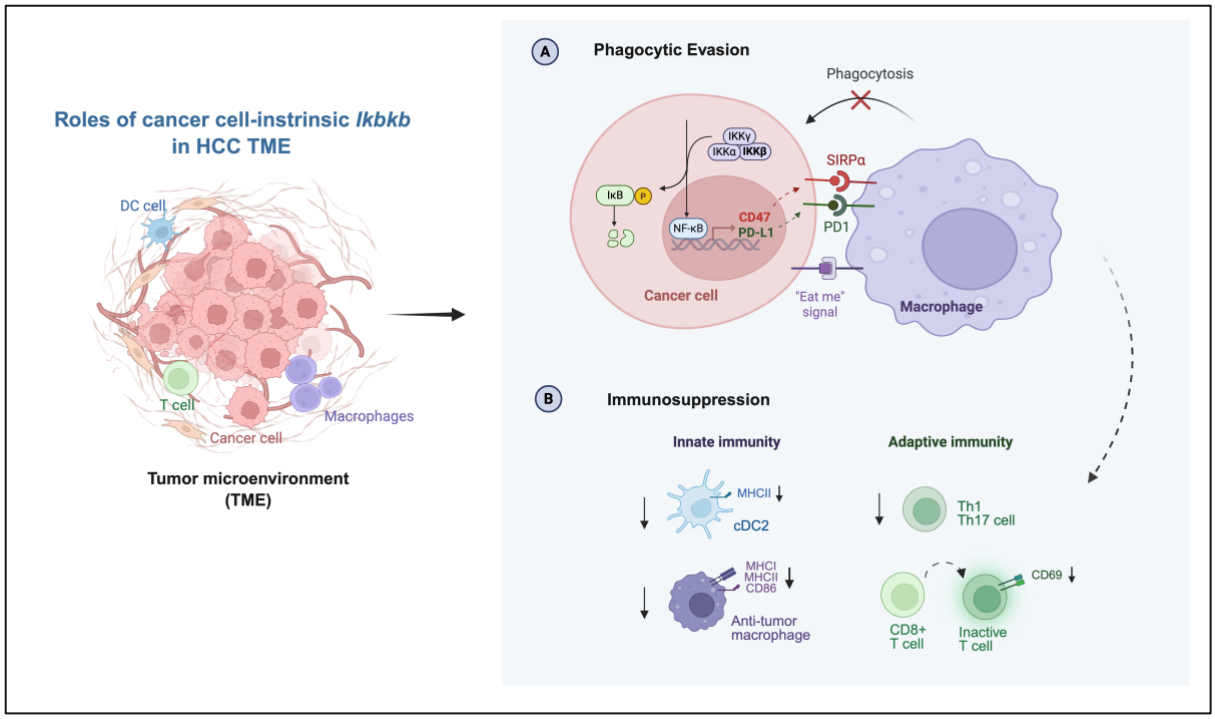

Figure 8. Schematic diagram showing the role of *Ikbkb* in immune regulation in HCC

References

Abou- Alfa, G. K. et al. Cabozantinib in patients with advanced and progressing hepatocellular carcinoma. N. Engl. J. Med. 379, 54–63 (2018).

Abou-Alfa Ghassan, K. et al. Tremelimumab plus durvalumab in unresectable hepatocellular carcinoma. NEJM Evid. 1, EVIDoa2100070 (2022).

Abou-Alfa, G.K. *et al.* (2022) 'Phase 3 randomized, open-label, Multicenter Study of Tremelimumab (T) and durvalumab (D) as first-line therapy in patients (PTS) with unresectable hepatocellular carcinoma (uHCC): Himalaya.', *Journal of Clinical Oncology*, 40(4_suppl), pp. 379–379. doi:10.1200/jco.2022.40.4_suppl.379.

Advani, R. *et al.* (2018) 'CD47 blockade by Hu5f9-G4 and Rituximab in Non-Hodgkin's lymphoma', *New England Journal of Medicine*, 379(18), pp. 1711–1721. doi:10.1056/nejmoa1807315.

Alloatti, A., Kotsias, F., Pauwels, A. M., Carpier, J. M., Jouve, M., Timmerman, E., ... & Amigorena, S. (2015). Toll-like receptor 4 engagement on dendritic cells restrains phago-lysosome fusion and promotes cross-presentation of antigens. *Immunity*, 43(6), 1087-1100.

Anderson, N., Minutolo, N., Gill, S., and Klichinsky, M., 2020. Macrophage-Based Approaches for Cancer Immunotherapy. *Cancer Research*, 81(5), pp.1201-1208.

Ansell, S.M. *et al.* (2021) 'Phase I study of the CD47 blocker TTI-621 in patients with relapsed or refractory hematologic malignancies', *Clinical Cancer Research*, 27(8), pp. 2190–2199. doi:10.1158/1078-0432.ccr-20-3706.

Antonangeli, F., Natalini, A., Garassino, M. C., Sica, A., Santoni, A., & Di Rosa, F. (2020). Regulation of PD-L1 expression by NF-KB in cancer. *Frontiers in Immunology*, *11*. doi.org/10.3389/fimmu.2020.584626

Barkal, A., Brewer, R., Markovic, M., Kowarsky, M., Barkal, S., Zaro, B., Krishnan, V., Hatakeyama, J., Dorigo, O., Barkal, L., and Weissman, I., 2019. CD24 signalling through macrophage Siglec-10 is a target for cancer immunotherapy. *Nature*, 572(7769), pp.392-396.

Bennett, S. R., et al. (1998). Help for cytotoxic-T-cell responses is mediated by CD40 signalling. *Nature*, 393(6684), 478–480.

Betancur, P. A., Abraham, B. J., Yiu, Y. Y., Willingham, S. B., Khameneh, F., Zarnegar, M., Kuo, A. H., McKenna, K., Kojima, Y., Leeper, N. J., Ho, P., Gip, P., Swigut, T., Sherwood, R. I., Clarke, M. F., Somlo, G., Young, R. A., & Weissman, I. L. (2017). A CD47-associated super-enhancer links pro-inflammatory signalling to CD47 upregulation in breast cancer. *Nature Communications*, *8*(1), 14802. doi.org/10.1038/ncomms14802

Bevan, M. J. (2004). Helping the CD8+ T-cell response. *Nature Reviews Immunology*, 4(8), 595–602.

Bian, J., Zhang, S., Yang, Y., Liu, Y., Sun, X., & Wang, Y. (2020). CCL2-CCR2 axis recruits tumor associated macrophages to induce immune evasion through PD-1 signaling in esophageal carcinogenesis. *Molecular Cancer*, *19*(1), 41.

Blum, J. S., Wearsch, P. A., & Cresswell, P. (2013). Pathways of antigen processing. *Annual Review of Immunology*, 31, 443-473.

Bogdanov, A. A., Lin, C. P., Simonova, M., Matuszewski, L., & Weissleder, R. (2002). Cellular activation of the Self-Quenched fluorescent Reporter probe in tumor microenvironment. *Neoplasia*, *4*(3), 228–236. doi.org/10.1038/sj.neo.7900238

Borst, J., Ahrends, T., Bąbała, N., Melief, C. J. M., & Kastenmüller, W. (2018). CD4+ T cell help in cancer immunology and immunotherapy. *Nature Reviews Immunology*, 18(10), 635–647.

Bruix, J. et al. Regorafenib for patients with hepatocellular carcinoma who progressed on sorafenib treatment (RESORCE): a randomised, double- blind, placebo-controlled, phase 3 trial. Lancet 389, 56–66 (2017).

Cabibbo, G. et al. A meta-analysis of survival rates of untreated patients in randomized clinical trials of hepatocellular carcinoma. Hepatology 51,1274–1283 (2010).

Cabibbo, G., Enea, M., Attanasio, M., Bruix, J., Craxì, A. and Cammà, C., 2009. A meta-analysis of survival rates of untreated patients in randomized clinical trials of hepatocellular carcinoma. *Hepatology*, 51(4), pp.1274-1283.

Cao, X., Chen, J., Li, B., Dang, J., Zhang, W., Zhong, X., Wang, C., Raoof, M., Sun, Z., Yu, J., Fakih, M. G., & Feng, M. (2022). Promoting antibody-dependent cellular phagocytosis for effective macrophage-based cancer immunotherapy. *Science Advances*, *8*(11), eabl9171. doi.org/10.1126/sciadv.abl9171

Cassetta, L., Pollard, J. Targeting macrophages: therapeutic approaches in cancer. *Nat Rev Drug Discov* 17, 887–904 (2018). doi.org/10.1038/nrd.2018.169

Chao, M., Alizadeh, A., Tang, C., Myklebust, J., Varghese, B., Gill, S., Jan, M., Cha, A., Chan, C., Tan, B., Park, C., Zhao, F., Kohrt, H., Malumbres, R., Briones, J., Gascoyne, R., Lossos, I., Levy, R., Weissman, I. and Majeti, R., 2010. Anti-CD47 Antibody Synergizes with Rituximab to Promote Phagocytosis and Eradicate Non-Hodgkin Lymphoma. *Cell*, 142(5), pp.699-713.

Chen, L., & Flies, D. B. (2013). Molecular mechanisms of T cell co-stimulation and co-inhibition. *Nature Reviews Immunology*, 13(4), 227–242.

Cheng, A., 2021. Pursuing efficacious systemic therapy for hepatocellular carcinoma. *Nature Reviews Gastroenterology & Hepatology*, 18(2), pp.95-96.

Cleary, S.P. *et al.* (2013) 'Identification of driver genes in hepatocellular carcinoma by exome sequencing', *Hepatology*, 58(5), pp. 1693–1702. doi:10.1002/hep.26540.

Daver, N. G., Vyas, P., Huls, G. A., Döhner, H., Maury, S., Novak, J., Papayannidis, C., Chamorro, C. M., Montesinos, P., Niroula, R., Fenaux, P., Esteve, J., Wu, S., De Voeght, A., Mayer, J., Valk, P. J., Johnson, L., Dong, M., Liu, K., . . . Murthy, G. S. G. (2025). The ENHANCE-3 study: venetoclax and azacitidine plus magrolimab or placebo for untreated AML unfit for intensive therapy. *Blood*, *146*(5), 601–611. doi.org/10.1182/blood.2024027506

De Waele, J., Verhezen, T., Van Der Heijden, S., Berneman, Z. N., Peeters, M., Lardon, F., Wouters, A., & Smits, E. L. J. M. (2021). A systematic review on poly(I:C) and poly-ICLC in glioblastoma: adjuvants coordinating the unlocking of immunotherapy. *Journal of Experimental & Clinical Cancer Research*, *40*(1), 213. doi.org/10.1186/s13046-021-02017-2

Deng, L., Liu, Y., Lin, N., Yao, Z., Zhang, J., Meng, W., Lu, Q., Tian, W., Zhu, J., & Song, Y. (2024). Phase Ib/IIa Study of Amulirafusp Alfa (IMM0306) in Combination with Lenalidomide in Patients with Relapsed or Refractory CD20-Positive B-Cell Non-Hodgkin's Lymphoma. *Blood*, *144*(Supplement 1), 3033. doi.org/10.1182/blood-2024-200539

Duan, Z., Luo, Y. Targeting macrophages in cancer immunotherapy. *Sig Transduct Target Ther* 6, 127 (2021). doi.org/10.1038/s41392-021-00506-6

Eggert, T. et al. Distinct Functions of Senescence-Associated Immune Responses in Liver Tumor Surveillance and Tumor Progression. *Cancer Cell* 30, 533–547 (2016).

El-Khoueiry, A. B. et al. Nivolumab in patients with advanced hepatocellular carcinoma (CheckMate 040): an open-label, non-comparative, phase 1/2 dose escalation and expansion trial. Lancet 389, 2492–2502 (2017).

Feng, M., Jiang, W., Kim, B.Y.S. *et al.* Phagocytosis checkpoints as new targets for cancer immunotherapy. *Nat Rev Cancer* 19, 568–586 (2019). doi.org/10.1038/s41568-019-0183-z

Ferrari de Andrade, L., Tay, R., Pan, D., Luoma, A., Ito, Y., Badrinath, S., Tsoucas, D., Franz, B., May, K., Harvey, C., Kobold, S., Pyrdol, J., Yoon, C., Yuan, G., Hodi, F., Dranoff, G. and Wucherpfennig, K., 2018. Antibody-mediated inhibition of MICA and MICB shedding promotes NK cell–driven tumor immunity. *Science*, 359(6383), pp.1537-1542.

Ferris, R. L., Saba, N. F., Gitlitz, B. J., Haddad, R., Sukari, A., Neupane, P., Morris, J. C., Misiukiewicz, K., Bauman, J. E., Fenton, M., Jimeno, A., Adkins, D. R., Schneider, C. J., Sacco, A. G., Shirai, K., Bowles, D. W., Gibson, M., Nwizu, T., Gottardo, R., . . . Cohen, E. E. W. (2018). Effect of adding Motolimod to standard combination chemotherapy and Cetuximab treatment of patients with squamous cell carcinoma of the head and neck. *JAMA Oncology*, *4*(11), 1583. doi.org/10.1001/jamaoncol.2018.1888

Finn, R. S. et al. Pembrolizumab as second-line therapy in patients with advanced hepatocellular carcinoma in KEYNOTE-240: a randomized, double-blind, phase III trial. J. Clin. Oncol. 38, 193–202 (2020).

Finn, R. S. et al. Phase Ib study of lenvatinib plus pembrolizumab in patients with unresectable hepatocellular carcinoma. J. Clin. Oncol. 38, 2960–2970 (2020).

Finn, R., Qin, S., Ikeda, M., Galle, P., Ducreux, M., Kim, T., Kudo, M., Breder, V., Merle, P., Kaseb, A., Li, D., Verret, W., Xu, D., Hernandez, S., Liu, J., Huang, C., Mulla, S., Wang, Y., Lim, H., Zhu, A. and Cheng, A., 2020. Atezolizumab plus Bevacizumab in Unresectable Hepatocellular Carcinoma. *New England Journal of Medicine*, 382(20), pp.1894-1905.

Finn, R.S. *et al.* (2020) 'Atezolizumab plus bevacizumab in unresectable hepatocellular carcinoma', *New England Journal of Medicine*, 382(20), pp. 1894–1905. doi:10.1056/nejmoa1915745.

Gelderblom, H., Palmerini, E., Blay, J., Van De Sande, M., Broto, J. M., Terés, R., Davies, M., Seltzer, E., Veltkamp, S., & Tinoco, G. (2025). A phase 3, randomized, double-blind, placebo-controlled study to assess the efficacy and safety of emactuzumab in patients with tenosynovial giant cell tumor (TANGENT). *Journal of Clinical Oncology*, *43*(16_suppl). doi.org/10.1200/jco.2025.43.16_suppl.tps11584

Greten, F. R., Eckmann, L., Greten, T. F., Park, J. M., Li, Z. W., Egan, L. J., ... & Karin, M. (2004). IKKβ links inflammation and tumorigenesis in a mouse model of colitis-associated cancer. Cell, 118(3), 285-296.

Gholamin, S., Mitra, S., Feroze, A., Liu, J., Kahn, S., Zhang, M., Esparza, R., Richard, C., Ramaswamy, V., Remke, M., Volkmer, A., Willingham, S., Ponnuswami, A., McCarty, A., Lovelace, P., Storm, T., Schubert, S., Hutter, G., Narayanan, C., Chu, P., Raabe, E., Harsh, G., Taylor, M., Monje, M., Cho, Y., Majeti, R., Volkmer, J., Fisher, P., Grant, G., Steinberg, G., Vogel, H., Edwards, M., Weissman, I. and Cheshier, S., 2017. Disrupting the CD47-SIRPα anti-phagocytic axis by a humanized anti-CD47 antibody is an efficacious treatment for malignant pediatric brain tumors. *Science Translational Medicine*, 9(381).

Gomez-Roca, C., Cassier, P., Zamarin, D., Machiels, J., Gracia, J. L. P., Hodi, F. S., Taus, A., Garcia, M. M., Boni, V., Eder, J. P., Hafez, N., Sullivan, R., Mcdermott, D., Champiat, S., Aspeslagh, S., Terret, C., Jegg, A., Jacob, W., Cannarile, M. A., . . . Marabelle, A. (2022b). Anti-CSF-1R emactuzumab in combination with anti-PD-L1 atezolizumab in advanced solid tumor patients naïve or experienced for immune checkpoint blockade. *Journal for ImmunoTherapy of Cancer*, *10*(5), e004076. doi.org/10.1136/jitc-2021-004076

Grotzke, J. E., Kozik, P., Morel, J. D., Impens, F., Pietrosemoli, N., Cresswell, P., & Amigorena, S. (2017). Sec61 blockade by mycolactone inhibits antigen cross-presentation independently of endosome-to-cytosol export. *Proceedings of the National Academy of Sciences*, 114(29), E5910-E5919.

Gül, N., Babes, L., Siegmund, K., Korthouwer, R., Bögels, M., Braster, R., Vidarsson, G., ten Hagen, T., Kubes, P. and van Egmond, M., 2014. Macrophages eliminate circulating tumor cells after monoclonal antibody therapy. *Journal of Clinical Investigation*, 124(2), pp.812-823.

Hagemann, T., Lawrence, T., McNeish, I., Charles, K. A., Kulbe, H., Thompson, R. G., Robinson, S. C., & Balkwill, F. R. (2008). "Re-educating" tumor-associated macrophages by targeting NF-κB. *The Journal of Experimental Medicine, 205*(6), 1261–1268.

Herter, S., Birk, M., Klein, C., Gerdes, C., Umana, P. and Bacac, M., 2014. Glycoengineering of Therapeutic Antibodies Enhances Monocyte/Macrophage-Mediated Phagocytosis and Cytotoxicity. *The Journal of Immunology*, 192(5), pp.2252-2260.

Hagemann, T., Lawrence, T., McNeish, I., Charles, K. A., Kulbe, H., Thompson, R. G., ... & Balkwill, F. R. (2008). "Re-educating" tumor-associated macrophages by targeting NF-κB. Journal of Experimental Medicine, 205(6), 1261-1268.

Huntington, N., Cursons, J. and Rautela, J., 2020. The cancer–natural killer cell immunity cycle. *Nature Reviews Cancer*, 20(8), pp.437-454.

Iborra, S., & Sancho, D. (2015). Signalling versatility following self and non-self sensing by myeloid C-type lectin receptors. *Immunobiology*, 220(2), 175–184.

Im, J., Buzzelli, J., Jones, K., Franchini, F., Gordon-Weeks, A., Markelc, B., Chen, J., Kim, J., Cao, Y. and Muschel, R., 2020. FGF2 alters macrophage polarization, tumor immunity and growth and can be targeted during radiotherapy. *Nature Communications*, 11(1).

Johnson, D. B., Sullivan, R. J. & Menzies, A. M. Immune checkpoint inhibitors in challenging populations. Cancer 123, 1904–1911 (2017).

Johnson, M., Dudek, A. Z., Sukari, A., Call, J., Kunk, P. R., Lewis, K., Gainor, J. F., Sarantopoulos, J., Lee, P., Golden, A., Harney, A., Rothenberg, S. M., Zhang, Y., & Goldman, J. W. (2022). ARRY-382 in Combination with Pembrolizumab in Patients with Advanced Solid Tumors: Results from a Phase 1b/2 Study. *Clinical Cancer Research*, *28*(12), 2517–2526. doi.org/10.1158/1078-0432.ccr-21-3009

Kamber, R., Nishiga, Y., Morton, B., Banuelos, A., Barkal, A., Vences-Catalán, F., Gu, M., Fernandez, D., Seoane, J., Yao, D., Liu, K., Lin, S., Spees, K., Curtis, C., Jerby-Arnon, L., Weissman, I., Sage, J. and Bassik, M., 2021. Inter-cellular CRISPR screens reveal regulators of cancer cell phagocytosis. *Nature*, 597(7877), pp.549-554.

Kato Y, Tabata K, Kimura T, Yachie-Kinoshita A, Ozawa Y, Yamada K, et al. Lenvatinib plus anti-PD-1 antibody combination treatment activates CD8+ T cells through reduction of tumor-associated macrophage and activation of the interferon pathway. PLoS One 2019;14(2):e0212513.

Kelley, R.K. *et al.* (2022) 'Cabozantinib plus atezolizumab versus sorafenib for advanced hepatocellular carcinoma (cosmic-312): A Multicentre, open-label, randomised, phase 3 trial', *The Lancet Oncology*, 23(8), pp. 995–1008. doi:10.1016/s1470-2045(22)00326-6.

Ko, A. H., Chao, J., Noel, M. S., Shankaran, V., Sohal, D., Crow, M., Oberstein, P. E., Scott, A. J., McRee, A. J., Lima, C. M. S. P. R., Fong, L., Keenan, B. P., Soto, M., Filbert, E. L., Hsu, F. J., & Yang, X. (2025). A Phase 2 Study of Sotigalimab, a CD40 Agonist Antibody, plus Concurrent Chemoradiation as Neoadjuvant Therapy for Esophageal and Gastroesophageal Junction Cancers. *Cancer Research Communications*, *5*(2), 349–357. doi.org/10.1158/2767-9764.crc-24-0513

Ko, M. S., Cohen, S. N., Polley, S., Mahata, S. K., Biswas, T., Huxford, T., & Ghosh, G. (2022). Regulatory subunit NEMO promotes polyubiquitin-dependent induction of NF-κB through a targetable second interaction with upstream activator IKK2. *Journal of Biological Chemistry*, *298*(5), 101864. doi.org/10.1016/j.jbc.2022.101864

Kudo, M. et al. Lenvatinib versus sorafenib in first-line treatment of patients with unresectable hepatocellular carcinoma: a randomised phase 3 non- inferiority trial. Lancet 391, 1163–1173 (2018).

Kudo, M. Sequential therapy for hepatocellular carcinoma after failure of atezolizumab plus bevacizumab combination therapy. Liver Cancer 10, 85–93 (2021).

Lecoultre, M., Dutoit, V., & Walker, P. R. (2020). Phagocytic function of tumor-associated macrophages as a key determinant of tumor progression control: a review. *Journal for ImmunoTherapy of Cancer*, *8*(2), e001408. doi.org/10.1136/jitc-2020-001408

Levin-Konigsberg, R., & Mantegazza, A. R. (2020). A guide to measuring phagosomal dynamics. *FEBS Journal*, *288*(5), 1412–1433. doi.org/10.1111/febs.15506

Li, H. et al. Tim-3/galectin-9 signaling pathway mediates T-cell dysfunction and predicts poor prognosis in patients with hepatitis B virus-associated hepatocellular carcinoma. *Hepatology* 56, 1342–1351 (2012).

Lin, Y. Y. et al. Immunomodulatory effects of current targeted therapies on hepatocellular carcinoma: implication for the future of immunotherapy. Semin. Liver Dis. 38, 379–388 (2018).

Liu, M., O'Connor, R. S., Trefely, S., Graham, K., Snyder, N. W., & Beatty, G. L. (2019). Metabolic rewiring of macrophages by CpG potentiates clearance of cancer cells and overcomes tumor-expressed CD47−mediated 'don't-eat-me' signal. *Nature Immunology*, *20*(3), 265–275. doi.org/10.1038/s41590-018-0292-y

Liu, Y., Wang, Y., Yang, Y. *et al.* Emerging phagocytosis checkpoints in cancer immunotherapy. *Sig Transduct Target Ther* 8, 104 (2023). doi.org/10.1038/s41392-023-01365-z

Llovet JM, Castet F, Heikenwalder M, Maini MK, Mazzaferro V, Pinato DJ, Pikarsky E, Zhu A X, Finn RS. Immunotherapies for hepatocellular carcinoma. Nat Rev Clin Oncol 2022;19:151-172.

Llovet JM, Ricci S, Mazzaferro V, Hilgard P, Gane E, Blanc JF, et al. Sorafenib in advanced hepatocellular carcinoma. New Engl J Med. 2008;359:378–90.

Llovet, J. M., Kelley, R. K., Villanueva, A., Singal, A. G., Pikarsky, E., Roayaie, S., ... & Finn, R. S. (2022). Hepatocellular carcinoma. *Nature Reviews Disease Primers*, *8*(1), 6.

Llovet, J., Kelley, R., Villanueva, A., Singal, A., Pikarsky, E., Roayaie, S., Lencioni, R., Koike, K., Zucman-Rossi, J., and Finn, R., 2021. Hepatocellular carcinoma. *Nature Reviews Disease Primers*, 7(1).

Llovet, J.M. *et al.* (2023a) 'Lenvatinib plus pembrolizumab versus lenvatinib plus placebo for advanced hepatocellular carcinoma (LEAP-002): A randomised, double-blind, phase 3 trial', *The Lancet Oncology*, 24(12), pp. 1399–1410. doi:10.1016/s1470-2045(23)00469-2.

Lossos, C., Liu, Y., Kolb, K. E., Christie, A. L., Van Scoyk, A., Prakadan, S. M., Shigemori, K., Stevenson, K. E., Morrow, S., Plana, O. D., Fraser, C., Jones, K. L., Liu, H., Pallasch, C. P., Modiste, R., Nguyen, Q., Craig, J. W., Morgan, E. A., Vega, F., . . . Weinstock, D. M. (2019). Mechanisms of lymphoma clearance induced by High-Dose alkylating agents. *Cancer Discovery*, *9*(7), 944–961. doi.org/10.1158/2159-8290.cd-18-1393

Malehmir, M. et al. Platelet GPIbalpha is a mediator and potential interventional target for NASH and subsequent liver cancer. *Nat. Med.* 25, 641–655 (2019).

Mantovani, A., Allavena, P., Marchesi, F. *et al.* Macrophages as tools and targets in cancer therapy. *Nat Rev Drug Discov* 21, 799–820 (2022). doi.org/10.1038/s41573-022-00520-5

Márquez-Rodas, I., Dutriaux, C., Saiag, P., De La Cruz Merino, L., Álvarez, E. C., Robert, C., Rodríguez-Moreno, J. F., Arance, A., Cerezuela-Fuentes, P., Montaudié, H., Sanmamed, M. F., González-Cao, M., Charles, J., Criado, M. P. L., Berrocal, A., De Miguel, E., Funck-Brentano, E., Prey, S., De La Gala, M. C. Á., . . . Dalle, S. (2025). BO-112 plus pembrolizumab for patients with Anti–PD-1–Resistant Advanced melanoma: Phase II Clinical Trial SPOTLIGHT-203. *Journal of Clinical Oncology*, *43*(25), 2806–2815. doi.org/10.1200/jco-24-02595

Maeda, S., Kamata, H., Luo, J. L., Leffert, H., & Karin, M. (2005). IKKβ couples hepatocyte death to cytokine-driven compensatory proliferation that promotes chemical hepatocarcinogenesis. Cell, 121(7), 977-990.

Mehta, A., Harb, W., Xu, C., Meng, Y., Lee, L., Yuan, V., Wang, Z., Song, P., Shen, J. H., & Gopal, A. K. (2021). Lemzoparlimab, a Differentiated Anti-CD47 Antibody in Combination with Rituximab in Relapsed and Refractory Non-Hodgkin's Lymphoma: Initial Clinical Results. *Blood*, *138*(Supplement 1), 3542. doi.org/10.1182/blood-2021-150606

Montero, A., Wisinski, K. B., Fang, B., McCann, K. E., Hurvitz, S., Yeung, K. T., Parajuli, R., Chaves, J., Brufsky, A., Kaufman, P. A., Patel, M.

Murray, P. J., & Wynn, T. A. (2011). Protective and pathogenic functions of macrophage subsets. *Nature Reviews Immunology*, 11(11), 723–737.

Noel, M., O'Reilly, E. M., Wolpin, B. M., Ryan, D. P., Bullock, A. J., Britten, C. D., Linehan, D. C., Belt, B. A., Gamelin, E. C., Ganguly, B., Yin, D., Joh, T., Jacobs, I. A., Taylor, C. T., & Lowery, M. A. (2019). Phase 1b study of a small molecule antagonist of human chemokine (C-C motif) receptor 2 (PF-04136309) in combination with nab-paclitaxel/gemcitabine in first-line treatment of metastatic pancreatic ductal adenocarcinoma. *Investigational New Drugs*, *38*(3), 800–811. doi.org/10.1007/s10637-019-00830-3

Padrón, L. J., Maurer, D. M., O'Hara, M. H., O'Reilly, E. M., Wolff, R. A., Wainberg, Z. A., Ko, A. H., Fisher, G., Rahma, O., Lyman, J. P., Cabanski, C. R., Yu, J. X., Pfeiffer, S. M., Spasic, M., Xu, J., Gherardini, P. F., Karakunnel, J., Mick, R., Alanio, C., . . . Vonderheide, R. H. (2022). Sotigalimab and/or nivolumab with chemotherapy in first-line metastatic pancreatic cancer: clinical and

immunologic analyses from the randomized phase 2 PRINCE trial. *Nature Medicine*, *28*(6), 1167–1177. doi.org/10.1038/s41591-022-01829-9

Pasparakis, M. (2009). Regulation of tissue homeostasis by NF-κB signalling: implications for inflammatory diseases. Nature Reviews Immunology, 9(11), 778-788.

Pathria, P., Louis, T. and Varner, J., 2019. Targeting Tumor-Associated Macrophages in Cancer. *Trends in Immunology*, 40(4), pp.310-327.

Petrova, P., Viller, N., Wong, M., Pang, X., Lin, G., Dodge, K., Chai, V., Chen, H., Lee, V., House, V., Vigo, N., Jin, D., Mutukura, T., Charbonneau, M., Truong, T., Viau, S., Johnson, L., Linderoth, E., Sievers, E., Maleki Vareki, S., Figueredo, R., Pampillo, M., Koropatnick, J., Trudel, S., Mbong, N., Jin, L., Wang, J. and Uger, R., 2016. TTI-621 (SIRPαFc): A CD47-Blocking Innate Immune Checkpoint Inhibitor with Broad Antitumor Activity and Minimal Erythrocyte Binding. *Clinical Cancer Research*, 23(4), pp.1068-1079.

Phipps, C., Chen, Y., Gopalakrishnan, S., & Tan, D. (2015). Daratumumab and its potential in the treatment of multiple myeloma: overview of the preclinical and clinical development. *Therapeutic Advances in Hematology*, *6*(3), 120–127. doi.org/10.1177/2040620715572295

Qi, J., Li, J., Jiang, B., Jiang, B., Liu, H., Cao, X., Zhang, M., Meng, Y., Ma, X., Jia, Y., Guo, J., Zhang, Y., Huang, W., & Wang, J. (2020). A Phase I/IIa Study of Lemzoparlimab, a Monoclonal Antibody Targeting CD47, in Patients with Relapsed and/or Refractory Acute Myeloid Leukemia (AML) and Myelodysplastic Syndrome (MDS): Initial Phase I Results. *Blood*, *136*(Supplement 1), 30–31. doi.org/10.1182/blood-2020-134391

R., Pluard, T., Salim, B., Shah, K. V., Guan, S., Tsiatis, A. C., Randolph, S., & Meric-Bernstam, F. (2025). Abstract PS8-09: Zanidatamab in combination with evorpacept in HER2-positive and HER2-low metastatic breast cancer: Results from a phase 1b/2 study. *Clinical Cancer Research*, *31*(12_Supplement), PS8-09. doi.org/10.1158/1557-3265.sabcs24-ps8-09

Rahma, O. E. & Hodi, F. S. The intersection between tumor angiogenesis and immune suppression. Clin. Cancer Res. 25, 5449–5457 (2019).

Razak, A. R., Cleary, J. M., Moreno, V., Boyer, M., Aller, E. C., Edenfield, W., Tie, J., Harvey, R. D., Rutten, A., Shah, M. A., Olszanski, A. J., Jäger, D., Lakhani, N., Ryan, D. P., Rasmussen, E., Juan, G., Wong, H., Soman, N., Smit, M. D., . . . Papadopoulos, K. P. (2020). Safety and efficacy of AMG 820,

an anti-colony-stimulating factor 1 receptor antibody, in combination with pembrolizumab in adults with advanced solid tumors. *Journal for ImmunoTherapy of Cancer*, *8*(2), e001006. doi.org/10.1136/jitc-2020-001006

Runde, A. P., Mack, R., Breslin, P., SJ, & Zhang, J. (2022). The role of TBK1 in cancer pathogenesis and anticancer immunity. Journal of Experimental & Clinical Cancer Research, 41(1), 135. https://doi.org/10.1186/s13046-022-02352-y

Sawa-Wejksza, K., & Kandefer-Szerszeń, M. (2017). Tumor-Associated macrophages as target for antitumor therapy. *Archivum Immunologiae Et Therapiae Experimentalis*, *66*(2), 97–111. doi.org/10.1007/s00005-017-0480-8

Schoenberger, S. P., et al. (1998). T-cell help for cytotoxic T lymphocytes is mediated by CD40–CD40L interactions. *Nature*, 393(6684), 480–483.

Shitara, K., Wainberg, Z. A., Tabernero, J., Van Cutsem, E., Coutzac, C., De La Fouchardiere, C., Lee, J., Rha, S. Y., Kang, Y., Fanning, P., An, G., Jin, F., Forgie, A. J., Pons, J., Tsiatis, A., Randolph, S., & Lee, K. (2025). Final analysis of the randomized phase 2 part of the ASPEN-06 study: A phase 2/3 study of evorpacept (ALX148), a CD47 myeloid checkpoint inhibitor, in patients with HER2-overexpressing gastric/gastroesophageal cancer (GC). *Journal of Clinical Oncology*, *43*(4_suppl), 332. doi.org/10.1200/jco.2025.43.4_suppl.332

Sung, H., Ferlay, J., Siegel, R., Laversanne, M., Soerjomataram, I., Jemal, A. and Bray, F., 2021. Global Cancer Statistics 2020: GLOBOCAN Estimates of Incidence and Mortality Worldwide for 36 Cancers in 185 Countries. *CA: A Cancer Journal for Clinicians*, 71(3), pp.209-249.

Shiha, G., & El-Emshaty, H. M. (2019). The role of IKKβ in hepatocellular carcinoma initiation and progression. Journal of Hepatology, 70(1), e118-e119

Takaesu, G., Surabhi, R. M., Park, K., Ninomiya-Tsuji, J., Matsumoto, K., & Gaynor, R. B. (2003). TAK1 is Critical for IκB Kinase-mediated Activation of the NF-κB Pathway. Journal of Molecular Biology, 326(1), 105–115. https://doi.org/10.1016/s0022-2836(02)01404-3

Tap, W. D., Gelderblom, H., Palmerini, E., Desai, J., Bauer, S., Blay, J., Alcindor, T., Ganjoo, K., Martín-Broto, J., Ryan, C. W., Thomas, D. M., Peterfy, C., Healey, J. H., Van De Sande, M., Gelhorn, H. L., Shuster, D. E., Wang, Q., Yver, A., Hsu, H. H., . . . Wagner, A. J. (2019). Pexidartinib versus

placebo for advanced tenosynovial giant cell tumor (ENLIVEN): a randomised phase 3 trial. *The Lancet*, *394*(10197), 478–487. doi.org/10.1016/s0140-6736(19)30764-0

US National Library of Medicine. ClinicalTrials.gov clinicaltrials.gov/ct2/show/NCT04039607 (2019).

Van Laethem, J., Borbath, I., Prenen, H., Geboes, K. P., Lambert, A., Mitry, E., Cassier, P. A., Blanc, J., Pilla, L., Batlle, J. F., Garrote, M. R., Pazo-Cid, R. A., Gallego, I., Smith, K. E., Ellmark, P., De Coaña, Y. P., Ambarkhane, S. V., & Macarulla, T. (2024). Combining CD40 agonist mitazalimab with mFOLFIRINOX in previously untreated metastatic pancreatic ductal adenocarcinoma (OPTIMIZE-1): a single-arm, multicentre phase 1b/2 study. *The Lancet Oncology*, *25*(7), 853–864. doi.org/10.1016/s1470-2045(24)00263-8

Vaughan, J., Wiggill, T., Mia, Z., & Patel, M. (2024). Tumor-associated macrophages in diffuse large B-cell lymphoma: the prognostic and therapeutic impact in a South African centre with high HIV seroprevalence. *Immunologic Research*, *72*(6), 1393–1403. doi.org/10.1007/s12026-024-09537-x

Wang-Gillam, A., O'Reilly, E. M., Bendell, J. C., Wainberg, Z. A., Borazanci, E. H., Bahary, N., O'Hara, M. H., Beatty, G. L., Pant, S., Cohen, D. J., Leong, S., Beg, M. S., Yu, K. H., Evans, T. J., Seufferlein, T., Okusaka, T., Phillips, P., Liu, X., Perna, S. K., & Le, D. T. (2019). A randomized phase II study of cabiralizumab (cabira) + nivolumab (nivo) ± chemotherapy (chemo) in advanced pancreatic ductal adenocarcinoma (PDAC). *Journal of Clinical Oncology*, *37*(4_suppl), TPS465. doi.org/10.1200/jco.2019.37.4_suppl.tps465

Wei, L., Lee, D., Law, C., Zhang, M., Shen, J., Chin, D., Zhang, A., Tsang, F., Wong, C., Ng, I., Wong, C., and Wong, C., 2019. Genome-wide CRISPR/Cas9 library screening identified PHGDH as a critical driver for Sorafenib resistance in HCC. *Nature Communications*, 10(1).

Weiskopf, K., Jahchan, N., Schnorr, P., Cristea, S., Ring, A., Maute, R., Volkmer, A., Volkmer, J., Liu, J., Lim, J., Yang, D., Seitz, G., Nguyen, T., Wu, D., Jude, K., Guerston, H., Barkal, A., Trapani, F., George, J., Poirier, J., Gardner, E., Miles, L., de Stanchina, E., Lofgren, S., Vogel, H., Winslow, M., Dive, C., Thomas, R., Rudin, C., van de Rijn, M., Majeti, R., Garcia, K., Weissman, I. and Sage, J., 2016. CD47-blocking immunotherapies stimulate macrophage-mediated destruction of small-cell lung cancer. *Journal of Clinical Investigation*, 126(7), pp.2610-2620.

Weiss, S. A., Sznol, M., Shaheen, M., Berciano-Guerrero, M., Couselo, E. M., Rodríguez-Abreu, D., Boni, V., Schuchter, L. M., Gonzalez-Cao, M., Arance, A., Wei, W., Ganti, A. K., Hauke, R. J., Berrocal, A., Iannotti, N. O., Hsu, F. J., & Kluger, H. M. (2023). A Phase II Trial of the CD40 Agonistic Antibody

Sotigalimab (APX005M) in Combination with Nivolumab in Subjects with Metastatic Melanoma with Confirmed Disease Progression on Anti-PD-1 Therapy. *Clinical Cancer Research*, *30*(1), 74–81. doi.org/10.1158/1078-0432.ccr-23-0475

Willingham, S., Volkmer, J., Gentles, A., Sahoo, D., Dalerba, P., Mitra, S., Wang, J., Contreras-Trujillo, H., Martin, R., Cohen, J., Lovelace, P., Scheeren, F., Chao, M., Weiskopf, K., Tang, C., Volkmer, A., Naik, T., Storm, T., Mosley, A., Edris, B., Schmid, S., Sun, C., Chua, M., Murillo, O., Rajendran, P., Cha, A., Chin, R., Kim, D., Adorno, M., Raveh, T., Tseng, D., Jaiswal, S., Enger, P., Steinberg, G., Li, G., So, S., Majeti, R., Harsh, G., van de Rijn, M., Teng, N., Sunwoo, J., Alizadeh, A., Clarke, M. and Weissman, I., 2012. The CD47-signal regulatory protein alpha (SIRPa) interaction is a therapeutic target for human solid tumors. *Proceedings of the National Academy of Sciences*, 109(17), pp.6662-6667.

Wu, K., Kryczek, I., Chen, L., Zou, W., & Welling, T. H. Kupffer cell suppression of CD8+ T cells in human hepatocellular carcinoma is mediated by B7-H1/programmed death-1 interactions. *Cancer Res.* 69, 8067–8075 (2009).

Wu, Q. et al. Blocking Triggering Receptor Expressed on Myeloid Cells-1-Positive Tumor-Associated Macrophages Induced by Hypoxia Reverses Immunosuppression and Anti-Programmed Cell Death Ligand 1 Resistance in Liver Cancer. *Hepatology* 70, 198–214 (2019).

Yang, J., Song, Y., Zhou, K., Li, Z., Zhang, M., Jing, H., Wang, Z., Yu, L., Meng, W., Lu, Q., Tian, W., & Shi, Y. (2024). Safety and efficacy of amulirafusp alfa (IMM0306), a fusion protein of CD20 monoclonal antibody with the CD47 binding domain of SIRPα, in patients with relapsed or refractory B-cell non-Hodgkin lymphoma: a phase 1/2 study. *Journal of Hematology & Oncology*, *17*(1), 123. doi.org/10.1186/s13045-024-01646-2

Yarchoan, M., Hopkins, A., and Jaffee, E., 2017. Tumor Mutational Burden and Response Rate to PD-1 Inhibition. *New England Journal of Medicine*, 377(25), pp.2500-2501.

Yau, T. et al. CheckMate 459: a randomized, multi-center phase III study of nivolumab (NIVO) vs sorafenib (SOR) as first-line (1L) treatment in patients(pts) with advanced hepatocellular carcinoma (aHCC). Ann. Oncol. 30, v874–v875 (2019).

Yau, T. et al. Efficacy and safety of nivolumab plus ipilimumab in patients with advanced hepatocellular carcinoma previously treated with sorafenib: the CheckMate 040 randomized clinical trial. JAMA Oncol. 6, e204564 (2020).

Yu, J., Li, S., Chen, D. *et al.* IMM0306, a fusion protein of CD20 mAb with the CD47 binding domain of SIRPα, exerts excellent cancer killing efficacy by activating both macrophages and NK cells via blockade of CD47-SIRPα interaction and FcγR engagement by simultaneously binding to CD47 and CD20 of B cells. *Leukemia* 37, 695–698 (2023). doi.org/10.1038/s41375-022-01805-9

Zeller, T. *et al.* (2023) 'Perspectives of targeting Lilrb1 in innate and adaptive immune checkpoint therapy of cancer', *Frontiers in Immunology*, 14. doi:10.3389/fimmu.2023.1240275.

Zheng, H., Peng, X., Yang, S. *et al.* Targeting tumor-associated macrophages in hepatocellular carcinoma: biology, strategy, and immunotherapy. *Cell Death Discov.* 9, 65 (2023). doi.org/10.1038/s41420-023-01356-7

Zhou, X. et al. Treatment-related adverse events of PD-1 and PD-L1 inhibitor-based combination therapies in clinical trials: a systematic review and meta-analysis. Lancet Oncol. 22, 1265–1274 (2021).

Zhu, A. X. et al. Ramucirumab after sorafenib in patients with advanced hepatocellular carcinoma and increased α-fetoprotein concentrations (REACH-2): a randomised, double- blind, placebo-controlled, phase 3 trial. Lancet Oncol. 20, 282–296 (2019).

Zhu, S. et al. Combination strategies to maximize the benefits of cancer immunotherapy. J. Hematol. Oncol. 14, 156 (2021).

Zhu, Y., Yang, J., Xu, D., Gao, X., Zhang, Z., Hsu, J. L., ... & Hung, M. C. (2019). Disruption of tumor-associated macrophage trafficking by the osteopontin-induced colony-stimulating factor-1 signalling sensitises hepatocellular carcinoma to anti-PD-L1 blockade. *Gut*, *68*(9), 1653–1666.

Zhuang, T. Z., Feng, L., Tyshevich, A., Shavronskaya, D., Alesse, J., English, N., Sheehan, L., Syzrantsev, N., Nesmelov, A., Chihara, D., Westin, J., Ahmed, S., Fayad, L., Henderson, J., Dent, K., McChesney, E., Neelapu, S., Flowers, C. R., & Strati, P. (2025). Abstract LB369: Final results of a phase I trial of evorpacept (ALX148), lenalidomide, and rituximab for patients with B-cell non-Hodgkin lymphoma. *Cancer Research*, *85*(8_Supplement_2), LB369. doi.org/10.1158/1538-7445.am2025-lb369